Bournemouth University

Investigating the Ideal Deltoid Kinematics and Tension in Reverse Shoulder Arthroplasty (RSA)

By:

Navid Aslani

A thesis submitted in partial fulfilment of the requirements of Bournemouth University for the degree of Doctor of Philosophy (Ph.D.)

Collaborating Establishment

Bournemouth Royal Hospital, Bournemouth, UK

Bournemouth University

Faculty of Science and Technology

2017

Abstract

The Shoulder is the one of the most active joints within the human body. Recruited in the majority of daily activities either in active use such as moving/carrying of objects or as a source of stability during locomotion. Therefore painful shoulder or its reduced mobility and function can be very debilitating hence affecting the quality of life.

While shoulder pain and restricted motion encompasses a diverse array of pathologies, the most common causes are due to infection, arthritis, or trauma. Arthroplasty (the surgical reconstruction or replacement of a joint) of the shoulder has offered the potential for improved function and pain relief where the native structures have been damaged. The conventional total shoulder replacement, however, is not beneficial for all patients and may result in further pain and limited motion in persons with arthritic shoulders with a deficient rotator cuff. For these patients Reverse Shoulder Arthroplasty (RSA), in which anatomic concavities of glenohumeral joint are inverted, is a popular treatment. However, for optimal restoration of motion, the correct positioning of the glenohumeral centre of rotation and initial setting of the deltoid length (Deltoid Tension) must play an important role in the surgery outcome.

A study of the key literature has shown that despite common use of RSA, its biomechanical characteristics during motion are not fully understood. This study investigates the influence of some of the key parameters on the intensity of forces and moments in the shoulder joint before, during and after RSA. These parameters include; geometry, kinematics and muscle passive force measurement (deltoid pretension measurement).

To investigate the effect of geometrical changes on kinematics of shoulder after RSA, a musculoskeletal model of the shoulder is developed and simulated. Geometrical parameters of the musculoskeletal model are extracted from previous published studies.

Results of the simulation enabled the detection of key parameters in reverse shoulder kinematics and its influence on determining the mechanical advantage of the shoulder mechanism. This identified the need for developing an X-ray imaging protocol and image processing tool that enable surgeons to predict optimum implants insertion position and estimate the performance of the shoulder before planning the operation.

Subsequently, an assessment tool was proposed to assess shoulder Range of Motion (ROM) and deltoid muscle activity to both quantify and validate the predicted outcome of the surgery.

The main purpose of this study is to measure the passive force exerted on the reverse shoulder joint during surgery as a criterion or measure of deltoid pretension. Hence a force sensor is designed, developed and tested in a custom built joint simulator.

As part of this research and to allow objective assessment of the joint, a series of tools/hardware/software were proposed, designed and developed, and then tested and evaluated for effectiveness and functionality. The introduction of a system proposed here provides data which could be recorded in a database along with geometrics and kinematics pre and post operatively, residual force in glenohumeral joint intraoperatively and shoulder performance in terms of range of motion and EMG muscle activity of individual patients pre and post operatively. Such a database in time will enable us to find correlations between these parameters and the outcome of surgery in the long term. It is hoped that this will provide a tool for surgeons in future operations to who choose to use a more quantitative and repeatable way of optimizing the implant size and position accordingly.

Abbreviations

AAE	Anterior Active Elevation
BMI	Body Mass Index
CAD	Computer-Aided Design
CT	Computed Tomography
CTA	Cuff Tear Arthroplasty
DOF	Degree of Freedom
EMG	Electromyography
GH	Glenohumeral Joint
GUI	Graphical User Interface
IMU	Inertial Measurement Unit
JPEG	Joint Photographic Experts Group
MOM	Muscle Optimization Model
NHS	National Health Service
NJR	National Joint Registry
NJRSC	National Joint Registry Steering Committee
RBCH	Royal Bournemouth and Christchurch Hospital
ROM	Range of Motion
RS	Reverse Shoulder
RSA	Reverse Shoulder Arthroplasty
SD	Standard Deviation
TSA	Total Shoulder Arthroplasty

Nomenclature

$[x_o, y_o, z_o]$	Origin of the Cartesian coordinate system
$\emptyset_a$	Actual diameter of the Glenosphere
$\emptyset_p$	Projected diameter of the Glenosphere in the nominal Grashey view
ΔR_i	Resistance i^{th} variation
D_i	Deltoid insertion
$\vec{\underline{F}}$	Deltoid force vector
F_D	Force vector generated by Deltoid
K_1	Coefficient for torsion of rectangular section
L_0	Initial Deltoid length at neutral arm position
L_{eff}	Effective lever arm
O_{xy}	Origin of an orthogonal 2D coordinate system
$[R]$	Rotation matrix
R_g	Resistance of strain gauge
R_l	Longitudinal components of resistance
R_t	Transversal component of resistance
V_r	Voltage ratio
ϵ_l	Longitudinal strain
ϵ_t	Transversal strain
h	Beam thickness
E	Young modulus
GF	Gauge factor of the strain gauge
I	Second moment of inertia
L	Vertical distance between COR and Deltoid insertion on Humerus
M	Moment intensity

R	Moment arm in Z direction
d	Muscle excursion
e	Horizontal distance between COR and Deltoid insertion on Humerus
i	Vertical (inferior) distance between COR and tip of Acromion
m	Horizontal (medial) distance between COR and tip of Acromion
n	Distance between acromion and centre of rotation
qw, qx, qy, qz	Quaternion elements
r	Mechanical lever arm
v	Poisson ratio
w	Beam width
x	Distance from constraint in X direction
y	Distance from constraint in Y direction
β	Angle between the moment arm and force vector of deltoid
δ	Rotation offset from the actual Grashey view
θ	Angle of abduction in Scapular plan
ϵ	Strain

Table of Contents

List of Figures

List of Tables

Acknowledgements

I would like to thank my supervisory team, Professor Siamak Noroozi, Mr Richard Hartley, Dr Philip Sewell, and Dr Mihai Dupac for their support and guidance during my research.

In addition, I want to thank my friends for pushing, supporting, caring, and putting up with me during this time. I could not have done any of this without all of you.

Finally, I would like to thank my family for their infinite support, love and understanding throughout my life. Because of you, no matter how far away I may be, I am able to carry home with me.

Published materials

Aslani, N., Noroozi, S., Hartley, R., Dupac, M., and Sewell, P., 2016. Assessment Of Key Parameters On The Performance Of The Deltoid Muscle In Reverse Shoulder Arthroplasty — A Modelling And Simulation-Based Study. *Journal of Mechanics in Medicine and Biology [online],* 1650072. Available from: http://dx.doi.org/10.1142/S021951941650072X.
 (published paper)

Aslani, N., Noroozi, S., Harvey, A., Hartley, R., Dupac, M., and Sewell, P., 2016. Kinematics study of the deltoid in Reverse Shoulder Arthroplasty using Standard Pre and Post-Operative X-Rays. *Journal of Clinical Biomechanics*. (Submitted on 4 October 2016. (submitted paper)

Aslani, N., Noroozi, S., Davenport, P., Hartley, R., Dupac, M., and Sewell, P., 2016. Development of a 3D workspace Shoulder Assessment Tool Incorporating Electromyography and an Inertial Measurement Unit. *Journal of Medical & Biological Engineering & Computing.* (submitted paper)

Aslani, N., Noroozi, S., Hartley, R., Dupac, M., and Sewell, P., 2017. Design and fabrication of transducer to measure joint passive force in Reverse Shoulder Arthroplasty (working paper)

Chapter 1 Introduction

1.1 Introduction

The Shoulder is the most complicated and active joint of the human body in daily activities. Pain in the shoulder has become the third most common musculoskeletal disorder observed in the primary care (Mitchell et al. 2008). Arthroplasty of the shoulder has offered the potential for improved function and pain relief where the native glenohumeral (GH) articulation has been damaged by infection, arthritis, or trauma (Flatow et al. 2011).

Reverse Shoulder Arthroplasty (RSA) has emerged as a good treatment for patients who suffer from pain and limited range of motion of the shoulder caused by rotator cuff tear (Walker et al. 2011). There are many factors pre, intra and post operatively which can affect the outcome of RSA. These factors are mostly divided into three areas;

1. **Geometrical** (anatomical and prosthetic parameters which are a function of implant parts selection and positioning).
2. **Kinematics** (influence of initial and surgical geometrical parameters on kinematics of motion both in native and reverse shoulder).
3. **Joint forces** (such as reaction or passive force generated by muscles (soft tissue) on glenohumeral joint due to tension in the deltoid).

The purpose of this study, which was funded by Royal Bournemouth and Christchurch Hospital (RBCH, http://www.rbch.nhs.uk) was to investigate what have been deemed the primary factors when assessing performance of reverse shoulder arthroplasty.

1.2 Shoulder Anatomy

Before the kinematics of the shoulder can be discussed it is important to fully understand the anatomy of the shoulder. The shoulder is comprised of three bones, eighteen muscle sections, eight ligaments and four joint surfaces. Even in the simplest shoulder activities all or many of these parts are activated to provide motion, force and balance.

Among all four joints (Figure 1-1), the glenohumeral joint has the biggest share in most shoulder motions in daily activities, having all three rotational degree of freedom, while deltoid muscle sections (Figure 1-2) provide the most force upon the glenohumeral joint. The glenohumeral joint is able to provide rotation along different axes causing flexion, extension, abduction, adduction and internal and external rotation. The humerus

head is also capable of translating across the glenoid surface making the glenohumeral joint the most unconstrained joint in the human body (Permeswaran 2014). A full list of shoulder bones, muscles and ligaments can be found in appendix (Appendix A.I)

Joints

Figure 1-1: Shoulder joints

- Glenohumeral (GH)
- Scapulothoracic (ST)
- Sternoclavicular (SC)
- Acromioclavicular (AC)

Muscles

Deltoid

Deltoid Muscle

- Posterior Deltoid
- Middle Deltoid
- Anterior Deltoid

Figure 1-2: Deltoid muscle sections

Rotator Cuff

Supraspinatus	Infraspinatus	Teres Minor	Subscapularis

Figure 1-3: Rotator cuff Muscles
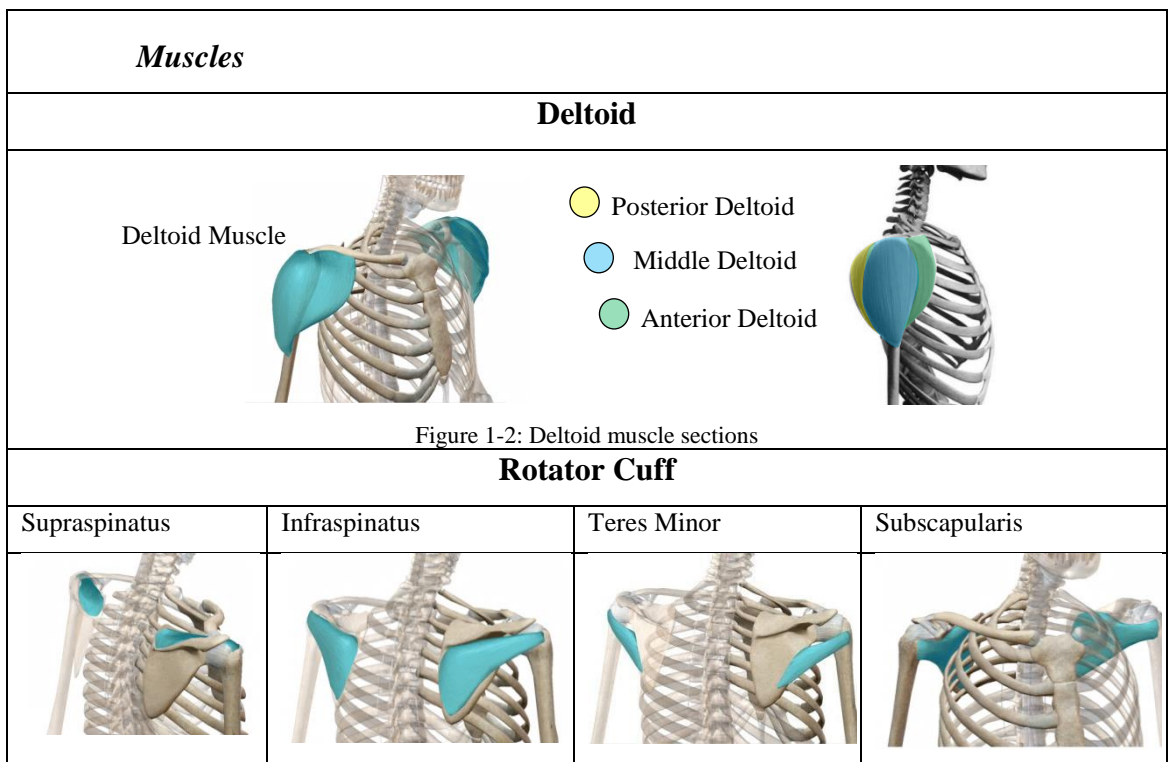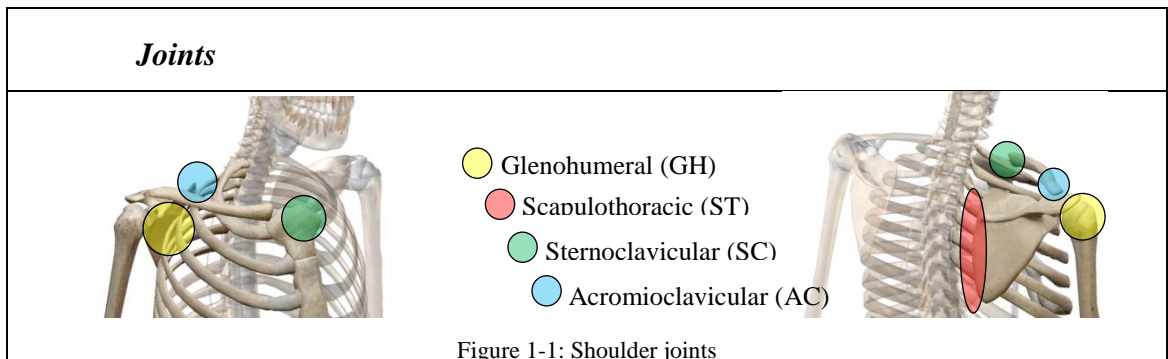
1.2.1 Biomechanics of Glenohumeral joint

Among all four joints of the shoulder the glenohumeral joint is the most active one, providing the greatest range of motion in daily activities (J.Tortora et al.2009). This joint consists of a spherical part (humerus head) constrained to the glenoid fossa on the scapula by both static and dynamic constraints. Static constraints include: The negative intra-articular pressure within the glenohumeral joint, the glenoid labrum and ligaments, tendons, and skeletal muscles surrounding the joint. Dynamic constraints which dynamically centre the humeral head within the glenoid fossa include: The rotator cuff

3

tendons (Figure 1-3) generating inferior and compressive force vectors. The strong deltoid muscle generating superiorly directed force and anterior and posterior force vectors are balanced by the subscapularis, teres minor, and Infraspinatus. Both static and dynamic constraints help to stabilise the glenohumeral joint in any position and motion.

1.2.2   Anatomy of Deltoid muscles

The Deltoid muscle (Figure 1-2) is the main elevator of the shoulder in different directions especially if the supraspinatus muscle is dysfunctional (Moser et al. 2013). The Deltoid muscle consists of three sections (Anterior, Middle and Posterior) and, depending on the direction of arm elevation, a share of each of these three sections is used in moving the arm.

1.2.3   Anatomy of Rotator Cuff

The Rotator cuff (Figure 1-3) is a group of muscles (Supraspinatus, Infraspinatus, Teres Minor, and Subscapularis). Before any motion at the glenohumeral joint rotator cuff muscles contract, limiting glenohumeral joint translation while providing dynamic stability for the shoulder. This group of muscles are also responsible for internal and external rotation (Permeswaran 2014).

Stability, strength and maneuverability of the shoulder is highly dependent on a healthy rotator cuff. Rotator cuff tear arthropathy is present in 2% of the ageing population ($\geq$ 70 years old) and can result in severe pain, with a pseudoparalysis arm and difficulty in performing daily activities (Naveed et al. 2011).

Rotator cuff tear is a tear of one or more of the tendons of the four rotator cuff muscles. A rotator cuff injury can include any type of irritation or damage to the rotator cuff muscles or tendons. There are different causes for rotator cuff tear such as: injury caused by lifting heavy object; overuse (especially after a period of inactivity); increasing age causing poor blood supply to rotator cuff and a gradual weakening of the tendons of the shoulder, often associated with impingement.

1.2.4   Rotator Cuff tear arthropathy

Cuff Tear Arthropathy (CTA) was first reported by Neer et al. (1983). Rotator cuff tear arthropathy caused by rotator cuff tears affects both shoulder strength and stability resulting in severe pain and difficulty in performing daily activities of living. A rotator cuff tear can cause secondary effects both mechanically and nutritionally in long term.

Mechanical factors cause humerus head migration upward by wearing into the acromion and acromioclavicular joint, and nutritional factors can cause reduced motion and function by losing pressure and quality of joint fluid which can lead to cartilage and subchondral collapse.

1.2.5   Rotator Cuff tear treatment

As discussed in the previous section, rotator cuff tear is a tear of one or more of the tendons of the four rotator cuff muscles. A rotator cuff injury can include any type of irritation or damage to the rotator cuff muscles or tendons.

There have been many suggestions about the treatments for rotator cuff tear summarised below (Nam et al. 2010, Flatow and Harrison 2011, Jazayeri and Kwon 2011, Sanchez-Sotelo 2011):

Non-operative management: including activity modification, oral medications, injections, fluid aspirations, and light motion exercises prior to surgery. This treatment can be useful for patients at early stages of treatment.

Resection arthroplasty: Resection arthroplasty has been attempted in the past as a treatment of shoulder with rotator cuff deficiency. However this kind of arthroplasty is mostly recommended for glenohumeral joint problems caused by sever osteoarthritis and injuries and not problems associated with deficiency of rotator cuff (Duncan et al. 2009).

Glenohumeral arthrodesis: Pain relief by eliminating shoulder motion (Figure 1-4-a). This method was used for patients who had multiple prior surgical procedures. Poor bone quality causes high risk of non-union in this treatment. Limited motion of glenohumeral joint causes excessive need for other shoulder joints motion resulting in pain making this method as an insufficient treatment for shoulders suffering from rotator cuff tear (Mimata et al. 2015).

Hemiarthroplasty: Broken humeral head is replaced with an artificial head and the fractured bone is reconstructed around the artificial spherical head (Figure 1-4-b). Just the spherical part of humerus is replaces with prosthesis while the scapula side remains native. In this method, Instability continues to be a long-term concern because of deficiency of rotator cuff still remains the big issue (Alentorn-Geli et al. 2014).

Constrained or conventional total shoulder arthroplasty: This method was one of the earliest designs introducing a fixed fulcrum as glenohumeral joint (Figure 1-4-c). Constrained total shoulder arthroplasty has been abandoned because the fixed joint caused excessive interface stresses resulting in rapid component loosening and failure (Post et.al 1983) .

Resurfacing implants: Implants without stem which cover humerus native head (Figure 1-4-d) with preserving bone stock and a good solution for patients with associated proximal humeral deformity although there is a big risk of fracture. This method does not seem to be a good alternative for rotator cuff tear treatment as it does not change biomechanical aspects of a shoulder to overcome rotator cuff deficiency (Mansat et al. 2013).

Total shoulder replacement: Damaged parts (the head of the humerus and the Glenoid fossa on scapula) are removed and replaced with artificial components (Figure 1-4-e). Total shoulder replacement is mostly used to treat severe shoulder fractures and different forms of arthritis. This implant required a functional rotator cuff to restore shoulder motion that's why they are not used for treatment of rotator cuff tear (Kiet et al. 2015).

Reverse shoulder Arthroplasty (RSA): Reverse Shoulder Arthroplasty (RSA), in which anatomic concavities of glenohumeral joint are inverted, is a popular treatment of arthritic shoulders with deficient rotator cuff (Figure 1-4-f).
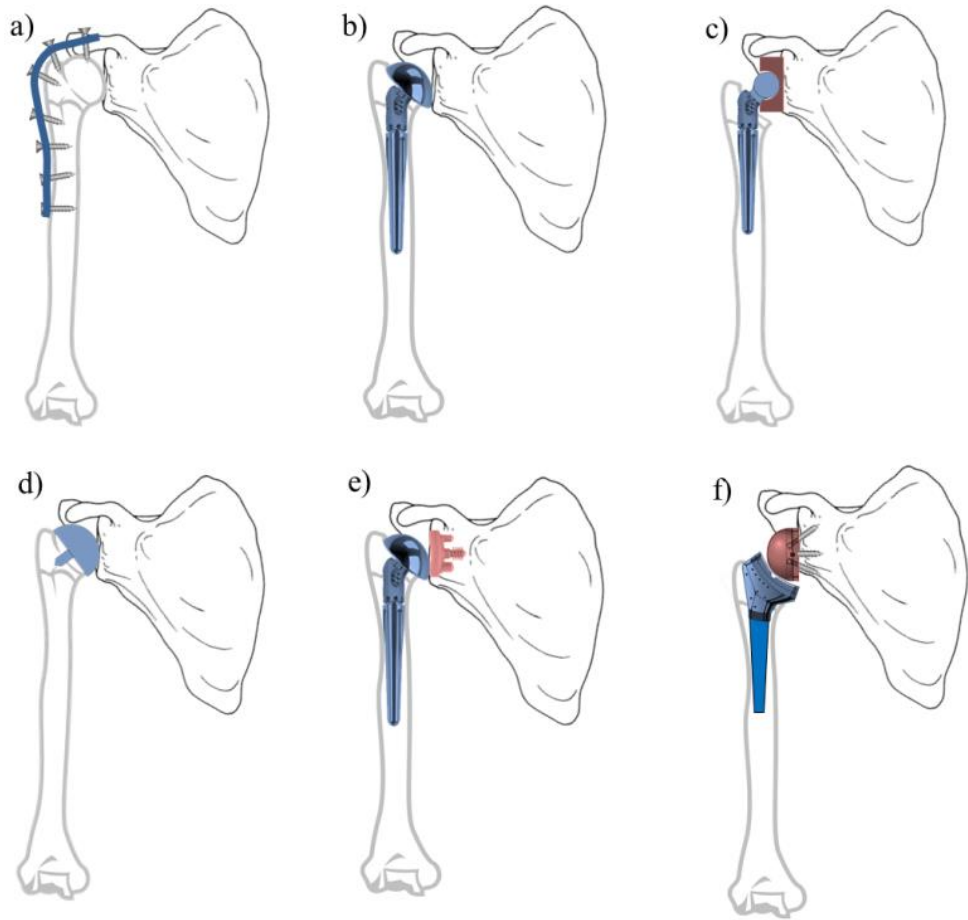
Figure 1-4: Suggested treatments for shoulders with rotator cuff tear

1.3 Reverse Shoulder Arthroplasty (RSA)

In 1985, Paul Grammont (Flatow and Harrison 2011) revolutionised shoulder arthroplasty by moving the centre of rotation of glenohumeral joint both medially and inferiorly relative to the native shoulder to increases the deltoid lever arm as well as the deltoid tension, allowing the muscles of the deltoid (anterior, middle and posterior) to compensate for rotator cuff deficiencies (Figure 1-5).
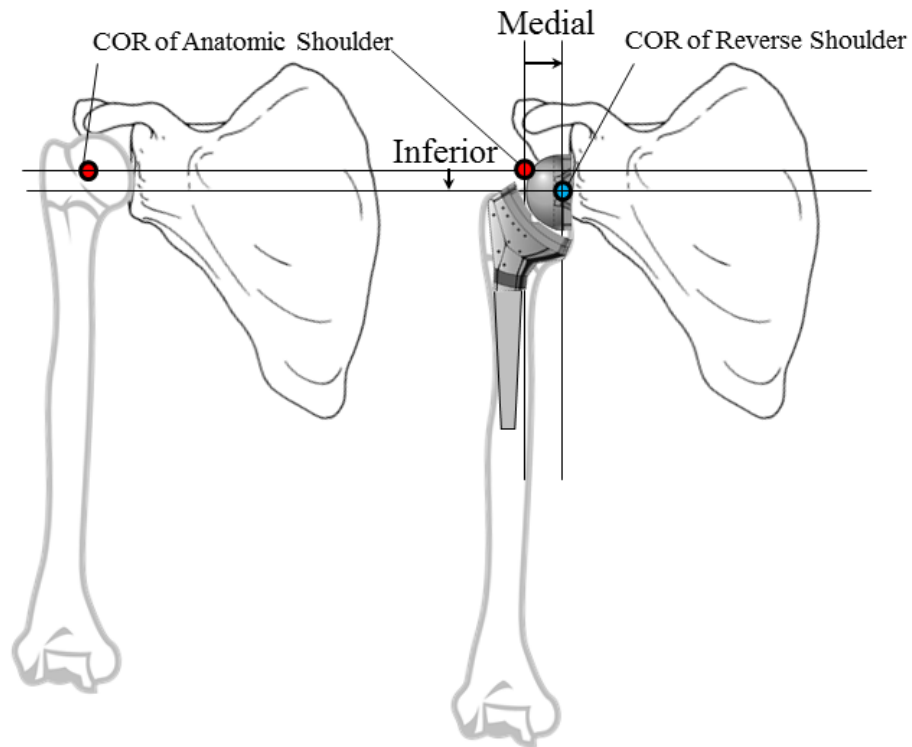
Figure 1-5: left: anatomic shoulder   right: reverse shoulder

The first prototype of the Grammont RSA was composed of a cemented glenosphere and an inverted polyethylene humeral stem. All the patients using this implant were reported to be pain free; however, the ranges of motion across the population as a result of surgery were reported to be variable. In 1991 a new variant of RSA was put into use, known as the DELTA implant (Jazayeri and Kwon 2011). This incorporated a mono-bloc humeral socket and a circular glenoid plate mounted on scapula having glenosphere screwed onto it (Figure 1-5). The plate was mounted on scapula with a central peg for press-fit impaction reinforced with two divergent screws and glenosphere directly screwed on the plate. There were further redesigns of Reverse Shoulder (RS) implants in later years; however, most of these were subject to loosening problems or impingement of prosthesis parts causing rapid deterioration. Currently there are many modern RS implants based on the Grammont design providing acceptable outcomes for shoulder with rotator cuff deficiency, reported to have a greater incidence of reliable pain relief and functionality of shoulder after surgery (Flatow and Harrison 2011, Jazayeri and Kwon 2011).

As the DELTA prosthesis has the longest reported outcome of any RS implant, this study focuses on two prosthesis released by DePuy (International Limited, Leeds, England) which are: Delta Xtend (Anon et al. 2007) and Delta CTA (Cta et al. 2004).

Figure 1-6: Delta Xtend   1: Diaphysis stem – 2:155o neck shaft – 3: Epiphysis cup – 4: monobloc stems (for use in proximal bone loss cases) – 5:+3, +6, +9 cup sizes – 6: glenosphere (38 and 42 mm) – 7: Metaglene – 8: Screws

Figure 1-7: Delta CTA   1: Diaphysis stem – 2: Epiphysis – 3: Lateralized Cup – 4: Glenosphere – 5: Metaglene – 6: Threaded head screws – 7: Spherical Head Screw

1.4 Reverse Shoulder Arthroplasty Applications

Reverse shoulder has been demonstrated to be a good treatment of several shoulder problems such as: Rotator cuff arthropathy, unsuccessful conventional shoulder arthroplasties, rheumatoid arthritis in patients associated with rotator cuff, proximal humeral tumors and proximal humeral fractures with antero-superior escape. However, RSA is the mostly used as treatment of shoulders with rotator cuff tear (Nam et al. 2010)

There are some theoretical advantages of RSA. The main ones include: improved stability; larger effective lever arm covering deficiency of rotator cuff; decreased mechanical failure; involvement of bigger portion of deltoid muscles by medicalisation; and a greater range of shoulder motion prior to impingement (Wright et al. 2015).

1.5 NJRSC Report

In the 12th edition of the annual report during the year 2014/15 (formal public report) released by National Joint Registry Steering Committee (NJRSC) nearly 2 milion records are managed and analysed for the period 1 April 2014 to 31 March 2015. This

report has the highest ever annual number of submissions at 226,871 as the largest arthroplasty registry in the world covering England, Wales and Northern Ireland (http://www.njrreports.org.uk/).

The NJR (National Joint Registry) is working with many sectors including patients, regulators, hospitals, universities, industry, individual surgeons and procurement to improve joint replacement outcomes.

The NJR established new economical arrangements in 2014 to reduce cost to the NHS and healthcare sector. In this year results of revision hip replacement and knee replacement are presented for the first time showing re-revision rates are almost an order of magnitude higher than the primary procedure. A summary of this report is presented in (Table 1-1).

According to this report, there are some patient factors which can notably influence the outcome and need for revision. Revision surgeries which are very expensive compared to primary procedure remains a problem in younger patients.

For example, the ten-year revision risk in male patients with cemented hip replacement shows 2.5 times more probability of revision for patients less than 55 years old in comparison to those over 75 years (7.26% in less than 55 years old and 2.83% in over 75 years old). The same trend is observed for the eleven-year revision risk in female patients with cemented, unconstrained, fixed bearing total knee replacement, having 4.5 time more risk of revision for patients less than 55 years in comparison to over 75 years (6.94% in less than 55 years old and 1.53% in over 75 years old).

The 12th Annual Report provides outcome data of all types of hip, knee, shoulder, elbow and ankle replacements. In this report 1,837,781 procedures are recorded including: 708,311 primary hip replacements and 772,818 knee replacements between 2003 and 2014, 2,554 ankle replacement between 2010 and 2014, 11,399 all types of shoulder replacement between 2012 and 2014 and 1,079 elbow replacement which is too small in number of procedures for further breakdown to be informative.

1.6 Shoulder Replacement

Between 2012 and 2014 11,399 shoulder replacements were recorded in NJRSC Report. There were more women (71.6%) than men (28.4%) undergoing primary procedures with median age of 73 years ranging between 19 and 99 years. Shoulder

replacement procedures are carried out by 553 consultant surgeons in 335 hospitals. The most used stem brand in all non-resurfacing procedures is Delta Xtend. 371 patients are reported to have replacements on both right and left sides, 12 of which were bilateral operations (right and left on the same day). 93.9% of patients with shoulder replacements are reported to have only one reason for primary operation.

The reasons for the primary operations are listed as: osteoarthritis (54.2%), cuff tear arthropathy (20.6%), Acute trauma (7.7%), Trauma sequelae (4.3%), Other inflammatory arthropathy (3.6%), avascular necrosis (1.8%) and other causes (1.8%).

Of all patients with shoulder replacement, RSA has the highest number of 4,127 primary procedures between 2012 and 2014. Over the last two years since the report was originally published there has been an increase in the use of Reverse implants from 31.1% (in 2012) to 39.9% (in 2014) showing there is an increasing demand for Reverse Shoulder Replacement.

According to the short period of data collection for shoulder replacements (from 2012 to 2014), only 165 revisions of primary operation are reported. It is expected to see a higher number of shoulder revisions in coming years as for hip and knee replacement with 11 years of follow up an increasing cumulative percentage probability of revisions are recorded versus years since primary operation.

The cumulative revision rate of reverse shoulder arthroplasty in the first 18 months after primary replacement is much worse in comparison to other types of shoulder replacements. RSA shows the highest percentage of first revisions among all type of primary shoulder replacement with 42.42% while total shoulder replacement is the second with 20.60%.

The main reason for 27.27% of revisions is due to instability, 18.78% cuff insufficiency, and 13.33% infection. Considering only reverse shoulder replacement, 37.14% of RSA revision surgeries performed are due to instability of shoulder joint, 21.42% indicates infection and 10% due to prosthesis fracture.

Among 165 revision surgeries reported, 60% of all had RSA as revision procedure while 22.42% had shoulder replacement.

70 reverse joint replacements were carried out at the Royal Bournemouth Hospital Shoulder Unit in the year 2012. The total number of Reverse joint replacements performed in the whole of UK is 2500 per year (Source Depuy Int). For hip replacement this is considerably more. Current NHS price/tariff for hip replacement and revision surgery alone is £5730 (R. Hartley, personal communication). Current NHS Price/tariff for reverse shoulder replacement surgery is £5888 (R. Hartley, personal communication). It is the same for revision surgery. The total cost of a revision shoulder surgery is between £12000 and £15000. Other additional costs to NHS include rehabilitation, hospital admission costs and physiotherapy. This makes the actual total cost of each revision as high as £15000 to £20000 (Source Depuy Int). In the UK alone this is estimated at £50m per year just for the shoulder.

	Number of procedures	Gender and median age (Primary surgery)	Fixation form/Replacement type	Cumulative percentage probability of revision (95%CI) after primary replacement
Hips	Primaries: 708,311 Revisions: 79,859 single-stage revision: 87.2% stage one of two-stage proceduers: 5.8% stage two of two-stage procedures: 6.9%	males 40.3%:females 59.7% Median Age: 69 years	36.1% Cemented 39.0% Uncemented 17.1% Hybrid 2.4% Reverse hybrid 5.3% Resurfacing	6.20% (6.04-6.36) at 11 years
Knees	Primaries: 772,818 Revisions: 47,829 single-stage revision: 76.7% stage one of two-stage procedures: 10.6% stage two of two-stage procedures: 12.6% (between 1 April 2010 and 31 December 2014)	males 43%:females 57% Median Age: 70 years	84.3% Cemented 4.7% Uncemented 1.1% Hybrid 8.7% Unicondylar 1.3% Patellofemoral	4.9% (4.77-5.04) at 11 years
Ankles	Primaries: 2,554 Revisions: 49 (between 1 April 2010 and 31 December 2014)	males 58%:females 42% Median Age: 68 years	2% Cemented 98% Unemented 0.04% Hybrid	3.46% (2.44-4.91) at 3 years
Shoulders	Primaries: 11,399 Revisions: 165 (between 1 April 2012 and 31 December 2014)	males 28.4%:females 71.6% Median Age: 73 years	5.2% Resurfacing total arthroplasty 29.4% Total prosthetic replacement 15.4% Hemiarthroplasty 13.8% Resurfacing hemiarthroplasty 36.2% Reverse polarity replacement	2.84% (2.35-3.42) at 2.5 years
Elbows	Primaries: 1,079 Revisions: 359	the numbers of elbows remains too small for further breakdown to be informative		

Table 1-1. A summary of NJRSC Report

1.7 Justification of research

In RSA the centre of rotation of the glenohumeral joint is moved medially and inferiorly, this is thought to improve the function of this joint and deltoid muscle. These geometrical changes in position of the centre of rotation will cause changes in kinematics of glenohumeral joint in comparison to the native shoulder. Deltoid tension could be another source of complexity. While a lack of tension leads to poor functionality of deltoid and glenohumeral joint instability and excessive deltoid tension causes pain and fracture of the acromion. For this reason it is the conclusion of this review that setting the right deltoid tension is crucial for outcome of RS surgery.

There are a huge number of factors influencing the outcomes of RSA. The most obvious factors are, surgeon's experience and expertise, design characteristics of the implant, characteristics of the individual's surgical technique, surgical instruments and measurement and assessment tools, type of approach and surgical planning, or post-operation care and rehabilitation, amongst others. Unfortunately, the analysis of the influence of the above factors on the outcomes of RSA has not been reported properly to date (Wright et al. 2015). One of the main purposes of this study was to investigate and categorise the main pre, intra and postoperative factors such as anatomical, geometrical, kinematics and force to investigate their effects on outcome of RSA.

All of the above can be due to unknown (excess or insufficient) levels of initial/residual tension in the deltoid or contact force at the joint. Currently surgeons do not have a value for these parameters to use as goal. Such information plus patient body mass data will allow surgeons/scientists to develop a link between deltoid tension and contact force which theoretically has to be the same for all (Kwon et al. 2010). At the moment surgeons rely solely on his or her experience (Gupta et al. 2016) and the haptic feel which is subjective and inaccurate at best.

Justifying the advantages of RSA over total shoulder replacement as a good revision procedure of shoulders with instability and rotator cuff insufficiency is a challenging question that needs better answer than is currently available. To achieve this, a better understanding of the effects of the main/chosen parameter on the expected outcome of the RSA is required. The main parameters are:

1) Correct kinematic location and orientation for the joint insertion.

2) Assessment method to evaluate performance of patient's shoulder pre and post operatively in terms of the range of motion and muscle activity.

3) Initial joint contact force during operation and the ability to adjust it to a desired setting and its effect on the outcome of RSA.

4) The ability to use positional data to predict the mechanical advantage based on force and lever arm plus the ability to adjust and optimize for best possible outcome.

1.7.1 Kinematics of shoulder gridle

Recent investigations have indicated a complete lack of consistencies in obtaining and assessing routine X-Ray images (Kwon et al. 2010, Ackland et al. 2011, Werner et al. 2015, Aslani et al. 2016). This lack of consistency does not allow any form of qualitative measurement or assessment of the joint needed to consistently predict the joint kinematics. This research proposes an introduction of an X-ray image protocol or standardisation method for imaging that will enable more accurate information to be extracted about the geometry and the kinematics of the joints prior to the surgical planning.

The RSA imaging protocol using a calibrated shoulder X-Ray identifies muscles origin, centre of rotation of the glenohumeral joint and muscle insertion point. By using the proposed protocol, this vital information can be extracted from X-ray images of patients both before and after the operation. A mathematical model of a shoulder joint will be developed that uses extracted geometrical data to calculate the differences in kinematics and mechanical advantages for various scenarios before each operation. The geometrical parameters can be inserted into kinematics equations to calculate muscle excursion and moment lever arm for a whole range of arm abduction.

1.7.2 Shoulder range of motion assessment and muscle activity

Different methods are available to evaluate shoulder performance during pre and post-operation in terms of pain free motion, manoeuvrability, strength and muscle activity, which are all qualitative and subjective making objective comparison/assessment difficult.

The available technologies are very expensive, not readily available in all clinics, require a dedicated space, [most] are not portable, and none have a high enough resolution to be useful for joint tracking in isolation. Also, they can substantially

increase the time needed for pre and post operation assessment. The most popular tracking systems are those used for human gait analysis which use optical motion capture and are fairly expensive and require a lab environment (Han et al. 2013). Recently low-cost wearable Inertial Measurement Unit (IMU) sensors have overcome many of the limitations of traditional motion tracking systems (Jung et al. 2010, Djurić-Jovičić et al. 2011, Palermo et al. 2014). These sensors include a 3 axis accelerometer (measuring linear acceleration), a 3 axis gyroscope (measuring angular velocity) and an additional 3 axis magnetometer (measuring magnetic field). These IMUs can have a very high resolution and can be attached to different body segments, even during operations.

This research proposes a new strategy and protocol as well as a novel transducer system to assess the performance of the shoulder by combining both ROM and EMG measurements. The GUI developed as part of this project will display the type and range of motion as well as deltoid's own activity levels, using a combination of IMU and EMG sensors.

The outcome of this investigation constitutes a leap forward in technology for RSA. It will replace the current practices which lack detail, accuracy and repeatability. In most cases the subject/patient will be asked to provide certain motions or trajectories such as abduction or flexion in certain 2D planes, all according to the defined protocol while capturing vital quantitative data.

1.7.3   Joint contact forces

It must be noted that every muscle in the shoulder girdle contributes to the shoulder movement according to its moment arm, line of action and the position of the glenohumeral joint. In the rotator cuff deficient shoulder, the most effective parameter that effects the glenohumeral motion is the deltoid muscle active and passive (residual) tension (Meyer et al. 2013). Hence setting the optimal residual tension (passive tension) in deltoid during RSA is one of the most important elements that affects the outcome of the surgery. In this proposal, the deltoid muscle initial tension (residual stress) is passively estimated via a novel transducer designed and developed as part of this project, to accurately measure and quantify the joint contact force. This measured load combined with kinematics data will help to establish a relationship that identifies the

ideal contact force for every individual based on their body mass, size, age and geometrical shoulder parameters.

Currently this is all done by feel and cannot be precisely measured, quantified or validated. This optimum tension level and contact force are at the discretion of the surgeons and is currently set based on their experience, skill, judgement and haptic their feedback. Using the proposed technologies can change all that. It is then down to the surgeon's skill and experience to find/select the best prosthesis size and position for the patient during the operation (Chih-Chiang Chang A 2013).

The introduction of the proposed system provides vital data, which is currently unavailable, which can be recorded in a dedicated database along with geometrical and kinematic data of individual patients. Such a database will enable correlations between the key parameters and the outcome of surgery to be determined in the long term. It is hoped that this will provide a tool for surgeons in future operations who choose to use a more quantitative and repeatable way of optimising the implant size and position accordingly.

In conclusion, this research aims to both identify and quantify kinematic parameters as well as initial deltoid tension that can control or influence the outcome of RSA. In this investigation a series of transducers, sensors, artefact, assessment and software will be designed and developed that in the long term will go a long way towards generating data and relationships that help surgeons to better understand and establish the links between these parameters and the functional outcome of shoulder surgeries. A simulation and optimisation of these parameters, when combined with individual's anatomical data captured before, during and after the operation should inform the operation planning and better placement of the implants by the surgeons.

Chapter 2 Literature Review

2.1 Introduction

As discussed, this thesis focuses on RSA and to be able to answer research question created in this chapter, a study of literature review is needed.

Despite RSA's success, this procedure has been associated with a relatively high complication rate both intraoperative (Wierks et al. 2009) and postoperative Flatow et al. (2011), while in some cases revision surgery is needed (Boileau et al. 2013). These complications include limited range of motion, pain, hematoma formation, infection, scapular notching, instability, acromial insufficiency, and glenoid component failures. A substantial numbers of these failures are due to excessive forces which are generated due to poor placement or wrong orientation and positional accuracy of the implant. With an aging population and increased use of this implant, this number is bound to increase.

X-Ray and MRI images of the shoulder girdle show a variety of morphology and dimensional differences amongst individuals (Werner et al. 2008, Frankle et al. 2009, Kircher et al. 2010, Gu and Yu 2013). Whilst no two individuals are the same, the normative range of motion of the arm for all healthy individuals should be relatively similar. However, the difference in anatomical sizes between individuals indicates there must exist an optimised relationship between relative values of these key parameters in order to obtain a defined abduction.

To date, limited data exists in regard to the influence of biomechanical and geometrical elements of an individual patients anatomic and post operation prosthesis parameters in terms of the functional outcome of RSA. For this reason, there is currently no information to link individual's initial anatomic and post operation shoulder girdle geometries on result of RSA.

There are to date many on-going studies aimed at investigating the multi-faceted properties of RSA in an effort to enhance the quality of life of its users. This project focuses on biomechanical factors effecting performance of RSA and these factors are categorized into two sections; "Geometrical parameters and kinematics" and "Deltoid Force Measurement". Assessment methods are also studied and discussed to evaluate outcome of RSA and compare it pre-operative performance of shoulder.

2.1.1 Geometrical parameters and kinematics

A healthy shoulder has specific characteristics in terms of range of motion, strength and manoeuvrability. In a shoulder with rotator cuff deficiency these characteristics are dramatically compromised and usually associated with severe pain in shoulder girdle (Meyer et al. 2013). As discussed before reverse shoulder arthroplasty is an effective treatment of a shoulder with rotator cuff deficiency (Nam et al. 2010, Sanchez-Sotelo 2011), where concavities of glenohumeral joint are inverted so to shift the centre of rotation medially (to increase effective lever arm) and distally (to set pre tension in deltoid muscle) and pain reduction as a result (Figure 1-5) (Kuechle et al. 2000, De Wilde et al. 2002, Terrier, Vogel, et al. 2008).

All of these variables play an important role in the shoulder's performance in terms of range of motion, strength and manoeuvrability. After RSA the geometry and kinematics of the glenohumeral joint will be totally changed. A standard RSA can result in different overall geometry depending on the original size of the individual and also in terms of the prosthesis size and positioning of prosthesis parts both on scapula and humerus for each patient.

Gutiérrez et al.(2008) reported the development of a 3D model of shoulder which was able to simulate abduction of glenohumeral joint in five surgical and implant-related factors. Their studies indicate small changes in placement of prosthesis parts could cause in impingement during abduction (Gutiérrez et al. 2008). Furthermore, this was followed by the same group examining the stability of RSA in experimental and theoretical models, suggesting stability of RSA is able to increase through joint compressive force generated largely by active and passive structures of soft tissue (Gutiérrez et al. 2008). These forces have been shown to vary greatly among individuals which concur with the findings of , Anglin et al. (2000) who characterizes six types of glenoid prosthesis demonstrating there the large variation in force ratio tolerated by prosthesis.

Kontaxis et al. (2009) developed a 3D biomechanical shoulder model consisting of six rigid bones and DELTA (DuPuy International, Leeds, United Kingdom) prosthesis. The model includes 31 muscles and three ligaments. A modified version of three dimensional Newcastle upper limb model (Charlton 2004) which in its original state represents a normal shoulder and elbow is used to simulate standardised daily activities.

The model also uses a contact detect algorithm to investigate possible impingement of prosthesis with the scapula. Results show in shoulder with rotator cuff tear deltoid muscle plays an important role to compensate for lack of rotator cuff muscles functionality by providing increased lever arm. It also reveals that modified contact forces in GH joint can cause more stability of joint in a reverse shoulder. Despite its advantages the contact detector algorithm shows impingement of prosthesis to scapula in some cases which could cause bone notches in long term.

Terrier et al. (2008) developed a finite element model of shoulder using geometries of scapula and humerus of a normal cadaver coming from CT (computed tomography) scan. Models of anatomical and reverse prosthesis were created to be compared. Middle deltoid, anterior deltoid, posterior deltoid, supraspinatus, subscapularis, and infraspinatus combined with teres minor were included in the model. Active abduction in scapular plane was performed in the scapular plane by a synchronised contraction of each muscle from 0 to 150 degree. The results show less needed deltoid force to achieve same amount of abduction because of increased lever arm of deltoid.

De Wilde et al. (2002) studied effect of deltoid elongation by using a computerized model of shoulder. The position and line of action of the force exerted by the different parts of the deltoid muscle was derived from serial transverse CT scans of a male subject. Muscle length–tension data were applied to obtain angle–force relationships. This study proves that stretching the deltoid muscle by 10% seems to result in a significantly more favourable position in case of shoulder elevation. This is a mathematical study and results are not validated against clinical or experimental tests.

2.1.2 RSA assessment:
There are some studies which investigate damages in RSA:

Gutiérrez et al. (2008) investigates hierarchy of stability factors in reverse shoulder arthroplasty to understand how to prevent and manage prosthetic instability. This study uses both experimental and theoretical models. The experimental model defines dislocation force as a dependent variable examined through three dependent variables which are compressive force, humerosocket depth and glenosphere radius in mechanical testing machine while the mathematical model calculates needed dislocation force assuming prosthesis parts as rigid bodies in contact with each other. Nam et al. (2010) discusses about current concepts, results, and component wear

analysis of RSA based on reports of clinical outcomes after RSA. Boileau et al. (2013) discusses revision surgery of reverse shoulder arthroplasty addressing even if revision may lead to several procedures in the same patient, preservation or replacement of the RSA is largely possible. This study uses 37 patients with RSA revision surgery with a minimum 2-years follow-up performing regular clinical and radiologic examinations preoperatively. Flurin et al. (2013) discusses scapular notching in RSA using 3D CAD (Computer-Aided Design) models to investigate impingement of prosthesis with scapula causing notching. Gutiérrez et al. (2008) investigates range of impingement-free abduction and adduction deficit after RSA using 3D CAD models.

There are some studies which investigate and discuss outcome of RSA:

Wright et al. (2015) presents a Systematic review of clinical and functional outcomes considering clinical outcomes depending on the type of approach-type of prosthesis concluding both medialization and laterization clearly improve outcome of RSA. Kim et al. (2012) discusses how scapula motion changes after reverse total shoulder arthroplasty using X-Ray Images of individuals pre and post operatively showing more scapular upward rotation after RSA. Naveed et al. (2011) investigate the mean maximum elevation in The Delta III reverse shoulder replacement in a clinical study showing patient satisfaction, no pain, improvement in activities of daily living and functional independence which are reflected as significant improvements in the American and Oxford scores which are Patient Reported Outcome questionnaire.

These studies investigate RSA based on some defined parameters. Roche et al. (2013) present a comparison of bone removed with Reverse Total Shoulder Arthroplasty using 3D computer model to quantify humeral and glenoid bone removal of three different implant designs. Jobin et al. (2012) investigate the clinical effect of deltoid lengthening and centre of rotation medialization using X-Ray images showing that deltoid lengthening improves active forward elevation after RSA for cuff tear arthropathy. Lädermann et al. (2012) studies Influence of arm lengthening in reverse shoulder arthroplasty using X-Ray images showing that shortening of the arm reduced AAE (anterior active elevation).

2.1.3   Range of motion
Different measurement tools can be used to analyse human movement. Traditionally these devices work using one of optical, mechanical, magnetic, structured light or

acoustic techniques. However for measurements of shoulder range of motion (ROM) in different planes the most common measurement tools are either mechanical systems used by operators manually or optical devices. Mechanical measurement tools such as the goniometer (Yu and Lee 2013), inclinometer and plurimeter (Sharma et al. 2015), rely on trained operators and have low accuracy and reliability, while vision based systems - using optical reflective markers attached to subject's limb to be tracked in 3D space are fairly expensive and time consuming due to the experimental setup for each subject (Rettig et al. 2015, Seminati et al. 2015). Recent studies have suggested use of kinect measurements as a better solution in terms of cost and availability for shoulder ROM tracking (Gritsenko et al. 2015, Lee et al. 2015).

Most of the studies investigating shoulder ROM measure either passive motion or a specific motion scenario in a specific plane (non-planar measurement) independently. (Haering et al. 2014) studied shoulder 3D ROM with all DOF (Degree of Freedom) interactions using a motion analysis system combined with an upper limb kinematic model. In similar study (Han et al. 2013) measured the 3D reachable workspace envelope surface area normalized to subject's arm length using a stereo camera.

2.1.4   Deltoid Electromyography (EMG)

The deltoid is involved the majority of shoulder activities, although in different shoulder movements different deltoid sections are involved in conjunction with other shoulder muscles. The anterior deltoid is more active in flexion, adduction and medial rotation; the middle deltoid has the biggest share in arm abduction among all shoulder muscles; the posterior deltoid provides extension, adduction and lateral rotation.(Moser et al. 2013)

Several studies document EMG activity of shoulder muscles during specific shoulder movement (Reinold et al. 2004, 2007, Nagai et al. 2013). There are two different types of EMG, intramuscular EMG using needle electrodes inserted into muscles and surface EMG, measured with sensors applied to the skin above the muscle belly. Although intramuscular EMG is more reliable in terms of recording actual muscle activity, previous studies have revealed that EMG of the deltoid muscle could be measured accurately using surface electrodes (Hodges et al. 1997, Kasman and Wolf 2002, Wickham and Brown 2012).

2.1.5 Deltoid Force Measurement

Each muscle of the shoulder girdle contributes to shoulder movement according to its moment arm, line of action and the position of the glenohumeral joint. In the rotator cuff deficient shoulder the most obvious influence on glenohumeral motion is the deltoid muscle (Meyer et al. 2013). Hence setting the optimal tension (passive tension) in deltoid during RSA is one of the most important keys on outcome of surgery. The individual muscle initial tension (residual stress) is difficult to estimate, but their indirect influence can be measured.

There are three different ways that forces in shoulder muscles are either modeled or their behaviors simulated.

Firstly, there are mathematical approaches in which muscles around joints are considered as force vectors and in specific arm positions. The following optimization algorithms calculate the force of each muscle in a known static position which can be converted to joint contact force.

Lin et al. (2011) predicts applied forces in arm by using an energy model in a specific motion scenario. Terrier et al. (2010) developed a musculoskeletal shoulder model based on pseudo-inverse and null-space optimization. The mechanical system includes 6 muscles of shoulder and GH joint. This study simulates several movements by solving dynamical equations. Veeger et al. (2002) studied load on the shoulder in low intensity wheelchair propulsion by inputting experimental data to a musculoskeletal model of upper extremity to approximate shoulder muscle forces. Favre et al. (2005) uses an algorithm for estimation of shoulder muscle forces by using a full-size epoxy model of shoulder joint and cables as muscle force vectors. The algorithm selects an appropriate group of muscles and step by step attributes small force increments to withstand the external moment while aiming at minimising the forces involved. Each muscle force increment is stored after every loop and eventually summed up defining stability of GH joint as the final determining factor Ribeiro et al. (2009) compares two model of shoulder muscle force estimations which are MOM (Muscle Optimization Model) and MODI 2D (2D Optimization Model) inputting experimental data. Steenbrink et al. (2009) investigated GH stability in simulated rotator cuff tears using Delft shoulder model (Nikooyan et al. 2010) having experimental data as inputs. The approaches detailed above require a multitude of anatomical measurements to create each model.

However, most of the studies using this method are based on case studies, which, due to the inherent complexity and variation of human body geometries seem not to be a satisfactory approach when predicting and optimizing implant selection and positioning on an individual case by case basis.

The second approach that is commonly found in the literature is cadaveric studies where muscles are replaced by steel cables passing through their origin and insertion points with fixed and pulley constraints. The shoulder is then kept in a static position attempting to provide the least amount of tension in each cable to approximate the force required by each muscles for known arm positions. These techniques have been used to great effects in both normal shoulder (Schamblin et al. 2009) and in reverse shoulder arthroplasty (Ackland et al. 2011) .

Onstot et al.(2013) investigates muscle force and excursion requirements along with a moment arm analysis of RSA which have been offset from the standard position in to a posterior and superior position. The joint reaction forces for the non-offset RSA and the posterior-superior offset RSA designs were compared with the joint reaction force of native shoulders in a cadaveric study. Kwon et al.(2010) analyses reverse total shoulder joint forces and glenoid fixation in a cadaveric study showing that during the elevation of the arm the calculated joint force in reverse shoulders is less than the joint force in the normal anatomic shoulders. Ackland et al.(2011) investigates muscle and joint-contact loading at the glenohumeral joint after RSA determining the contributions of each shoulder muscle to glenohumeral joint force during abduction and flexion in both the anatomical and post-operative shoulder and to identify factors that may contribute to the incidence of glenoid component loosening/failure and joint instability in the shoulder after RSA in a cadaveric study showing after RSA superior orientation of deltoid is significantly increased.

The practicality of these approaches *in vivo* has been unachievable to implement during surgery, not only because of the complexity and the time it requires but also the risk of secondary trauma such test retest conditions may induce.

The final common approach used to measure forces in shoulder muscles and joints during surgery is placing force sensors inside the new prosthetic glenohumeral joint to measure directly the force *in vitro*. Bergmann et al. (2007) were able to measure glenohumeral joint contact force *in vivo* using an instrumented shoulder implant

mounted permanently on a patient's shoulder with humeral head arthritis. A clinically established implant was used to measure all 6 components of forces and moments on humeral head using 6 strain gauges mounted on the prosthesis. Westerhoff et al. (2009) used the same sensor to investigate shoulder joint loads during daily activities. Schwartz et al. (2013) based on a cadaveric study discussed importance of anterior deltoid in RSA. In this study eight cadaveric shoulders were evaluated with a 6-axis force/torque sensor to assess the direction of rotation and 3D moment arms for all 6 segments of the deltoid both before and after the placement of a reverse shoulder prosthesis. They concluded that the 3D moment arms of the deltoid were significantly altered by the placement of the reverse shoulder prosthesis. The anterior and middle deltoid abduction moment arms significantly increased after placement of the reverse prosthesis.

Sensors are mostly used in other types of human joints such as knee. Crescini et al. (2011) designs and tests an autonomous sensor for force measurement in human knee implants using magnetoresistors. The deformation on polyethylene insert changes the distance between magnetoresistor and the permanent magnet modifying the magnetic field and data are transmitted wirelessly. Forchelet et al. (2014) presented the design, fabrication and testing of an instrumented insert performing force sensor containing micro fabricated polyimide thin-film piezoresitive strain gauge. Jacq et al. (2014) investigates a polymer thick-film piezoresistor force sensor design Nusser et al. (2012) presented a preliminary studies for validation of a novel sensor fiber to measure tension forces in the artificial ligaments.

Cristofolini et al. (2000) developed a novel transducer for measuring cement-prosthesis interface forces in cemented orthopedic devices specifically hip using a piezoelectric load-cell Damm et al. (2010) developed a new instrumented hip joint prosthesis for in vivo force measurement using 6 strain gauges.

2.2 Conclusion

The above investigation shows that RSA improves the performance of the glenohumeral joint. It should be noted that in the literature, medialization of the GH joint causing in increase of deltoid lever arm is addressed as a primary advantage of RSA for shoulders suffering from Rotator Cuff tear while deltoid lengthening is discussed as a secondary advantage. However most of the mentioned studies have

investigated consequences of initial geometrical changes in GH joint rather than their effect on kinematics of this joint in different motion scenarios.

In terms of pre and post-operative assessment of shoulder a gap in the literature is observed hence possible quantitative performance assessments (range of motion assessment and EMG muscle activity) are discussed.

Direct measurement of force in joint contact area using a force sensor seems to be the most feasible approach to predict correct implant selection and positioning while a database is generated based on measured force and its correlation to the outcome of surgery.

Tissues have similar properties and ultimate strength and theoretically they should all fail under the same load intensity. Hence the correlation between contact force and muscle volume or body mass can inform surgeons about what should be the nominal force that can be deemed acceptable. A transducer system that allows intraoperative forces to be measured is highly desirable because over time this information can lead to surgeons getting the passive contact load right first time during surgery.

Currently there are no simple tool that can inform the surgeon about the muscle tension during the operation ensure passive forces are within the acceptable range. Excessive un-accounted load results in fatigue, premature failures and excessive wear which results in looseness and change in kinematics.

2.3 Research question and objectives

Based on the review of the current issues associated with RSA surgery described above, the following research question will be answered:

 "Can the kinematics and forces in shoulder joint be quantified to inform the design of tools for surgeons to assess quality of RSA pre, intra and post-operatively?"

Based on the research question, an in-depth literature review was studied in this chapter presenting the current state of knowledge on theoretical and methodological contributions to Reverse Shoulder, shoulder kinematics, shoulder assessment and force measurement in joints.

The following four objectives were set so that this question could be answered:

1. Development of a simulated model of shoulder and study of kinematics of deltoid pre and post operatively.
2. Development of an image processing tool to assess standardised X-rays of individuals pre and post operatively by extracting geometrical parameters and calculating kinematics.
3. Development of a shoulder range of motion and Electromyography assessment tool to quantify and comparing shoulder performance pre and post-operatively.
4. Development of a force transducer for intraoperative force measurement.

In Chapter 3 the simulated musculoskeletal model was developed using geometrical parameters of previous studies. The X-ray tool was developed and assessed using X-rays of 10 patients and results were discussed in Chapter 4. The shoulder ROM and EMG assessment tool was designed, developed and tested on 7 subjects and results were discussed in Chapter 5. A new force sensor was proposed, designed and developed and performance of the sensor in a physical test rig were discussed in Chapter 6.

Chapter 3
Musculoskeletal Model

3.1 Introduction

As mentioned in Chapter 1, the main parameters affecting the outcome of RSA are Geometric/Kinematic and deltoid passive force (deltoid pre-tension), which have not been studied well in the literature, Chapter 2. The approach adopted is based on a simulated model of shoulder helping to investigate and understand the quantitative behaviour of GH joint and deltoid muscles pre and post operatively.

To construct the simulated model, all pre-operative and post-operative data can be extracted for further assessment of the positional and orientation accuracy of the placement of the implant (Saltzman et al. 2010, Lädermann et al. 2012):

-   Bones size and morphology
-   The origin of the deltoid on the acromion
-   The insertion points of the deltoid on the humerus
-   The centre of rotation of glenohumeral joint in 3D space
-   The available space and size of the glenoid sphere

All the geometrical measurements (both pre and post operatively) are extracted from previous studies (Werner et al. 2008, Frankle et al. 2009, Kircher et al. 2010, Saltzman et al. 2010, Lädermann et al. 2012, Gu and Yu 2013) (Figure 3-1).
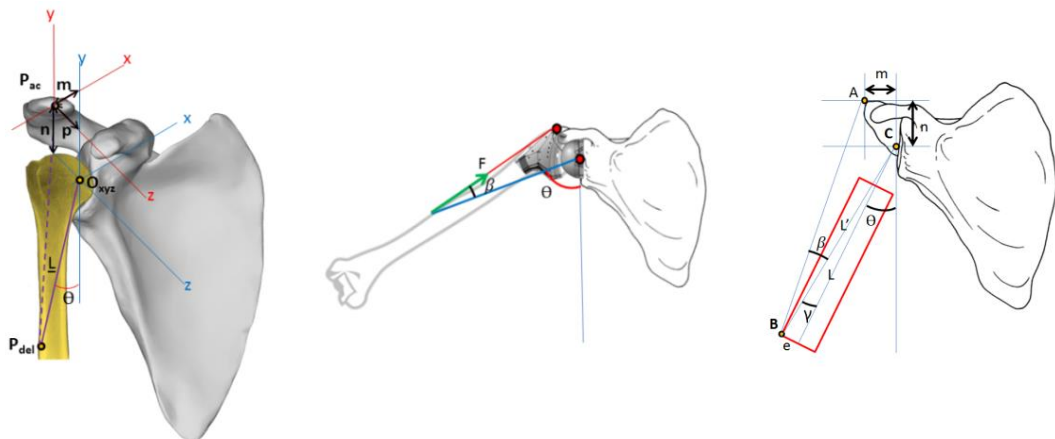
Figure 3-1: 3D Biomechanical Model of Shoulder (left) –Scapular Plane View (middle) – Parametric Scapular Plane View (Right)

3.1.1 Musculoskeletal model

An adjustable musculoskeletal model of shoulder is developed in Autodesk Inventor (Autodesk, Inc.) and then imported into MSC ADAMS (MSC Software) software including glenohumeral joint, scapula, humerus and two segments of deltoid (anterior

and middle). A precise 3D model of DELTA prosthesis was developed in the same software and inserted in bones following standard Surgical Technique of Delta Xtend Anon et al. (2007). This implant model is created using precise reverse engineering measurement of prosthesis parts in surgical theatre. All the parameters used to create and develop the CAD models can be easily changed to follow (fit) the dimension and morphology of any individual pre and post-operatively (Figure 3-2). To develop CAD model of the bones, all the dimensions are visually approximated while key parameters including origin and insertion of muscles relative to the coordinate of the origin (centre of GH) are extracted from previous studies as mentioned above and in the previous chapters.
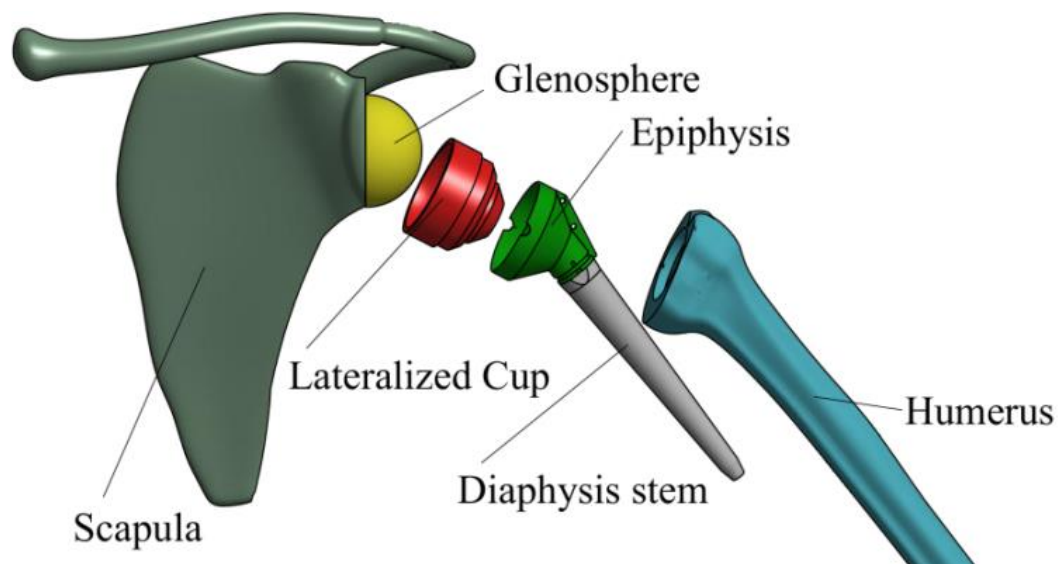
Figure 3-2: CAD model of RS

The Centre of rotation of GH joint is defined as the centre of the humerus spherical head in anatomic shoulder and the centre of prosthesis glenoid in reverse shoulder. Both anterior and middle deltoids are modelled by linear springs connected to the origin and insertion coordinates of deltoid on scapula and humerus (Figure 3-3). Spring deformation is considered as muscle contraction while these springs are also considered as muscular actuators (muscles) applying forces on the bones (Terrier, Reist, et al. 2008, Kontaxis and Johnson 2009). The 3D model developed as part of the project can be easily adjusted to each patient's specific dimensions and shapes while other muscles can be added to the model easily knowing their origin and insertion coordinates. This model can be used to investigate the shoulder performance (muscle contraction, muscle effective lever arm) in shoulder motion.
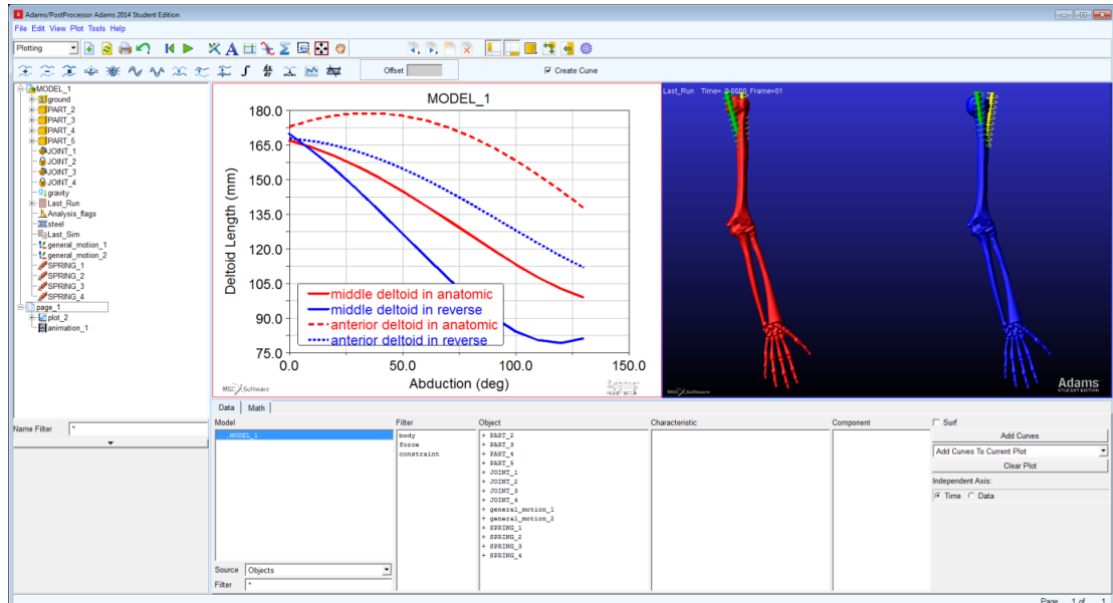
Figure 3-3: 3D model developed in MSC ADAMS

Limitations of kinematics models

It should be noted that, these kinematics models only consider geometry and kinematics of the glenohumeral joint while there are many other patient characteristics such as muscle fibre type, muscle volume and bone shapes which have not been taken into account in this study. Therefore, the prediction of subjective outcomes (pain relief and range of motion) needs more studies including mathematical and clinical approaches together.

3.2 Results

3.2.1 Deltoid excursion

The simulated model showed that the deltoid (Middle Deltoid, Anterior Deltoid) after RSA excurses (moves) more than the anatomic shoulder during abduction (0°-120°) (Fig.3-4) (Meyer et al. 2013). This longer excursion can cause a huge reduction in the deltoid range of available active force according to Force-Length graphs (Hill's Muscle model) (Berthonnaud et al. 2010, Millard et al. 2013) . Hill's Muscle model indicates muscles can provide the maximum force at the neutral position and a decreasing force as the muscle contracts. According to previous studies, the deltoid has its neutral length at approximately 30° of arm abduction (Flavio Almeida Salles 2002, Terrier, Vogel, et al. 2008, Terrier et al. 2010). However, Berthonnaud *et al*. (2010) assume that the deltoid has its maximum force at its neutral position (0° of abduction).
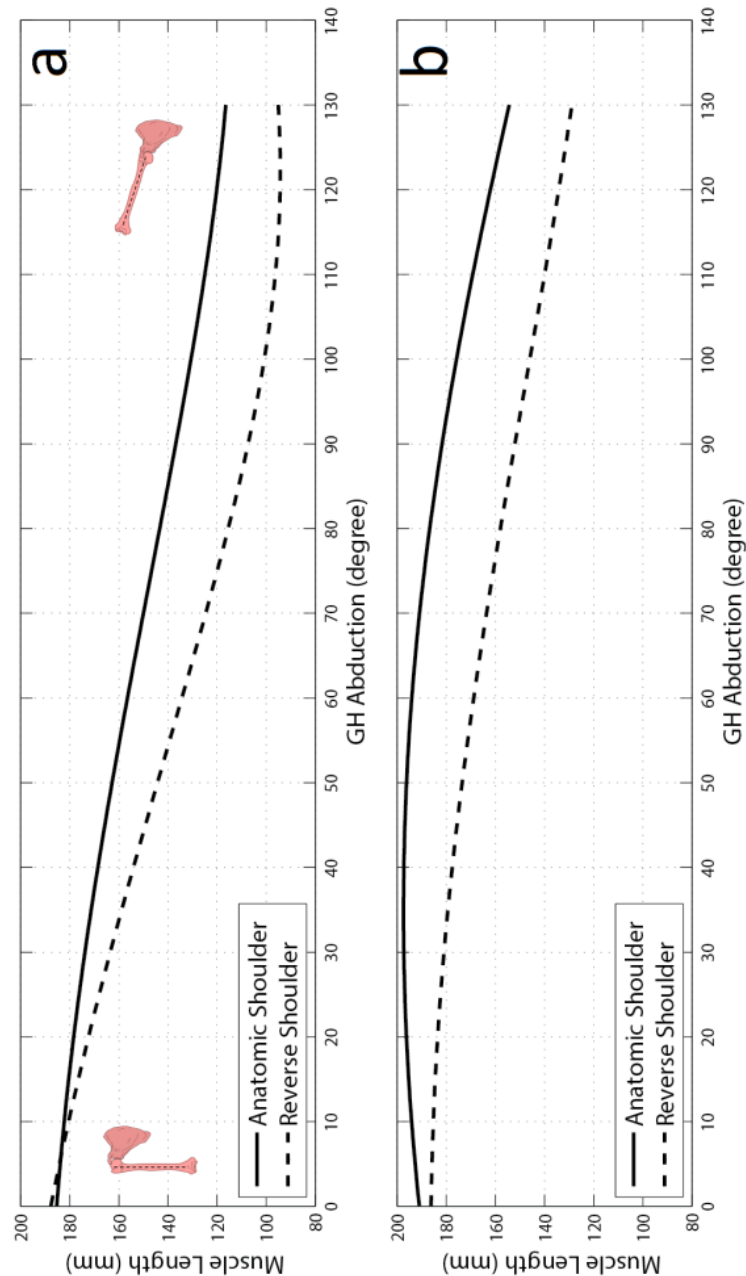
Fig.3-4: Deltoid Length VS Abduction of GH joint in scapular plane (a) Middle Deltoid (b) Anterior Deltoid

This accelerating contraction of the deltoid in reverse shoulder causes dramatic reduction in the available active force in it due to the muscle reaching the end of its contraction range. In some cases the deltoid may exceed its working range where it no longer can generate any force.

The Force-Length graph of the middle deltoid in the anatomic shoulder (Fig.3-5) shows that when the glenohumeral joint is in 0 degree of abduction, there exists little passive

force in the muscle having an available active force close to its maximum. As the arm abducts more, the middle deltoid reaches its maximum available active force at approximately 30° of abduction (where muscle reaches its neutral length). At larger angles, the available active force decreases towards zero (Maximum Abduction Angle). While in the reverse shoulder, the middle deltoid starts its excursion approximately at the same muscle length as the anatomic shoulder (0° of abduction) but it excurses more than the anatomic one during abduction arriving almost at zero force (Fridén and Lieber 2001). Generally, the available maximum active force of the Middle Deltoid in reverse shoulder is less than that of anatomic shoulder during the same range of abduction angles. While for Anterior Deltoid, the reverse shoulder can provide more force than the anatomic one at the lower abduction angle. Effectively, the higher abduction angle follows the same trend as that of the Middle Deltoid (Fig.3-6).
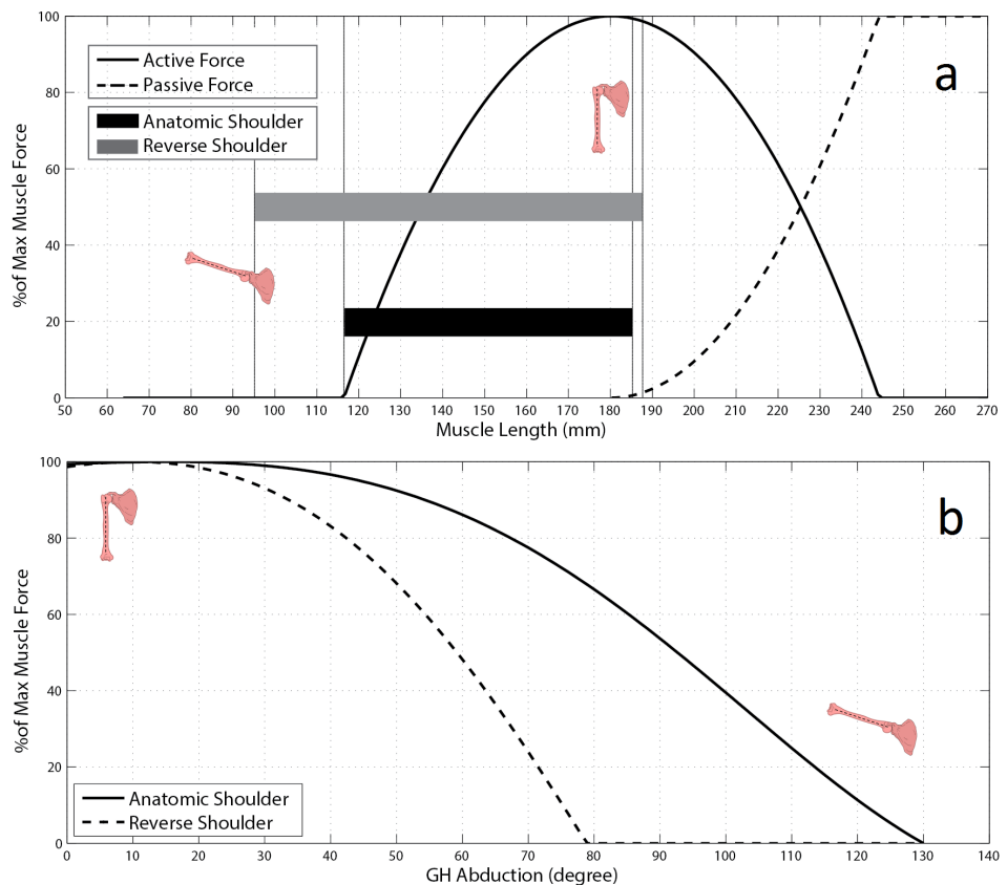
Fig.3-5: (a) Available active force in middle deltoid VS muscle length   (b) Available active force in middle deltoid VS glenohumeral abduction angle

(Horizontal bars indicate deltoid excursion in anatomic and RS from 0° to 130° of Glenohumeral joint abduction)

Fig.3-6: (a) Available active force in anterior deltoid VS muscle length   (b) Available active force in anterior deltoid VS glenohumeral abduction angle

(Horizontal bars indicate deltoid excursion in anatomic and RS from 0° to 130° of Glenohumeral joint abduction)

The moment intensity is the function of the moment arm (distance between Centre of Rotation of the humerus and the deltoid insertions on humerus: **L**), deltoid force vectors (the vectors connecting deltoid insertion points on the humerus and origins of the deltoid on acromion: $\vec{\boldsymbol{F}}$) and $\boldsymbol{sin}$ of the angle between the moment arm and force vector of deltoid, $\boldsymbol{sin(\beta)}$ (Figure 3-1). They are related by the following function (Terrier, Reist, et al. 2008, Kontaxis and Johnson 2009, Schwartz et al. 2013).

$$M = F \times L \times sin(\beta) \quad (eq.1)$$

Effective lever arm is the product of Moment arm: (**L**) multiplied by $\boldsymbol{sin(\beta)}$.

$$L_{eff} = L \times sin(\beta) \quad (eq.2)$$

$$M = F \times L_{eff} \quad (eq.3)$$

Plotting Effective Lever Arm (Leff) versus abduction angle in anatomic shoulder and reverse shoulder shows different trends:

Middle Deltoid: This section of the deltoid experiences higher values of the effective lever arm in the reverse shoulder than in anatomic shoulders for a limited abduction angle. It then drops dramatically getting close to zero (Fig.3-7-a). At Zero degrees the glenohumeral joint mechanism is locked and cannot be abducted any more due to the loss of the effective lever arm and generates a pure compression force pulling on the arm towards the centre of rotation instead of rotating about it.

Leff may not cross absolute zero in its range of motion but this increased Leff shows closer (or even smaller) values compared to anatomic ones during higher abduction. This means that the provided increase of Leff by medialization does not provide a constant or sustained boost to rotation moment through the whole range of the motion. Previous studies mention that the lever arm in reverse shoulder is bigger than the anatomic one thanks to medialization of COR, but this investigation using a kinematic model has shown this theory can only be correct during a limited range of abduction (Jazayeri and Kwon 2011, Jobin et al. 2012).
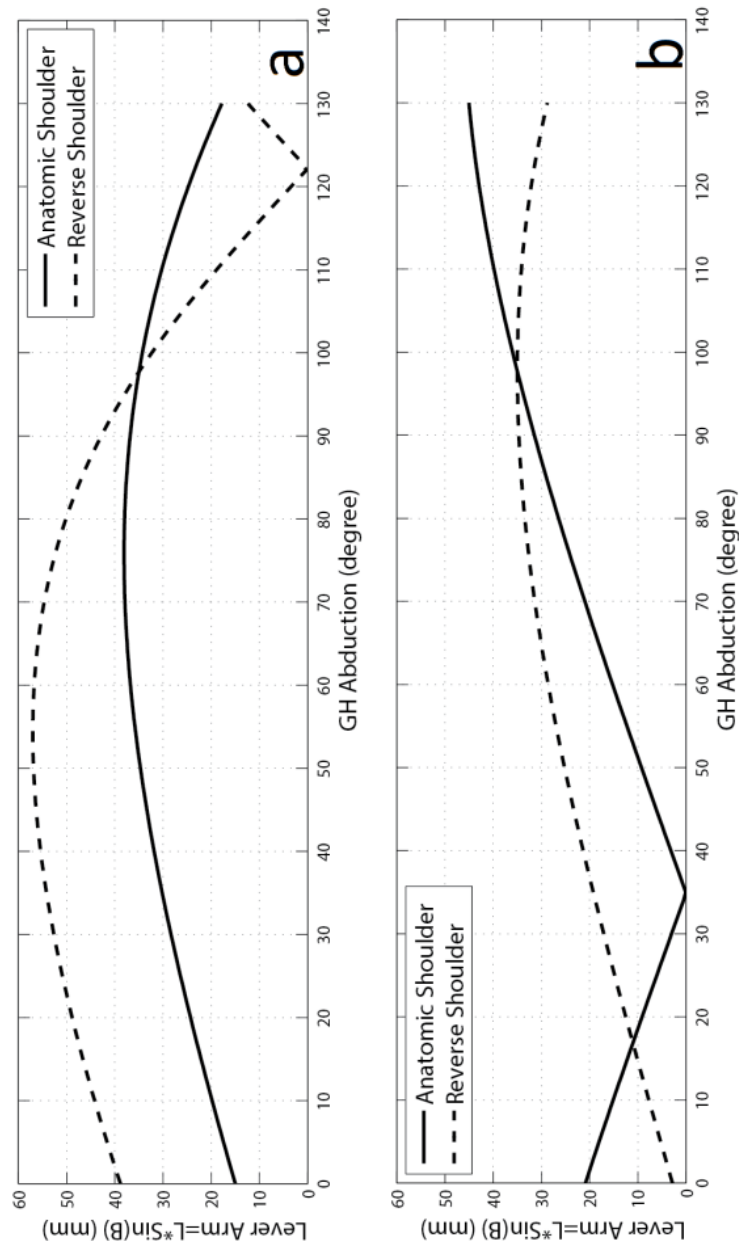
Fig.3-7: deltoid Effective Lever Arm VS Abduction of GH joint (a) middle deltoid   (b) anterior deltoid

For example, looking at Fig.3-7-a, at 10 degrees of GH joint abduction the effective lever arm in anatomic shoulder has a value equal to 20 mm while the prosthetic shoulder has an effective lever arm equal to 45 mm which is more than twice that of the anatomic one of the same patient. However, at 80 degrees of glenohumeral abduction the anatomic shoulder has an effective lever arm equal to 40 mm while at this angle the prosthetic reverse shoulder is 50mm. The results show that the rate of change of the lever arm does not follow a linear trend and this medialization in RS is only advantageous during a limited range of abduction.

Anterior Deltoid: As shown in Fig.3-7-b, in reverse shoulder, Leff of the Anterior Deltoid will increase at the beginning of abduction while its effect decreases in higher abduction. Fig.3-7 clearly shows the effect of the change in Lever arm length and its dependency on the subtended angle (β). In these graphs absolute values of Leff have been demonstrated. The anatomic Leff graph has intersected zero effective lever arm at an approximate angle of 35° of abduction. Regarding absolute value before this angle, Leff has a negative value which means it does not assist the arm to abduct in low abduction whilst reverse shoulder has positive Leff during whole abduction which is useful.

Deltoid pre-tensioning as a solution? The Deltoid length can be defined as the distance between origins of the deltoid on the acromion and its insertion points on the humerus. In reverse shoulder arthroplasty the deltoid is lengthened to increase its efficiency and it must be performed by increasing the distance between the origin of the deltoid on the acromion and its insertion point on the humerus (De Wilde et al. 2002, Saltzman et al. 2010, Jobin et al. 2012, Lädermann et al. 2012).

There are two solutions to increase this length which are:

(1) Increasing **L** (Figure 3-1) (Distance between the centre of rotation and insertion of deltoid on humerus). **L** depends on the position of the socket of the prosthesis on the humerus, diameter of the ball of the prosthesis and the size of the spacers used. Increasing this value will result in middle deltoid working range, a shift to the right on Force-Length graphs as shown in Figure 3-8-a. As can be seen in Figure 3-8-b, increased **L** is not affecting Leff .The same trend is observed for Anterior Deltoid as shown in Figure 3-8-c,d.
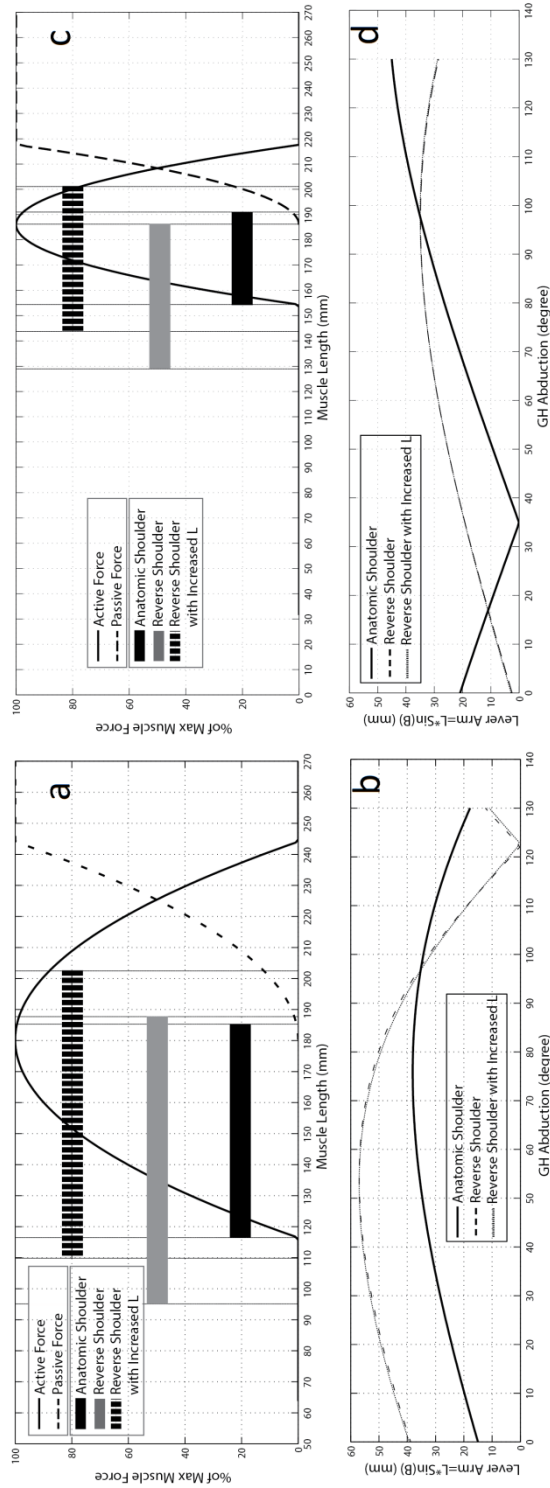
Figure 3-8 (a) %of Max Muscle Force VS Muscle Length in middle deltoid.
Horizontal bars show Muscle Excursion. Black graph reveals passive force in muscle
(b) Effective Lever Arm VS GH Abduction
(c) %of Max Muscle Force VS Muscle Length in anterior deltoid.
Horizontal bars show Muscle Excursion. Black graph reveals passive force in muscle
(d) Effective Lever Arm VS GH Abduction

(2) Increasing **n** (distance between acromion and centre of rotation) (Figure 3-1). This requires placing the ball of the prosthesis more inferiorly on scapula. As shown in Figure 3-9-a, when the COR is moved in the reverse shoulder more inferiorly, initial middle deltoid length will be increased while more excursion of deltoid occurs during abduction with a shift in the working range of deltoid to right in the Force-Length graph. As shown in Figure 3-9-b Leff trend will generally improve still showing a drop in higher abduction. Excessive movement of COR inferiorly can result in over stressing that can result in stress fracture (Schamblin et al. 2009, Boileau et al. 2013). Figure 3-9-a,b shows that deltoid tensioning can optimise deltoid excursion in Force-Length graph with a **developed** effect on the effective lever arm. The same trend is observed for Anterior Deltoid as shown in Figure 3-9-c,d.
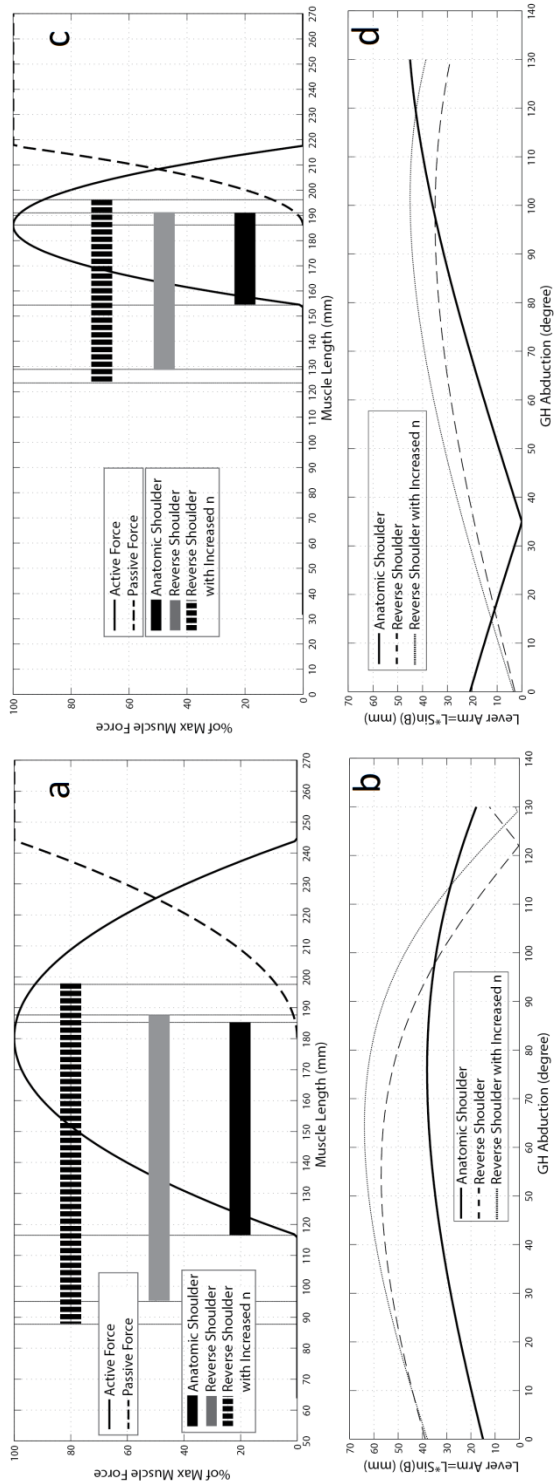
Figure 3-9 (a) %of Max Muscle Force VS Muscle Length in middle deltoid.
Horizontal bars show Muscle Excursion. Black graph reveals passive force in muscle
(b) Effective Lever Arm VS GH Abduction
(c) %of Max Muscle Force VS Muscle Length in anterior deltoid.
Horizontal bars show Muscle Excursion. Black graph reveals passive force in muscle
(d) Effective Lever Arm VS GH Abduction

Deltoid Pre-Tensioning Upper Limit in RSA, passive tension of deltoid is directly linked to the position of COR on the scapula, origin of the deltoid on the acromion and insertion point of the deltoid on the humerus.

As mentioned previously, increasing the tensioning parameters (**n** and **L**) shifts the working range of the deltoid towards the right hand side of the Force-Length graph of the muscle Figure 3-8-a,d and Figure 3-9-a,d. However, as shown in Fig.3-10, the more it is shifted to the right the more passive tension in the deltoid muscle is generated which can result in loosening of the prosthesis and fracture of the acromion due to high load intensity or stress (Schamblin et al. 2009, Boileau et al. 2013).
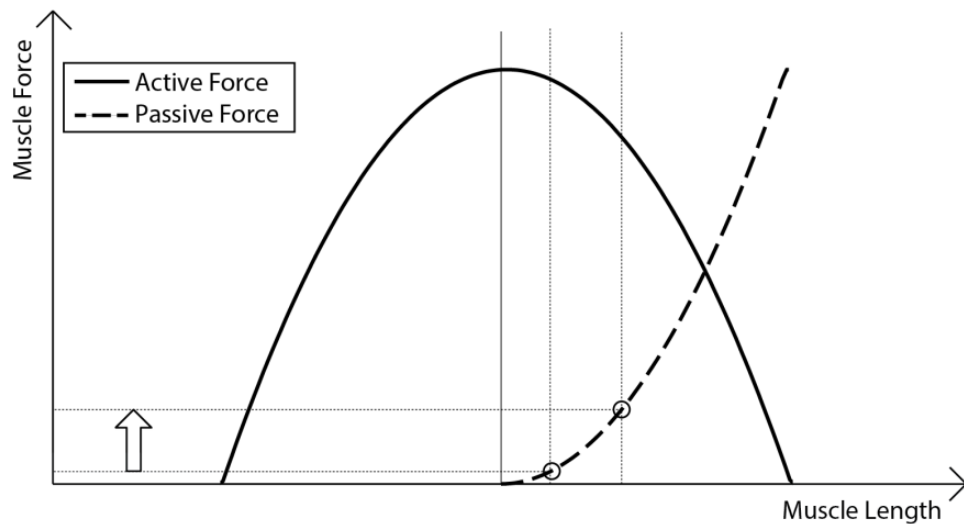
Fig.3-10: Muscle Force VS Muscle Length   the more shift to right side, the more passive force in muscle

Active force is generated in the muscle when needed while passive force is a permanent spring effect of muscle while it is stretched (not contraction).

The results show that RSA improves the effective lever especially if the glenohumeral centre of rotation is moved both medially and inferiorly. It is also shown that because of tension of deltoid muscle its active force will be improved after RSA according to Hill's Muscle model. These two factors (improved effective lever arm and deltoid's active force) directly contribute to improvement of moment intensity of the glenohumeral joint generated by the deltoid. It must be taken into account that excessive deltoid tension could be a cause of scapula fracture. It is also shown that deltoid muscle excursion

increases after RSA which could be a drawback while the deltoid reaches its maximum range of effectiveness.

3.3 Discussion

There are some modelling studies of reverse shoulder in the literature. Based on a cadaveric study, Schwartz *et al* (2013) discusses the importance of anterior deltoid in RSA concluding after RSA surgery the anterior deltoid's moment arm increases. Kontaxis and Johnson 2009 and Terrier, Reist, et al. (2008) studied biomechanics of RSA, based on a modelling study, and also concluded both middle and anterior deltoid moment arms increase after RSA. De Wilde et al. (2002), based on a computerised study, proves that the deltoid muscle force will be improved after RSA. Jobin et al. (2012 investigated the clinical effect of deltoid lengthening and centre of rotation medialisation concluding Deltoid lengthening improves active forward elevation after RSA for cuff tear arthropathy.

The results from this study are in agreement with previous literature. In addition, the results provide new information regarding details of improvement of deltoid moment arm, deltoid excessive excursion after RSA and deltoid lengthening effect of increasing the deltoid's force. This study demonstrated that all of the geometrical parameters, both in normal shoulder and reverse shoulder either individually or in combination can play an important role on the outcome of the surgery for each individual (Frankle et al. 2009, Saltzman et al. 2010, Hoenecke et al. 2012).

A mathematical and 3D model of the anatomical shoulder and RSA were developed using data from X-Ray and MRI images of previous studies. Different geometrical parameters were defined in each model (anatomic and RS) and the effect of small changes in each one (in isolation) on the overall kinematics and kinetics of the shoulder was investigated.

These parameters identify the centre of rotation of glenohumeral joint and the force vector of the deltoid knowing the origin of the deltoid on the scapula and its insertion point on the humerus both for the anatomic and RSA shoulder.

The behaviours of the deltoid muscle was simulated and investigated during glenohumeral joint full abduction both before and after RSA. The factors considered for comparison of the functional outcome are classified as: 1) Deltoid Excursion, 2) Effective Lever Arm, 3) Deltoid Tensioning and 4) Deltoid Tensioning Upper Limit. Also, the differences these geometrical parameters made on the outcome of the simulation were discussed.

Using the simulation, it was also possible to show the importance of the initial geometrical differences in individuals and how it can inform the placement of the implants. It also enables users to visualise the effect of lever arm beyond the range of motion possible by the deltoid contraction. This will have an effect on design of new implants glenoid to better control the lever arm length during abduction.

Using an image database of individuals' pre and post operatively, calculating the discussed kinematics parameters for each and correlating them with the outcome of surgery in long term, could inform surgeons intraoperatively about optimised placement of prosthesis to provide the maximum possible range of motion and least amount of pain.

It should be highlighted, that these models only consider geometry and kinematics of the glenohumeral joint while there are many other patient characteristics such as muscle fibre type, muscle volume and bones shape which have not been taken into account in this study. Therefore, the prediction of subjective outcomes (pain relief and range of motion) needs more studies including mathematical and clinical approaches together.

Reverse Shoulder Arthroplasty (RSA), in which anatomic concavities of glenohumeral joint are inverted, is a popular treatment of arthritic shoulders with deficient rotator cuff. The correct positioning of the glenohumeral centre of rotation and initial setting of the deltoid length (Deltoid Tension) plays an important role in the outcome of the reverse shoulder arthroplasty. A study of the key literature has shown that despite common use of RSA, its biomechanical characteristics during motion are not fully understood. This study investigates the influence of some of the key parameters (geometry, kinematics and muscle passive force measurement) on the intensity of the moment in a shoulder after RSA.

According to literature review some aspects of RSA are not fully investigated. We divided these factors into three categories:

- Geometries both on native and reverse shoulder which are function of normal anatomy and implant selection and positioning after RSA.
- Kinematics which are function of anatomical and prosthetic initial geometries and their variation in arm motion.
- Muscle passive force measurement which can be measured as resultant force acting on glenosphere.

An adjustable 3D musculoskeletal model (MSC ADAMS) of the anatomical and RSA are developed using data from X-Ray and MRI images coming from previous studies (Werner et al. 2008, Frankle et al. 2009, Kircher et al. 2010, Saltzman et al. 2010, Lädermann et al. 2012, Gu and Yu 2013). Some parameters are defined in models identifying the Centre of rotation of glenohumeral joint and the force vector of the deltoid knowing origin of the deltoid on the scapula and its insertion point on the humerus both for the anatomic and RS shoulder.

The behaviours of the deltoid muscle is simulated and investigated during glenohumeral joint full abduction both before and after RSA. The factors considered for comparison of the functional outcome are classified as: 1) Deltoid Excursion, 2) Rate of deltoid contraction 3) Effective Lever Arm, 4) Deltoid Tensioning and 5) Deltoid Tensioning Upper Limit. Also, the differences these geometrical parameters made on the outcome of the simulation were discussed. This simulation study helps us to detect and investigate biomechanical factors involved in reverse shoulders. This information is needed to develop a tool for X-ray processing of patients pre and post operatively discussed in Chapter 4.

Chapter 4 X-Rays assessment tool

4.1 Introduction

In this chapter some key geometrical parameters (discussed in Chapter 3) are extracted from standard X-rays of individuals pre and post-operatively in the neutral arm position. These X-rays are currently being taken as part of patient's treatment. Kinematics of the Glenohumeral joint across the whole range of arm abduction is calculated and simulated based on measured initial geometries and defined kinematics equations using a graphical user interface (GUI) developed in MATLAB (Mathworks, USA).

The kinematics equations relate all independent geometrical parameters to deltoid performance across the whole range of abduction and data can be documented in a database which in the long term can be used to inform surgeons about best implant selection and positioning according to individuals shoulder morphology and dimensions.

4.2 Subjects

Ten patients (six women and four men) undergoing RSA at Royal Bournemouth Hospital, Bournemouth, UK were included in this study, with a mean age of 74.6 years (SD 5.8 years) and a mean body mass index (BMI) of 29.7 (SD 6.9). The Rotator cuff tear arthropathy was the main reason for the surgery in all of the participant's shoulders. All shoulders received the same Delta Xtend (DePuy, Warsaw, IN, USA) prosthesis (Saltzman et al. 2010).

The X-ray images of the shoulder were taken both pre and post-operatively in the true anteroposterior (Grashey) plane and in the plane of the scapula. Having all images in the Grashey view helps to prevent overlap of the Humeral head and Glenoid fossa (Koh et al. 2013). Of all 10 volunteers 4 were incomplete and it did not fully comply with the inclusion criteria and for that reason the X-ray images were excluded from the study.

4.3 Ethical considerations

The protection of the rights, dignity, health, safety, well-being and privacy of the participants was paramount in this study. UK National Health Service (NHS) ethical approval was obtained by the collaborating consultants before the start of this study (Appendix A.II). A NHS-approved informed consent document for human subjects was

read and signed by all patients before participation in the study to allow anonymised X-ray of their shoulders to be used in this study (Appendix A.III).

4.4 Imaging inclusion exclusion criteria

The scapular plane has a 30° to 45° angular offset from the Coronal plane. To provide the Grashey view while imaging, subjects are asked to rotate posteriorly by 30 to 45 degrees, such that the Scapula plane is parallel to the imaging plate (Forte et al. 2009, Koh et al. 2013). Although all of the images are taken in the same plane (Grashey view) following the same protocol, it is difficult to prevent overlap of the Humeral head and Glenoid fossa in healthy shoulders, and the Glenosphere and Humerus stem in reverse shoulders, due to variations in the Scapula orientation (15 degrees) between individuals. If the subject is correctly oriented to the imaging plate, the hemispherical Glenosphere should be seen as a semicircle in 2D images. In most cases, however, this does not happen (Figure 4-1). In this study, the amount of angular offset from the Scapular plane is determined from the calibrated 2D images by Equation 1.

$$\text{Sin}(\delta) = \frac{\emptyset_p}{\emptyset_a} \qquad \text{(eq. 1)}$$

Where δ is the rotation offset from the actual Grashey view, $\emptyset_p$ is the projected diameter of the Glenosphere in the nominal Grashey view, and $\emptyset_a$ is the actual diameter of the Glenosphere.

A rotation offset of $15°$ is equivalent to a 3.5% error in the medial direction (as $\text{Cos}(15)$ = 0.965). If the rotation offset from the Grashey view is more than $15°$, the image is not included in the measurements.
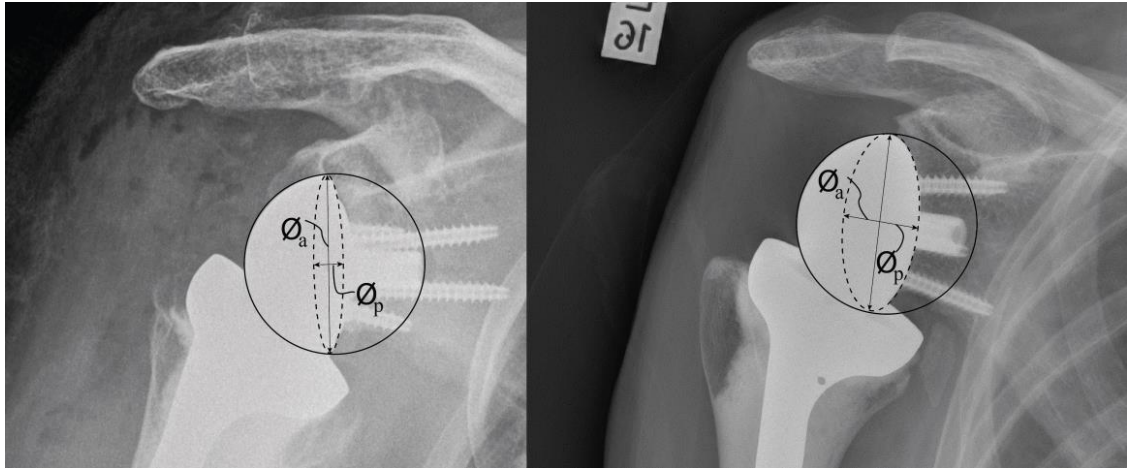
Figure 4-1: rotation offset calculations for two patients from the same view   left: accepted image   right: eliminated image

4.5 X-ray processing

The initial protocol required a careful positioning and placement of a 26mm diameter steel disc in the same plane as the patient's coronal plane (in line with the shoulder) for calibration. The X-ray images are imported to the GUI in Joint Photographic Experts Group (JPEG) format. The developed GUI (Figure 4-2) utilising MATLAB (the code can be found in Appendix A.IV) is used to calibrate all the dimensions using the image magnification factor measured by selecting two ends of the disc in the image (Jobin et al. 2012). The COR of the Glenohumeral joint is assumed to be the centre of the native Humeral head in the intact (Native) shoulder. The centre of the Glenosphere in the reverse shoulder is assumed to be the COR which can be estimated by measuring and curve fitting the best-fit circles drawn about the predicted centre. A wider field of view of the shoulder must be taken to enable detection of the deltoid insertion point on the Humerus.

The deltoid muscle is considered as a component with adjustable length acting as a linear actuator, linking its origin and insertion (Favre et al. 2009, Kontaxis and Johnson 2009). The deltoid fibre originates from the Infero-lateral Acromion tip all the way to the middle of Humeral shaft. There it is inserted into the midpoint of the deltoid tuberosity in the middle of the Humeral shaft (Sakoma et al. 2011, Jobin et al. 2012). Curvature of deltoid tuberosity is differentiated visually and a curve is fitted to it. The middle of the curve is the chosen as deltoid insertion on the humerus. While the patient's arm is at neutral position (De Wilde et al. 2002, Jobin et al. 2012), the distance between these two points dictates the initial Deltoid length. Figure 4-2, shows the free

body diagram representing the biomechanical model of the shoulder superimposed on the X-ray. It consists of the Deltoid muscle, Humerus and Glenohumeral joint.

The Glenohumeral joint has three full rotational degrees of freedom plus a small amount of translation displacement along all three orthogonal axes. In this study translational movement of the Humerus head is neglected and COR of Glenohumeral joint is fixed to the centre of the Glenohumeral head in the anatomic shoulder while in RSA geometries the Glenohumeral joint is totally reversed and moved, hence COR is fixed on the Scapula and is treated as the new centre of the Glenoid (Terrier, Vogel, et al. 2008, Saltzman et al. 2010, Naveed et al. 2011).
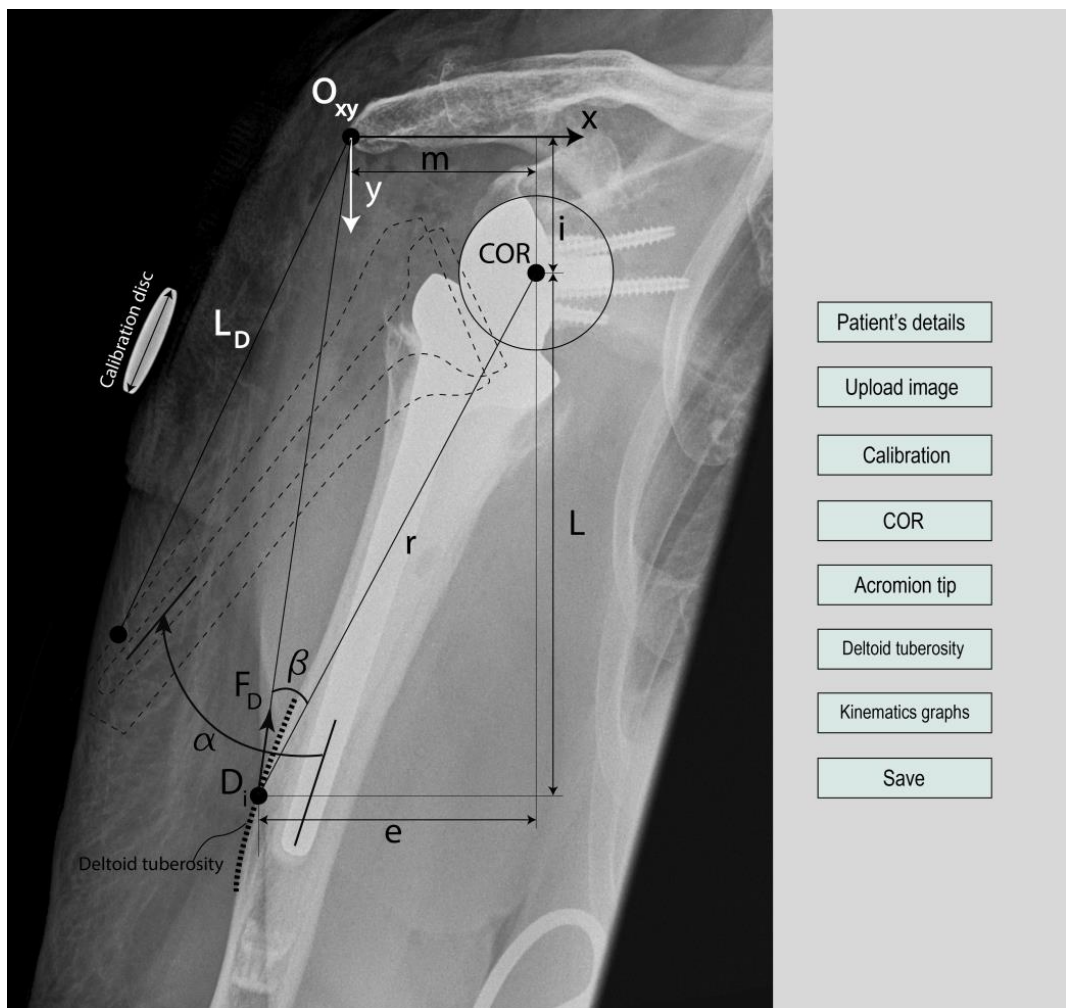
Figure 4-2 : Developed X-ray processing GUI - geometrical parameters affecting kinematics and dynamics of deltoid in glenohumeral joint abduction

The tip of the Acromion (origin of Deltoid) is chosen as the origin of an orthogonal 2D coordinate system (**Oxy**) with medially oriented **x** axis and is inferiorly parallel to the bodies longitudinal axes oriented **y** axis.

As mentioned previously, standard X-Rays are provided in the Anteroposterior (Grashey) view and all the geometrical parameters are defined in the Scapular 2D plane. Hence in this study kinematics of the deltoid are investigated for abduction in the Scapular plane. All the dimensions are measured and calibrated by a calibration factor in x and y directions.

4.6 Definition of Deltoid excursion

In the developed biomechanical model of the shoulder, the Humerus is considered as a mechanical lever arm (**r**) connecting the COR to **Di** having a rotational degree of freedom around the COR and the Deltoid acts as a linear actuator connecting **Oxy** to **Di** while providing force (**FD**) on the mechanical lever arm (**r**). The mechanical system is described in a 2D coordinate with origin of **Oxy**.

To calculate Deltoid excursion during abduction in the scapular plane, it is assumed that the Glenohumeral joint has one rotational degree of freedom while its translation is neglected (Terrier et al. 2010). The length of the Deltoid at any given abduction angle is addressed as deltoid excursion and calculated using Equations 2 and 3

$$L_{deltoid} =$$

$$\sqrt{[m - L_0 * sin(a + \tan^{-1}(e/L))]^2 + [i + L_0 * cos(a + \tan^{-1}(e/L))]^2} \text{ (eq. 2)}$$

$$L_0 = \sqrt{L^2 + e^2} \qquad \text{(eq. 3)}$$

Where; m = horizontal (medial) distance between COR and tip of Acromion; i = vertical (inferior) distance between COR and tip of Acromion; L_0 = Initial Deltoid length at neutral arm position; L = vertical distance between COR and Deltoid insertion on Humerus; e = horizontal distance between COR and Deltoid insertion on Humerus; θ = angle of abduction in Scapular plan.

4.7 Definition of moment arm

Based on the calibrated Xray obtained using our proposed protocol, described above, a model for determining the moment arm was proposed, developed and is presented here. It can be used to calculate or determine the generated moment in the Glenohumeral joint needed to abduct the arm (Equation 4).

$$M_D = F_D * r * \sin(\beta) \text{ and } \beta = a + \tan^{-1}(e/L) - \tan^{-1}\left(\frac{L_0 * \sin(a + \tan^{-1}(e/L)) - m}{L_0 * \cos(a + \tan^{-1}(e/L)) + i}\right)$$

(eq. 4)

Where; F_D = Force vector generated by Deltoid; r = Vector between COR and Deltoid insertion (Lever arm); β = angle between Deltoid force vector and lever arm.

During full arm abduction both the Glenohumeral and Scapulothoracic joint articulate together while two third of the motion (90° to 120°) covered at the Glenohumeral joint and one third at Scapulothoracic joint, known as Scapulohumeral rhythm (Ludewig et al. 2010, Matsuki et al. 2012). The deltoid is the main actuator in Glenohumeral joint articulation, meaning 90° to 120° of arm motion is dependent on the Deltoid. As wrapping of the Deltoid around the Humerus head takes place in a limited range of low abduction its effect on Deltoid excursion and lever arm is neglected (Johnson et al. 1996, Klepps et al. 2004, Berthonnaud et al. 2010, Moser et al. 2013).

4.8 Results

After Delta Xtend replacement, postoperative radiographs showed that the COR was displaced by 6 mm (SD 4 mm) inferiorly and 25 mm (SD 6 mm) medially relative to the fixed origin of the coordinate system proposed here. Also the Deltoid length was increased initially by 25 mm (SD 7 mm) due to increased Acromiohumeral distance postoperatively causing an additional 17% Deltoid initial elongation. The X-rays results based on the 6 patient's X-ray measurements are summarised in Table 4-1. Summary of 6 patient's X-ray measurements

Medialisation of the COR is addressed as the main advantage of RSA compared to TSA (Total Shoulder Arthroplasty) due to an increase of the Deltoid moment arm. While inferior displacement of the COR associated with Deltoid lengthening leads to a better Deltoid performance after RSA (Kontaxis and Johnson 2009, Jobin et al. 2012)

Radiographic measurements			
	Native Shoulder	Reverse Shoulder	Change
Measurements	Mean (SD)	Mean (SD)	Mean (SD)
Deltoid initial length (mm)	137 (13)	162 (12)	25 (7)
Medial distance (mm)	11 (4)	25 (6)	13 (7)
Inferior distance (mm)	28 (2)	34 (5)	6 (4)

Table 4-1. Summary of 6 patient's X-ray measurements

Based on geometrical parameters, Deltoid excursion was plotted against Glenohumeral joint abduction angle using Equation 2 both for native (pre-op) and reverse shoulders

(post-op). As shown in Figure 4-3, Deltoid contraction in native shoulders showed a constant slope for the whole range of abduction while in the reverse shoulder, from the neutral arm position until almost 90° of abduction, the deltoid contracts with a flatter gradient. At higher abduction, the Deltoid length remains constant meaning the muscle is reluctant to contract anymore.
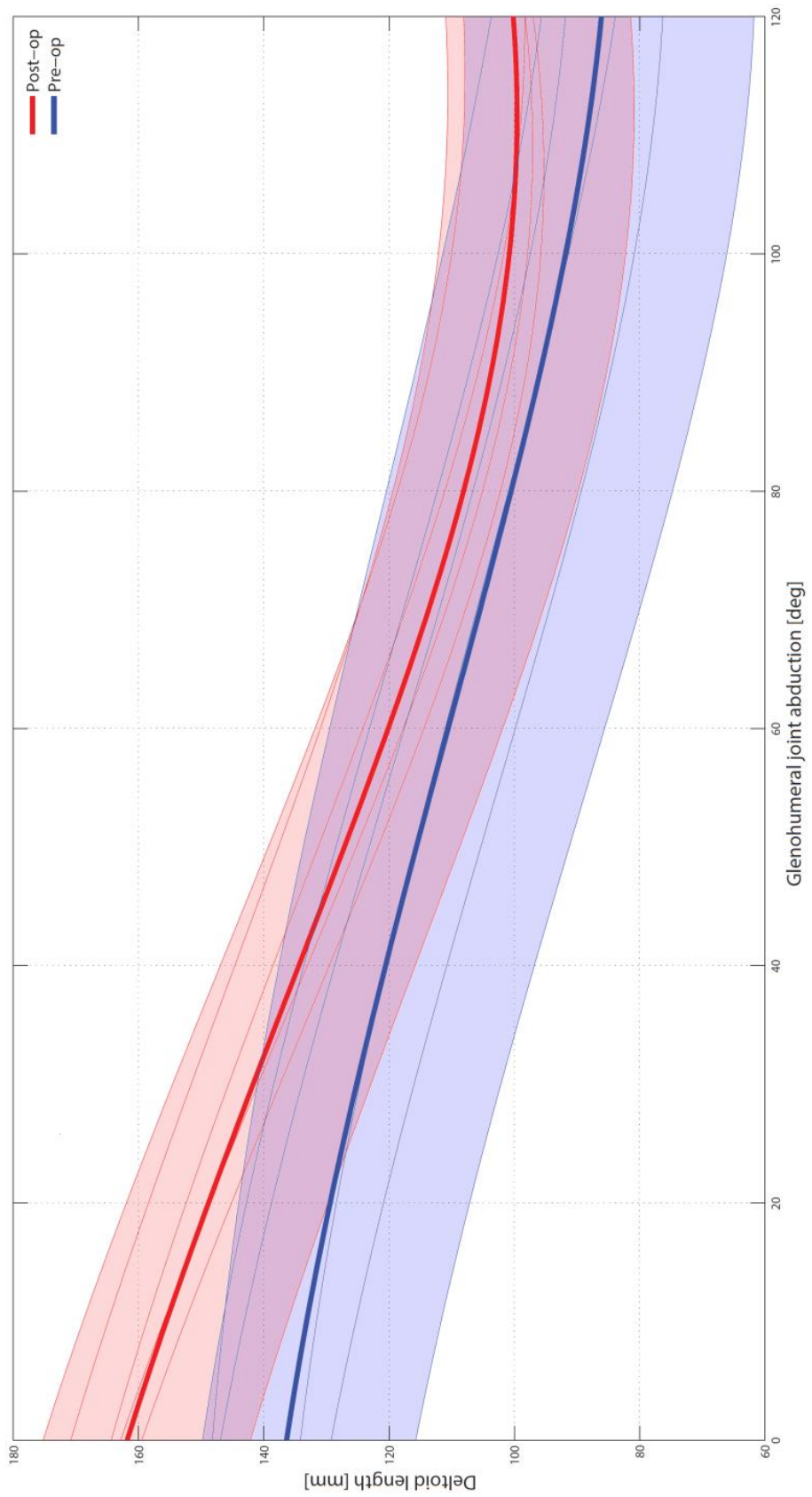
Figure 4-3: deltoid excursion versus Glenohumeral abduction.
Solid bold lines: average of all patients. Transparent ones: ±SD

Mechanical work generated in the Deltoid to abduct the arm is defined in Equation 5.

$$W = F \times d \qquad\qquad\qquad\qquad\qquad\qquad\qquad (eq.5)$$

Where **F** is muscle force and **d** is muscle excursion. Observed quasi-zero Deltoid excursion in higher abduction in the reverse shoulder is equivalent to zero displacement of the muscle in Equation 5 where no mechanical work is generated by the Deltoid and the mechanism locks.

Medialisation of the COR in reverse shoulders increased the initial lever arm of the Deltoid at the neutral arm position by 206%. However, the effect of improved lever arm in reverse shoulder is more dominant in lower abduction. In higher abductions (approximately 60°) a sudden drop in reverse shoulder lever arm is observed. At approximately 110° of Glenohumeral abduction the Deltoid has no lever arm and no further abduction can occur.
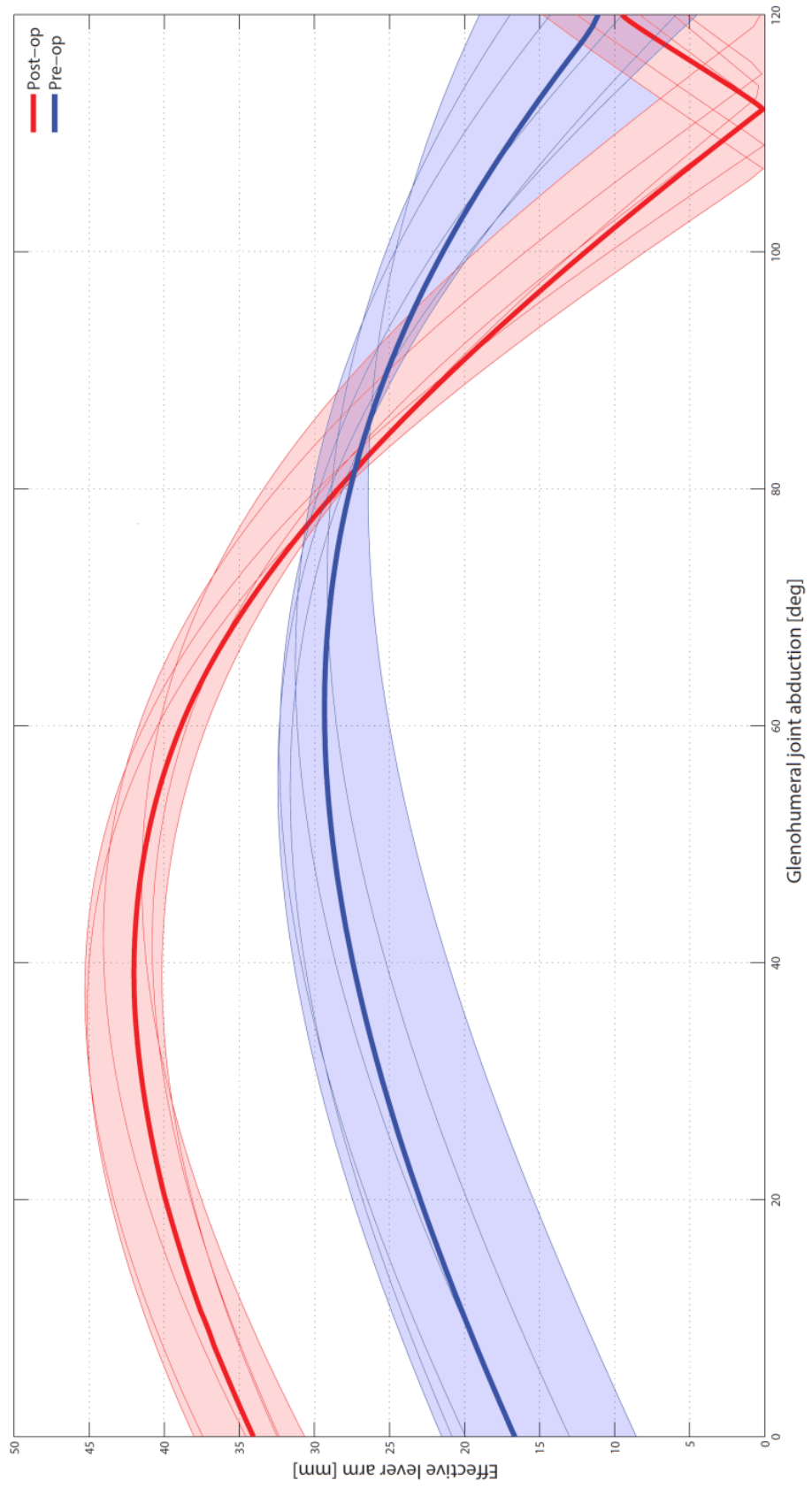
Figure 4-4: Deltoid effective lever arm versus Glenohumeral abduction.
Solid bold lines: average of all patients. Transparent ones: ±SD

4.9 Discussion

Correct implant selection and positioning into bones play an important role in the outcome of surgery. To find the optimum implant size and right positioning for individuals, the effect of geometrical parameters on the kinematics of the shoulder pre and postoperatively needs to be investigated and better understood. The considered geometrical parameters directly affect the modified lever arm, Deltoid performance and its excursion.

Although there are some imaging and documentation protocols addressed in the literature (Saltzman et al. 2010, Lädermann et al. 2012) the effect of anatomical and prosthetic geometrical parameters on Deltoid performance have not been well understood. In this study it is proposed that uniform and standardised X-ray images need to be obtained and analysed using a GUI developed here for detailed analysis in order to better understand the link between mechanical advantage and geometrical parameters.

A mathematical model of the shoulder joint was developed (Figure 4-2) that uses extracted geometrical data to calculate and simulate the differences in kinematics and mechanical advantages before and after RSA. The geometrical parameters can then be inserted into kinematics equations to calculate muscle excursion and moment lever arm for a whole range of arm abduction.

Initial COR medialisation and Deltoid lengthening is observed in all patients. Based on the measured parameters, Deltoid excursion and moment lever arm in the Glenohumeral are plotted for the whole range of abduction. Increased moment intensity due to COR medialisation in RSA is in agreement with literature although it does not show a constant trend and drops at higher abduction angles. Deltoid lengthening in literature is addressed as initial increase of the Deltoid length in the neutral arm position while Deltoid excursion in reverse shoulders is not well studied. This study shows the Deltoid excurses more in the reverse shoulder than the native shoulder.

Initial Deltoid lengthening increases its performance due to a shift of the muscle working range to the right in Hill-type graphs (Figure 4-5) (Thelen 2003). According to the Hill-type muscle model, each muscle is able to provide both passive and active forces according to its length while maximum available active force can be generated at initial muscle length. Available active force decreases as the muscle excurses

(contracts) more and more. Arm lengthening in reverse shoulder causes initial shift of muscle stroke to the right in Hill model where bigger passive tension exists in the muscle. While COR medialisation leads to more muscle excursion in the reverse shoulder compared to the native shoulder for the same amount of abduction. Deltoid lengthening associated with medialisation of the COR causes flat gradient of muscle excursion in higher abductions where no mechanical work can be generated. Excessive muscle excursion may also damage axillary nerves (Grant et al. 1999).
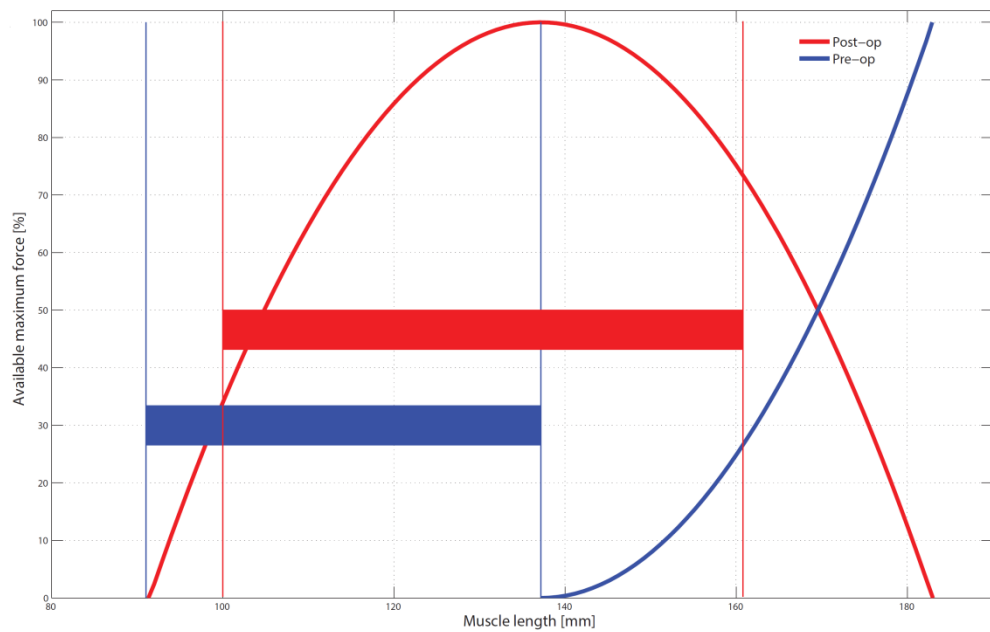
Figure 4-5: Available active and passive force in deltoid VS muscle length

Solid lines: average of all patients.

Horizontal bars indicate deltoid excursion in full arm abduction Blue: native shoulder, Red: Reverse shoulder

In the long term, an imaging database can be created/developed that includes geometrical and kinematic parameters and their correlation to the outcome of surgery. This database would allow for a more objective assessment of the joint mechanical advantage than the subjective process currently employed. By getting it right first time the number of revision surgeries due to mechanical failure required would be reduced due to better joint force balance and equilibrium. This database should reduce cost due to reduction in the number of revision surgeries, improve and optimise both the range of motion and the mechanical advantage resulting in a better and more deterministic surgical outcome.

4.10 Conclusion

RSA changes geometries and kinematics of the Glenohumeral joint to improve clinical outcome as well as pain relief. However, improved range of motion varies among individuals and currently there is no tool to predict optimum prosthesis size and placement into bones with regard to individual's anatomic morphology.

Despite anatomical differences between individuals' shoulders in terms of size, joints, bone morphology and muscle quality, a healthy shoulder is expected to provide a defined range and amount of manoeuvrability. Anatomic geometries of the shoulder are changed after RSA leading to a new mechanical system with new joint kinematics. To be able to restore the same amount and range of manoeuvrability and functionality as a healthy shoulder after RSA, performance of the Deltoid is crucial. This study defines two key kinematics parameters (Deltoid excursion and Deltoid effective lever arm) that can be calculated from standard X-rays of the shoulder to investigate performance of the Deltoid on the shoulder joint pre and post-operatively.

Currently there is no assessment tool to quantify key geometrical parameters and their influence on kinematics of the shoulder in RSA. A dedicated and user-friendly GUI (developed by the author using MATLAB), has enabled the standard shoulder X-rays of individuals to be used to extract key geometrical data of the shoulder, pre and post-operatively, to simulate, monitor and compare kinematics of the Deltoid. The kinematic equations/theories presented here relate all independent geometrical parameters to the Deltoid performance throughout the whole range of abduction. The GUI also stores this data in a database which in the long term which could be used to inform surgeons about the ideal joint contact force or ideal deltoid load intensity or tension to determine the optimal position and orientation of the implant.

Kinematics of six shoulders during abduction were investigated using standard pre and post-operative X-rays and results are discussed. It must be noted that this study uses a standard X-ray of the shoulder taken in anteroposterior following the same protocol for all the patients. More geometrical parameters can be extracted from other radiographic views to investigate different deltoid sections in different motion scenarios.

Small differences in anatomic and prosthetic geometrical parameters in individuals can have a large influence on the outcome. Under these circumstances and in the absence of quantitative data (sub optimal) even the most experienced surgeon must rely on

personal judgment or the most advanced prosthesis will not last or reach the anticipated or the expected life. Implant placements based on better informed and quantified data will assist surgeons to achieve the best possible results first time.

The aim is such information, in the long term will give the surgeon a means to interpolate what would be the ideal implant size and positioning on an individual's bones in order to get it right first time by creating shoulders that are not overloaded, have a good range of motion and will last the life of the user without the need for any revision surgery.

Chapter 5   Shoulder assessment

5.1 Introduction

As discussed in Chapter 1 one of the objectives of research is proposing a method to quantify shoulder motion and activity.

The shoulder and more specifically the glenohumeral joint provides the largest range of motion in human body. A healthy shoulder is expected to provide a certain amount of pain-free motion and strength. Shoulder disorders are the third most common location for a musculoskeletal problem, after knees and hips (Kolber et al. 2013). Most common shoulder disorders can be divided into soft tissue disorders, articular injury or instability, and arthritis causing pain and motion loss leading to difficulties in performing daily activities (Dinnes et al. 2003, McClure and Michener 2014, Do Moon et al. 2015).

The deltoid muscle plays an important role as the main shoulder abductor and glenohumeral joint stabilizer. It consists of three separate sections, known as the anterior deltoid, middle deltoid and posterior deltoid (Figure 5-1). The anterior deltoid originates from the anterior surface of the distal clavicle and the anterior edge of the acromion, the middle deltoid starts from the superior surface of the acromion and the posterior deltoid originates from the posterior scapular spine head and all three sections are inserted into the deltoid tuberosity on the lateral section humerus (Klepps et al. 2004, Moser et al. 2013, Schwartz et al. 2013).

Recently, low-cost wearable inertial measurement unit (IMU) sensors have overcome many of the limitations of traditional motion tracking systems (Jung et al. 2010, Djurić-Jovičić et al. 2011, Palermo et al. 2014). These sensors include 3 axis accelerometers (measuring linear acceleration), 3 axis gyroscopes (measuring angular velocity) and a 3 axis magnetometer (measuring magnetic north to compensate for orientation drift). These sensors in combination lead to a more accurate dynamic orientation calculation. A number of IMU can be attached to different body segments to track their motion individually in real time and 3D space.

Shoulder performance can be assessed objectively using different criteria such as the shoulder range of motion, electromyography (EMG) at the shoulder muscles and by using questionnaires completed by patients (Kolber et al. 2013).

In this study, an IMU sensor combined with an EMG sensor is used to measure the maximum reachable envelope of motion in 3D space with simultaneous collection of deltoid activity. Such a tool can be used to quantify and compare performance of shoulder pre and post operatively. However in this study, performance of the developed tool is tested on healthy and frozen shoulder and not patients undergoing RSA as ethical approval process will exceed deadline of this research.

Figure 5-1: Deltoid sections and surface electrode placement E0: ground; E1/E2: anterior deltoid; E3/E4: middle deltoid; E5/E6: posterior deltoid

5.2 Range of Motion Assessment

Orientation of objects in 3D space can be described using different forms such as 3 Euler angles, 4 element quaternion vector or a 3*3 rotation matrix. Euler angles suffer from a singularity error known as "gimbal lock". Gimbal lock is loss of one degree of freedom in 3D space which causes loss of track of orientation in higher angles for a short period of time, while both quaternion and rotation matrix techniques do not have any discontinuity across the range of possible 3D orientations (Palermo et al. 2014, Valenti et al. 2015).

The assessment tool consists of an IMU sensor (BNO055 intelligent 9-axis absolute orientation sensor) (Appendix A.V), an EMG sensor (MyoWare Muscle Sensor) (Appendix A.VI), a microcontroller (ATmega328) and a Bluetooth module (HC-05) (Appendix A.VII). The sampled quaternion (calculated using a 32-bit microcontroller running the proprietary BSX3.0 FusionLib software) and EMG signals are transmitted to the microcontroller. The microcontroller processes the received sensor data and

transmits them to a personal computer through a Bluetooth module at 100 Hz (Figure 5-2) (Appendix A.VIII). Software developed in MATLAB (Appendix A.IX) is used to analyse the data in real time and the analysed data is visualized as an animated figure moving its arm. In this way the performance of the sensor on individuals can be visually inspected during each test. Then the recorded data is processed and results are presented in graphs.
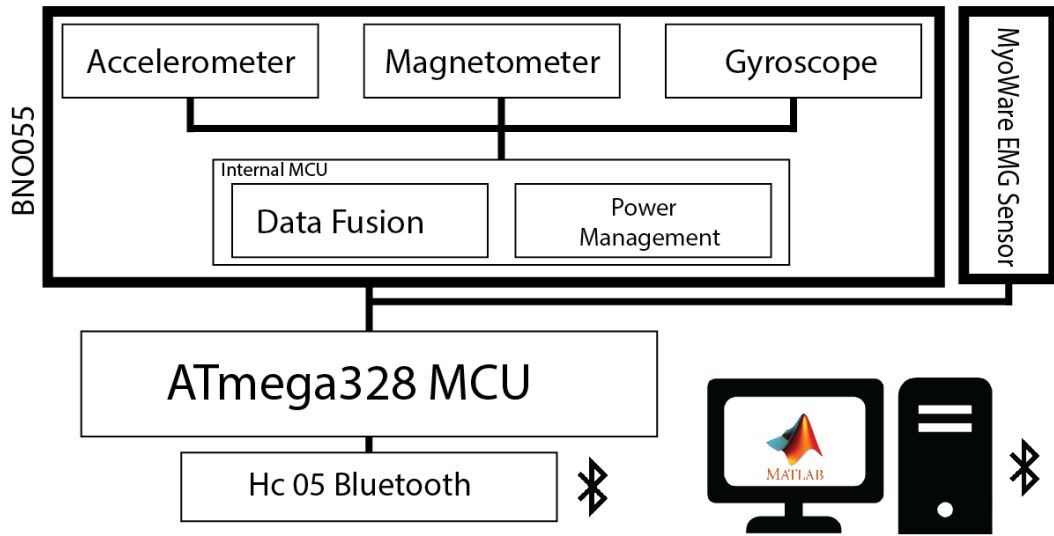
Figure 5-2: Schematic of sensor

The device weighs 230 grams and it is attached to the subject's arm with an adjustable band in such a way as not to impede movement and so that the subject feels comfortable during the required tests.

5.2.1 Processing data

A Quaternion (q) is a vector with one real element and three complex elements. Any arbitrary orientation of an object in 3D space can be represented by unit quaternion as defined below:

$$q = qw + i\, qx + j\, qy + k\, qz \quad \text{(eq.1)}$$

where qw, qx, qy, qz are quaternion elements. All four quaternion elements are calculated by the microcontroller embedded in BNO055 to be analysed in MATLAB. The quaternion representation can be transformed into a unique rotation matrix using the equation below:

$$R =$$

$$\begin{bmatrix} qw^2 + qx^2 - qy^2 - qz^2 & 2*qx*qy - 2*qw*qz & 2*qx*qz + 2*qw*qy \\ 2*qx*qy + 2*qw*qz & qw^2 - qx^2 + qy^2 - qz^2 & 2*qy*qz - 2*qw*qx \\ 2*qx*qz - 2*qw*qy & 2*qy*qz + 2*qw*qx & qw^2 - qx^2 - qy^2 + qz^2 \end{bmatrix}$$

(eq.2)

The rotation matrix of the arm in a neutral position ($[R_0]$) is considered as a reference. The rotation matrix of any arbitrary arm orientation relative to this reference is as follows:

$$[R] = [R_0]^{-1} * [R] \quad \text{(eq.3)}$$

In this study we are aiming to define arm motion using spherical coordinate parameters (azimuthal angle and elevation angle). Spherical coordinates helped to avoid Codman's paradox (Pearl et al. 1992, Wolf et al. 2009) by ignoring the axial rotation of arm around the long humerus axis (Figure 5-3).

To do so first we need to define a Cartesian coordinate system using the rotation matrix and then convert it into spherical coordinates.
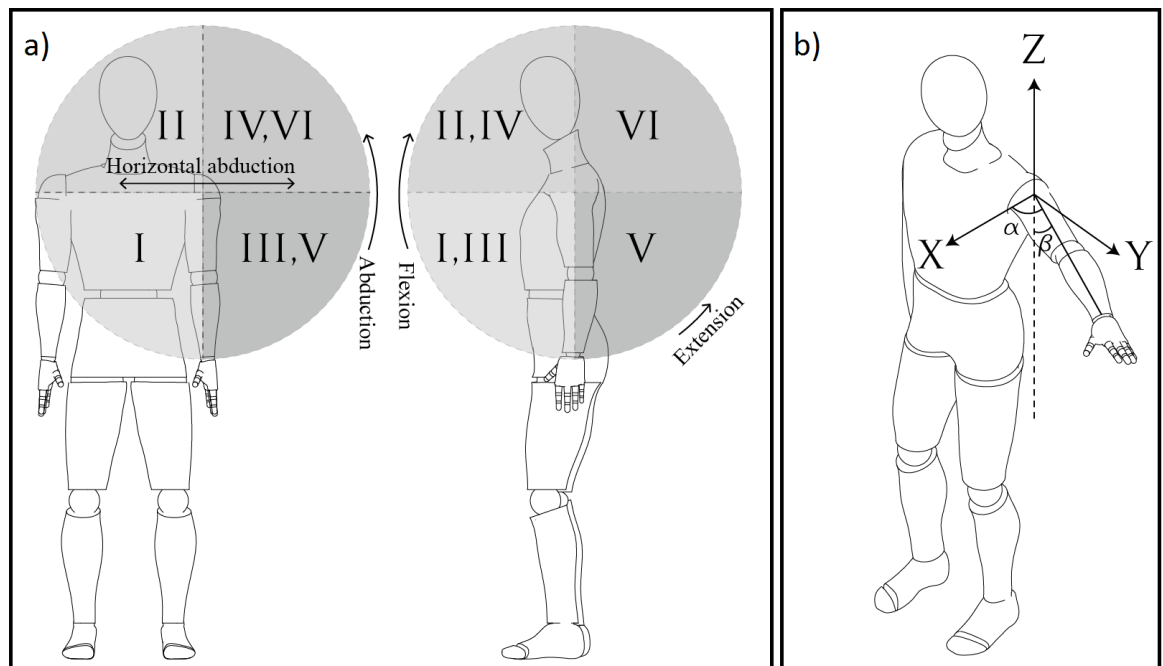
Figure 5-3a: ROM regions   2b: Arm spherical coordinates where α represents azimuthal angle and β is the elevation angle

The origin of the Cartesian coordinate system ($[x_o, y_o, z_o]$) is defined at the shoulder joint when the arm is in its neutral position and coordinate of an arbitrary point on the arm having distance of **r** from the origin is defined as $[X_n, Y_n, Z_n]$. While the arm moves in 3D space, the new coordinate of this arbitrary point is calculated using:

$$[X_n, Y_n, Z_n] = [R] * [x_o, y_o, z_o] \qquad (eq.4)$$

Region	Shoulder motion
I	Higher medial elevation
II	Higher lateral elevation
III	Higher posterior elevation
IV	Lower medial elevation
V	Lower lateral elevation
VI	Lower posterior elevation

Table 5-1: ROM regions in spherical coordinate

In this study rotation around the z axis (azimuthal angle) of human body is considered as horizontal abduction and rotation around x axis (elevation angle) as abduction. Hence the Cartesian coordinate of moving arm can be transformed to the spherical coordinates using the equation below:

$$r = \sqrt{x_n^2 + y_n^2 + z_n^2} \qquad (eq.5)$$

$$\beta = \cos^{-1}\left(\frac{z_n}{r}\right) \qquad (eq.6)$$

$$\alpha = \tan^{-1}\left(\frac{y_n}{x_n}\right) \qquad (eq.7)$$

ROM regions in spherical coordinate are shown in Table 5-1.

5.2.2 IMU performance

A gimbal test stand was built (Appendix A.X) to quantify IMU sensor performance and compare its calculations against known angle rotations (Appendix A.XI). The gimbal is able to provide full pitch and yaw motion using a pair of servomotors (HS-7950TH - Hitec Rcd USA, Inc) (Appendix A.XII). The IMU sensor is placed on the gimbal test stand and initial orientation recorded as the arm orientation in rest condition (Figure 5-4).
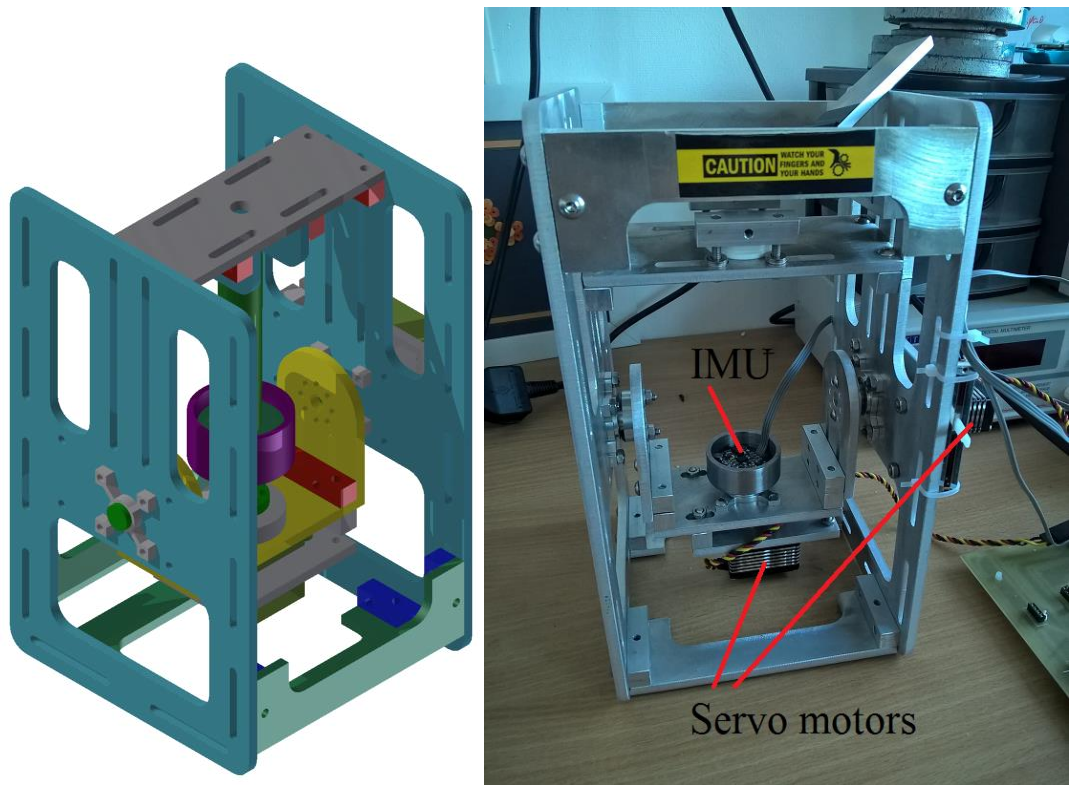
Figure 5-4: Left: Technical drawing; Right: Gimbal test rig setup

To evaluate accuracy and repeatability of the IMU sensor full arm elevation in different abduction planes as well as horizontal abduction is simulated by the gimbal mechanism (each test was repeated three times) and input angles provided by servo motors are compared to measured spherical coordinate angles by IMU. Maximum error of 3° for elevation angle and maximum error of 2° azimuthal angle were recorded during the tests. The results showed the validity of the sensor performance since they are comparable with precise rotation angles provided by servo motors.

5.2.3 Subjects

Six volunteer subjects with healthy shoulders (4 men, 2 women) with average age of 27.3±3.4 years, average height of 173±6 cm and average weight of 73±8 kg and one male participant with frozen shoulder (age 42, height 176cm and weight of 75kg) were studied. None of the subjects with healthy shoulders reported a history of shoulder injury, pain or instability.

5.2.4 Ethical considerations

The study was approved by the research ethics committee of Bournemouth University (Appendix A.XIII). All subjects gave their written informed consent before inclusion in the study. (Appendix A.XIV)

5.3 Experimental procedures

Prior to electrode placement, the skin on the shoulder was shaved and cleaned using alcohol. Six disposable surface electrodes were placed over the muscle belly by visual inspection and palpation of the muscle sections parallel to the muscle fibre direction, with a centre to centre distance of 3.5cm (Sakaki et al. 2013). Electrodes for recording the anterior deltoid were placed 2.5 cm below the anterior crest of the acromion, electrodes for the middle deltoid were located halfway between the acromion and the deltoid tubercle and electrodes for the posterior deltoid were positioned 2.5 cm below the posterior crest of the acromion. The reference electrode was positioned over the scapula (Kasman and Wolf 2002, Reinold et al. 2004, 2007, Boettcher et al. 2008). Electromyography of all three sections of the deltoid were evaluated in response to shoulder elevation in 3D space. EMG values were normalized to the highest value recorded by each muscle section during each test (Reinold et al. 2004).

The subjects stood in a stationary position facing the same direction during the experiment. Two practice motions were performed before each test. The subjects were verbally instructed to move their arm as far as they can in all directions at their own comfortable speed (Figure 5-5).

The assessment tool was attached to subjects arm. Individuals were instructed to move their arms with the elbow fully extended. They were asked to provide the maximal voluntary elevation envelope of the arm in 3D space in multiple attempts starting from a small movement envelope going to the biggest possible in four consecutive circuits. Each subject was asked to start his arm elevation medially, then anteriorly, cranially, posteriorly, laterally and then back to the initial rest position.

A demonstrator performed the movements in front of the subject to show the order of movements while asking the subject to provide their maximal voluntary elevation. Participants were advised not to move their legs and chest and to keep their torso facing the same direction throughout the movement. To evaluate the repeatability of each test, each subject performed the test three times. EMG of muscles was recorded simultaneously with arm motions from each of the three deltoid sections sequentially.
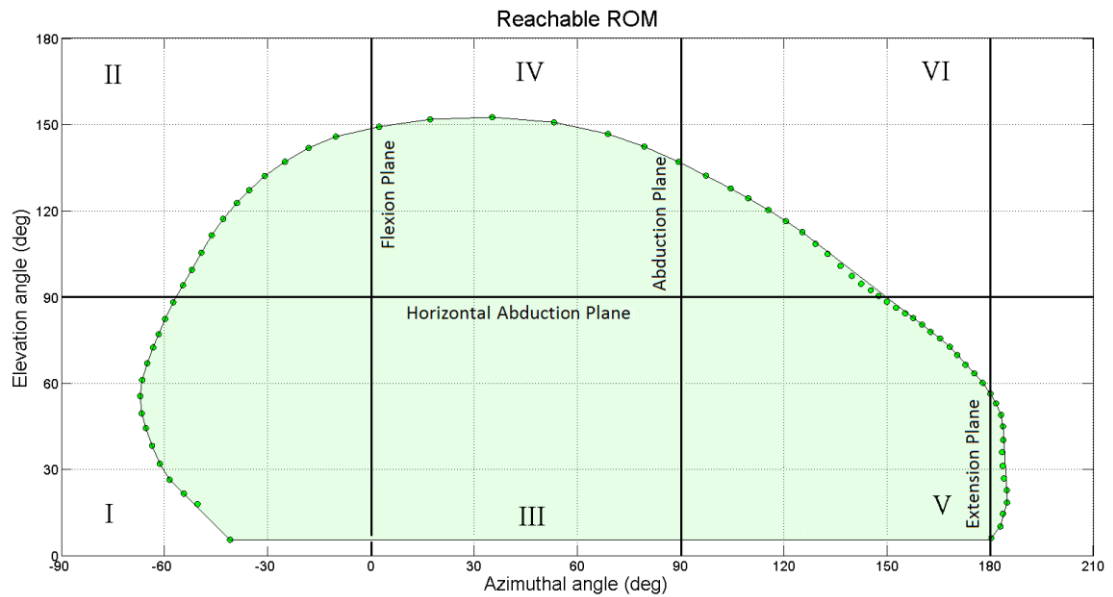
Figure 5-5Sample ROM data collection

In the case that any extra body movements such as bending or trunk rotation were observed by the demonstrator, the test was repeated. In all three tests, subjects were informed that comfortable axial rotation could be utilised if necessary. As Spherical coordinates are used in this study, only two angles of azimuthal (α) and elevation (β) are considered while rotation of humerus around its axis is ignored.

5.4 Results

Azimuthal angle versus elevation angle of arm movement in 3D space are plotted while EMG intensity of any arm position is presented by colour to quantify maximum reachable surface area of shoulder, maximum shoulder elevation in different planes separately and EMG activity of each section of deltoid at any arbitrary orientation of shoulder. Then the results within six healthy shoulders and one frozen shoulder are compared.

Each subject repeated the same test three times and although envelope profiles are slightly different, maximum variation coefficient of 8.3% was found across all subjects. An average ROM surface area of 27478±710 deg^2 was found with a variation coefficient of 4.8% among all six healthy individuals. The subject suffering from a frozen shoulder was able to provide only 13571±308 deg^2 showing 68% difference from average of healthy shoulders. ROM and maximum elevation of each individuals arm in different planes is represented in Table 5-2.

As shown in Figure 5-6, all the healthy shoulders were able to fill majority of region I, III and IV where most daily activities are performed. According to the graphs, it seems all three sections of deltoid show more EMG activities in higher elevation angles where II, III and VI are located for healthy shoulders and regions I, III and V for frozen shoulder.

It is also observed that moving from posterior deltoid toward anterior deltoid maximum of EMG is drawn from region VI to IV and then II for healthy shoulders and from region V to I for the frozen shoulder.

Comparison of the average surface area as well as maximum values from the mean of six shoulders and the one frozen shoulder showed a significant difference (67.8%). Results are compared in Table 5-2.

	Average surface area (deg2)	Coefficient of variation	Max Flexion	Max Abduction	Max extension	Max horizontal abduction
h1	28193	3.3	146	138	63	195
h2	26590	3.9	140	131	42	200
h3	26844	3.2	146	137	57	190
h4	27122	5	162	160	55	190
h5	28002	8.3	150	124	60	205
h6	28119	5.2	142	159	56	210
Healthy Mean	27478	4.8	148±8	141±15	55±7	198±8
i1	13571	3	86	64	NA	NA

Table 5-2. ROM measurements   h: healthy shoulders, i: injured shoulder
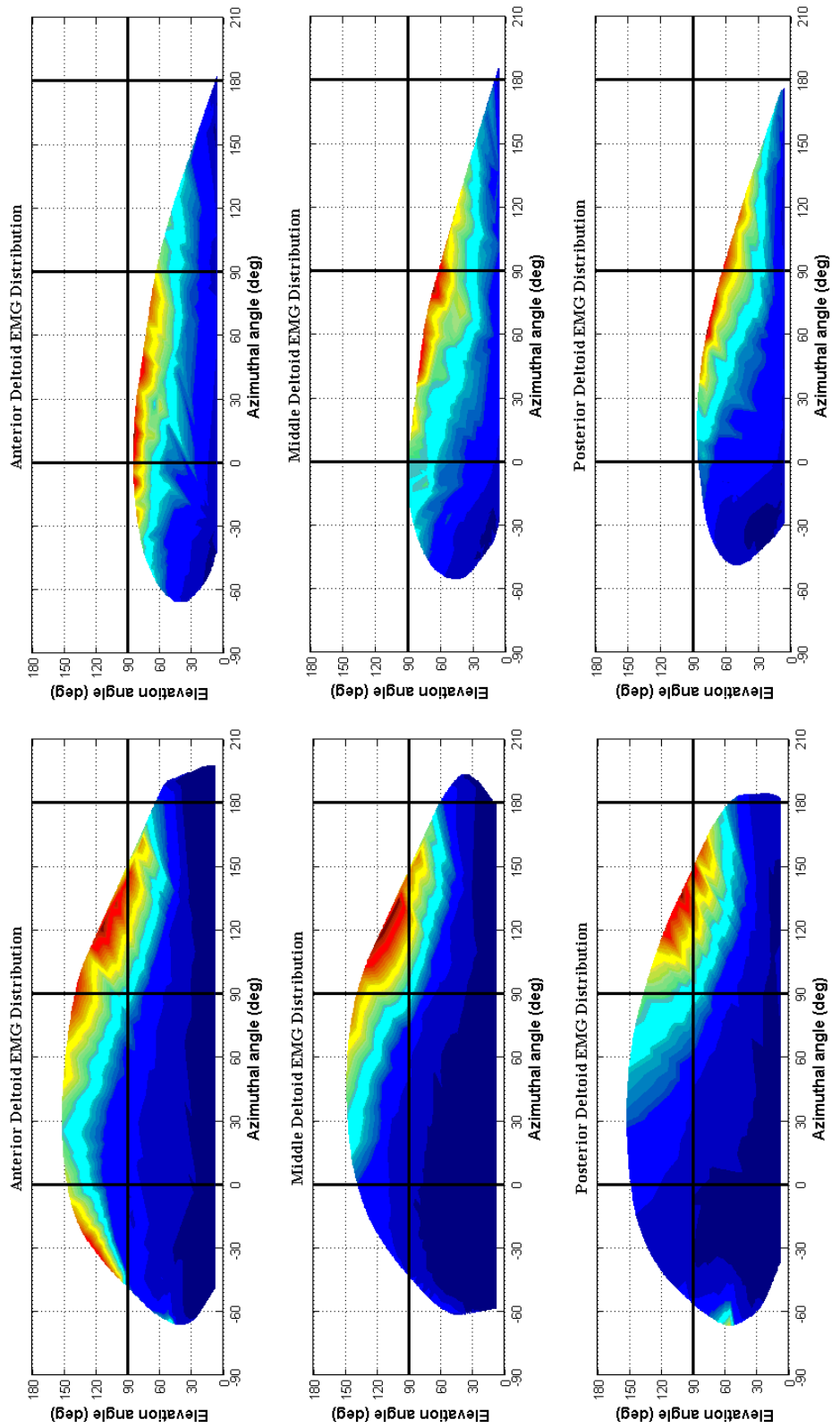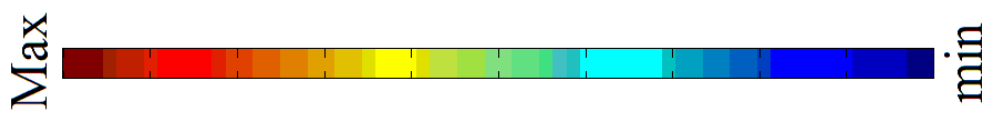
Figure 5-6: ROM and EMG activity comparison, left; a healthy shoulder (h1)   right; the frozen shoulder (i1)

There are different methods to evaluate shoulder performance in terms of pain free motion, manoeuvrability, strength and muscle activity. To measure ROM at the shoulder there are different methods, protocols and tools mentioned in the literature. Most protocols study shoulder ROM in single plane of motion. However, in this study we have proposed using an IMU sensor to measure the maximum envelope of motion in 3D space. Using an EMG sensor combined with the IMU aids in the evaluation muscle activity of deltoid sections.

All the subjects performed the requested arm movement with an extended elbow, using comfortable arbitrary axial rotation when needed. Each test was performed three times and each time EMG of one section of the deltoid was recorded. Results are represented in graphs which gives figures for both EMG and ROM.

In terms of reachable surface area, the subjects showed a maximum variation coefficient of 8.3% across three tests. A coefficient of variation of 4.8% was observed between all 6 healthy shoulders. The subject with frozen shoulder showed 13571 deg2 which was only 67.8% of the average of healthy shoulders. Measured maximum values in separate planes are in an agreement with the values from literature where maximum values are measured in separate single planes (Doriot and Wang 2006, Maier et al. 2014, Han JJ, de Bie E, Nicorici A, Abresch RT, Anthonisen C, Bajcsy R, Kurillo G 2015).

In terms of EMG all three sections of the deltoid showed higher activity in higher elevation angles while moving from posterior deltoid to anterior deltoid EMG distribution changed from region VI to II in healthy shoulders and IV to I in the frozen one.

5.5 Limitations

In this study arm movement is considered while the body is stationary. Both glenohumeral and scapular joint contributed to the arm movement although using one IMU attached to subjects arm does not allow us to differentiate the scapula rhythm involved in each subject movement. Adding two more IMU, one on thorax and one attached to the scapula enables the investigation of the effect of scapula rhythm of individuals as well an improved means of detecting if the subject moves his body to reach the maximum ROM or not. In this study interaction of all shoulder joints are

simplified as a spherical joint moving in 3D space while its motion is described by spherical coordinate angles (elevation and azimuthal angles).

5.6 Conclusion

Using wearable IMU to track human motion can be used instead of complex camera-based tracking systems or mechanical measurements tools suffering from inaccuracy. The IMU sensor was attached to six healthy shoulders and one impaired frozen shoulder and results are compared. At the same time, EMG activity of subjects during 3D movements was monitored and compared for each of the anterior deltoid, middle deltoid and posterior deltoid.

The graphs give information on the shoulder range of motion in specific standard planes such as abduction, flexion etc. as well as any point of interest in the whole 3D range of motion. It also provides information on relative magnitude of EMG in each section of deltoid across the whole range of motion.

EMG of the shoulder shows that in all cases, all three sections of deltoid were highly active at higher elevation. A prominent feature is that a significantly higher EMG is observed in region II, IV and VI in healthy shoulders and I, III and VI in the frozen shoulder.

The minimal setup time needed for the sensor and low cost makes the proposed system a practical assessment tool for individuals, surgeons and physiotherapist for objective assessment of shoulder motion as well as muscle EMG monitoring.

Chapter 6 Force measurement

6.1 Deltoid passive force

While many of the parameters that are taken into account when designing and performing a restorative surgery are objective, there are some parameters that cannot be measured or quantified. These are usually felt and not precisely measured and their intensity or levels are at the discretion of the surgeons and based on their experience. For theses subjective measures, it is down to the surgeon's skill and experience to find the best prosthesis size and position during operation. The most important parameter, which is set by the surgeon during surgery, is the force applied to the contact area of glenohumeral joint during motion. This force is mostly generated by the passive reaction of the deltoid muscle on glenosphere within the glenohumeral joint and currently there is no mechanism except surgeons experience to measure and record this. This is achieved by moving patient's arm in different directions passively and feeling involved forces and their intensities using fingers natural haptic feedback based on surgeon's experience. This force can be adjusted by placing different trial implants of various sizes to choose the best fit.

Different ways of measuring the force in glenohumeral joint were investigated in Chapter 2, concluding that direct force measurement on glenosphere using force transducer would be the most effective.

The overall purpose of this transducer is to measure the passive force exerted on the reverse shoulder joint during surgery as a criterion or measure of deltoid pretension. The introduction of a system proposed here provides data which are to be recorded in a database along with geometry and kinematics of individual patients. Such database will enable surgeons to find correlations between these parameters and the outcome of surgery in the long term. It is hoped that this will provide a tool for surgeons in future operations to use a more quantitative and repeatable way of optimizing the implant size and position accordingly.

According to literature currently there is no mechanism to quantify surgeon's experience in choosing implant parts size and their positioning on bones intraoperatively. However recently Chih-Chiang et al (2013) has released a new design of force transducer for RSA which employs strain gauges on the stem of a customized glenosphere during surgery to measure force on GH joint.

A new sensor is designed and developed and can be easily used to measure deltoid pretension intraoperatively with minimum distraction for surgeon and maximum easiness without any change in surgical workflow.

6.2 Passive force in Glenohumeral joint

During RSA the surgeon has some geometrical choices to adjust the implant parts on humerus and scapula in such a way to have the best outcome after surgery (Figure 6-1). These geometrical parameters are partly a function of the patient's anatomy and partly of prosthetic parameters effecting deltoid passive tension. Among all, the parameters which can be adjusted intraoperatively are:

On scapula side:

- Bone cut in medial direction
- Glenosphere size (38 and 42mm)
- Glenosphere position on scapula on inferior direction

On humerus side:

- Bone cut on humerus head
- Cup (spacer) size in diameter which is a function of glenosphere size (38 and 42mm)
- Cup (spacer) width (+3, +6, +9)

There are trial implants in all RSA which let the surgeon find the best combination of all these adjustable parameters. Currently surgeon's decision is made by feeling the passive force acting on glenosphere as a result of combination of all anatomic and prosthetic parameters.
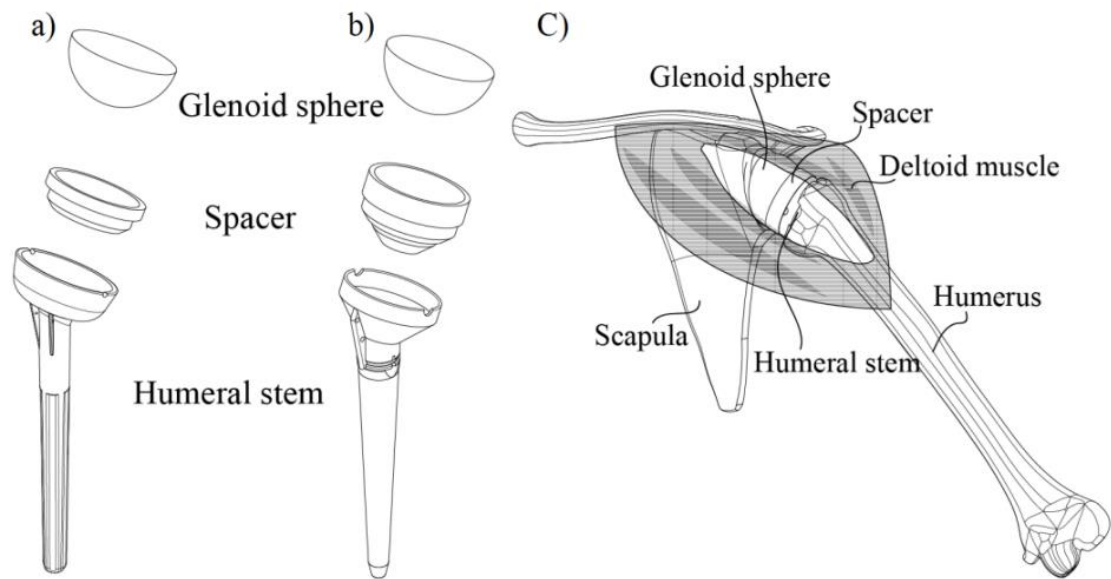
Figure 6-1: Delta Xtend prosthesis; b) Delta CTA prosthesis; c) Prosthesis placement in RSA

6.3 Potential sensor principles

Different force sensor types were studied and compared. The review of available literature was summarised and tabulated in Table 6-1 (Fässler 2010, Hunt et al. 2013). Based on advantages and disadvantages of load sensing, a design based on strain gauges is proposed.

Sensor type	Description	Advantages	Disadvantages
Semiconductor strain gauge	Strips of semi-conductive silicon changing their resistance due to strain.	- Linear response - Low hysteresis - Low creep - Large k-factor - Inexpensive - Small and thin	- Temperature dependant - Can not be shaped - They purge the need for bonding agents
Metal strain gauge	Consist of an insulating flexible backing which supports a metallic foil pattern	- Robust - Inexpensive - Small size - High sensitivity - Can be employed to measure both static and dynamic force	- Temperature dependent - Low k-factor
Thin film strain gauge	Thin film gauge is molecularly bonded to the specimen by sputtering or evaporating thin films of metals or alloys onto the elastic element.	- Stable installation - Small drift	- several stages of evaporation and sputtering - expensive
Piezoelectric crystal (quartz force transducer)	Electrical voltage is produced on the crystal in proportion to the change of applied force	- very suitable for dynamic loads - high overload - small size	- can not be used for static load - lower sensitivity while increasing temperature

Capacitive	The sensor consists of two parallel conductive plates placed opposite each other and displacement of the plates caused by applied force changes the gap between the plates leading to a change in electrical capacitance	- able to measure both normal and shear force - properties of the sensor depends on the elastic plate between two conductive plates causing design flexibility - temperature stability	- complex circuit - susceptible to noise
Hall effect	Magnetic field changes, caused by elements deflection due to the forces, are measured	- robust - low hysteresis - linear response - able to measure normal and shear force	- measures field in one direction - susceptible to magnetic field
Magnetoelastic	Magnetoelastic sensors are made of Magnetostrictive material able to change their magnetic permeability while subjected to deformation.	- Good sensitivity - Good linearity - Low hysteresis	- Complex circuit - Susceptible to noise
Optical	Strain of optical fibres due to applied force results length changes in the fibre which can be detected by measuring the phase differences of monochromic light beams.	- Flexible	- Complex construction
FSR (Force Sensitive Resistor)	FSR consists of a conductive polymer which changes resistance while strained by a force	- Thin and lightweight - Small - Cost effective	- Limited working range - drift

Table 6-1. summary of different force sensor types

6.4 Strain gauge based design

In all human joints there is a passive force created by ligaments and muscles around the joint. Setting the right passive tension in muscles after prosthesis placement in patient's joints is crucial for outcome of the surgery. The reaction of soft tissue as passive force that acts on joint's parts is directly proportional to the tension in the muscles. Hence finding the correlation between implanted joint contact force and muscle volume or body mass of individuals can inform surgeons about what should be the nominal force that can be deemed acceptable. A transducer system that allows intraoperative forces to be measured is highly desirable because over time this information can lead to surgeons to set the best possible passive contact load/force in the joint and get it right first time during surgery.

A cup sensor was developed that can be inserted temporarily during surgery to measure the normal force without any change in the surgical workflow (Figure 6-2). The sensor replaces the plastic spacer (Figure 6-1) used in reverse shoulder implants and normal force is measured while the joint is articulated passively by the surgeon (Figure 6-3).

Measured force generated by the muscles tension can inform the surgeon to choose proper implant size and alignment during surgery.

Figure 6-2: Prototype of the transducer

The transducer has the same overall dimension as the plastic spacers used in original implants. The force imposed on joint by the muscle passive tension can be measured during passive articulation and the values of contact force and the associated feel can be correlated or quantified to give an objective data that one can use to standardise/normalise the load intensities that a deltoid needs to experience depending on the total mass of the deltoid and the overall contact force.
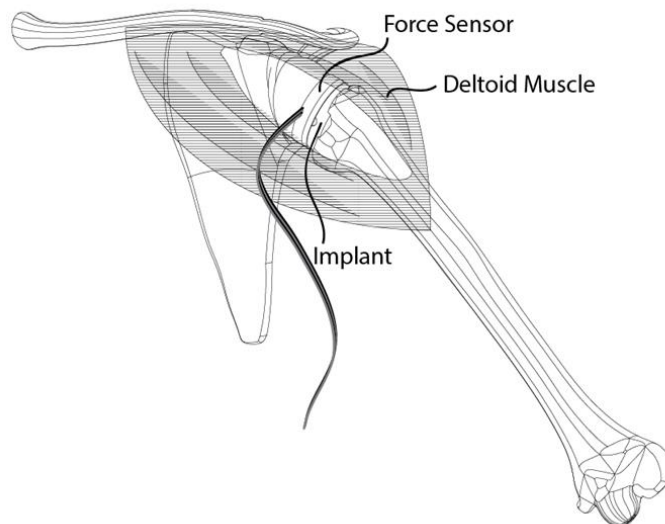
Figure 6-3: Intraoperative sensor placement

This design relates generally to joint implant and more specifically to a transducer which measure force components on Reverse Shoulder implants joint of all types and

designs. The transducer can be used for any joint implant which includes a plastic spacer between implant parts to be replaced by the transducer intra operatively.

6.4.1 Architecture of the sensor

There are different type of reverse shoulder implants with different designs and sizes They all consist of three main components; humeral stem, to be implanted in the patient's humerus; glenoid sphere, to be implanted on the scapula and plastic spacer, to be used on top of humeral stem to create a universal joint that allow articulation on bearing surface of glenoid sphere (Figure 6-1).

Some of the requirements to be considered can be summarized as below:

- The transducer must be the same size as plastic spacer
- The transducer should be design base on clinically available types of prosthesis and surgery procedure should remain unchanged.
- The rings must be able to adjust sensor height to simulate different spacer sizes
- The transducer must be sensitive to force in normal direction only.

The transducer includes a load bearing plate which articulates on glenosphere while directing the force generated by passive tension of deltoid muscle to support post whose load-dependent deflection is measured by strain gauges mounted on its flexure members (Figure 6-4). The measured deflections are converted to electrical signals by strain gauges and according to load distribution pattern on flexure members, normal directions of force is measured while the other two components of force are ignored. The applied force on contact area is transferred to flexure members through a rod to the strain gauge area that collectively represent the absolute force through the joint.

Dimensions of the transducer follows exact 3D dimensions of chosen implant therefore its bearing surface can easily articulate on bearing surface of glenoid sphere while measuring the force. Main body of transducer occupies the cavity of cup of humeral stem with the same manner as plastic spacer does.
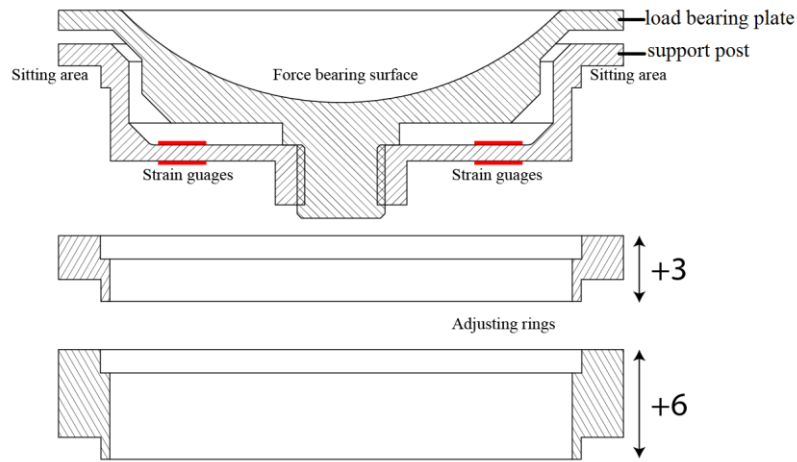
Figure 6-4: Basic structure of the device (cross section of the force sensor parts)

The transducer is accompanied with multiple calibrated spacers (Adjusting rings) which can be easily inserted between bearing ring area of the sensor and bearing ring area of the cup of humeral stem. This is to adjust depth of transducer according to surgeon's will.

Transducer structure includes two main components which are integrated as a unitary body and can be made from aluminum or titanium alloy or any other suitable metallic materials (Figure 6-5); load bearing plate consist of a bearing spherical surface in contact with glenoid sphere and support post including flexure members and reinforced structure of greater thickness to have minimum strain. Half bridge setup of strain guages helps compensates for temperature effect on output voltage of the bridge.
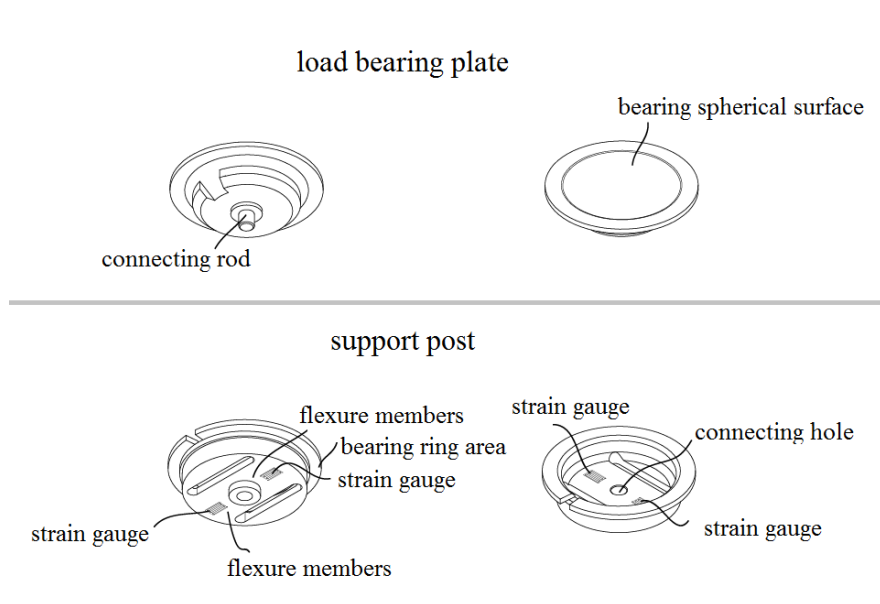
Figure 6-5: Description of the transducer

6.4.2   Mathematical model of the sensor

To investigate sensor performance in different loading conditions, simplifications based on following assumptions are applied:

- Implant parts form a spherical joint in which the whole force is transmitted through the ball to the ring of the sensor
- Beams are identical and applied force through the rod acts on the centre of the beam.
- Due to applied force in agreement with the safety factor the deformation occurs in elastic range.
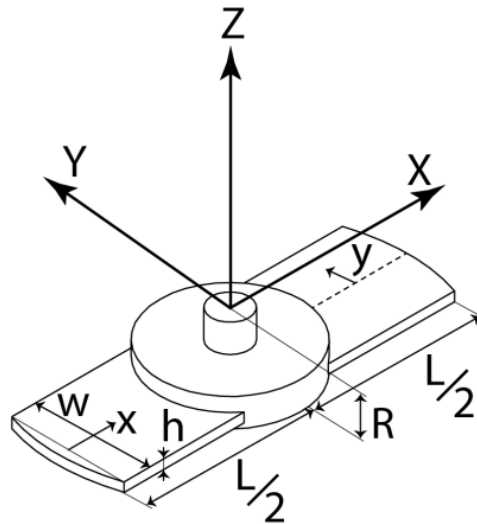
Figure 6-6: geometry of load carrying structure of the sensor

The force sensor principle and its dimensions are shown in (Figure 6-6). Three different loading scenarios (resultant force in X, Y and Z directions) are studied separately and strain on left and right membranes (Figure 6-7), both on upper and lower surfaces, are calculated using the equations below:
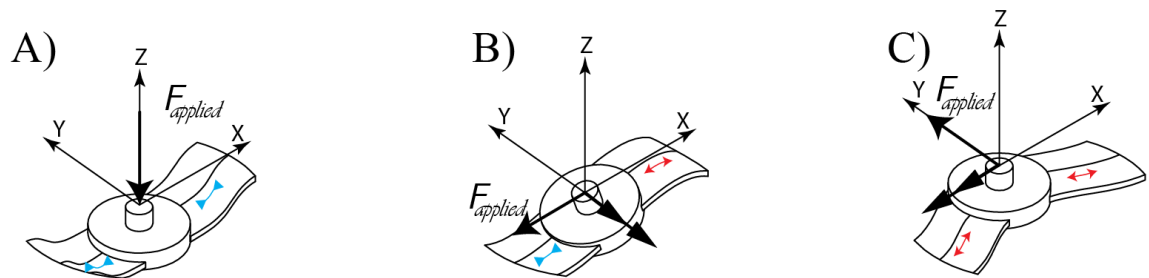
Figure 6-7: A) Normal force in Z direction; B) Normal force in X direction; C) Normal force in Y direction

A) Resultant force in Z direction

$$\varepsilon_{1,x}^u = \frac{hF(4x-L)}{16EI_{yy}}, x = (0,\tfrac{L}{2}) \qquad \varepsilon_{2,x}^u = -\frac{hF(4x-3L)}{16EI_{yy}}, x = (\tfrac{L}{2},L) \qquad \varepsilon_{1,x}^l = -\frac{hF(4x-L)}{16EI_{yy}}, x =$$

$$(0,\tfrac{L}{2}) \quad \varepsilon_{2,x}^l = \frac{hF(4x-3L)}{16EI_{yy}}, x = (\tfrac{L}{2},L)$$

B) Resultant force in X direction: creating an axial load along X as well as a moment around Y.

$$\varepsilon_{1,x}^u = \frac{FRh}{8EI_{yy}} + \frac{F}{hw} \qquad \varepsilon_{1,x}^l = -\frac{FRh}{8EI_{yy}} + \frac{F}{hw} \qquad \varepsilon_{2,x}^u = -\frac{FRh}{8EI_{yy}} - \frac{F}{hw} \qquad \varepsilon_{2,x}^l =$$

$$\frac{FRh}{8EI_{yy}} - \frac{F}{hw}$$

C) Resultant force in Y direction: creating a bending in Y direction as well as a moment around X.

$$\varepsilon_1^u, \varepsilon_1^l = \frac{FR(1+v)}{K_1 Ewh^2} \qquad \varepsilon_2^u, \varepsilon_2^l = \frac{FR(1+v)}{K_1 Ewh^2}$$

$$\varepsilon_{1,x}^{u,l} = \frac{yF(4x-L)}{16EI_{zz}}, x = (0,\tfrac{L}{2}) \quad \varepsilon_{2,x}^{u,l} = -\frac{yF(4x-3L)}{16EI_{zz}}, x = (\tfrac{L}{2},L)$$

Where F is resultant force; h is beam thickness; x is distance from constraint in X direction; L is length of each membrane; E is young modulus; I is second moment of inertia; w is beam width; R is moment arm in Z direction; v is Poisson ratio and K_1 is coefficient for torsion of rectangular section.

6.4.3   Wheatstone bridge

The Wheatstone bridge (Figure 6-8) is one of the best circuits able to measure small variation of resistance. In this circuit input voltage of V$_{Ex}$ is applied to the four resistance bridge and output voltage (V_{Out}) is measured. The sensor consists of a single beam with a fixed loading point in the middle, dividing the beam into two membranes (right and left). Strain gauges on each membrane form a separate half bridges by mounting one strain gauge on upper surface (R_u) and one on lower one (R_l). Each membrane will be sensitive only to bending moment while ignoring axial strains.
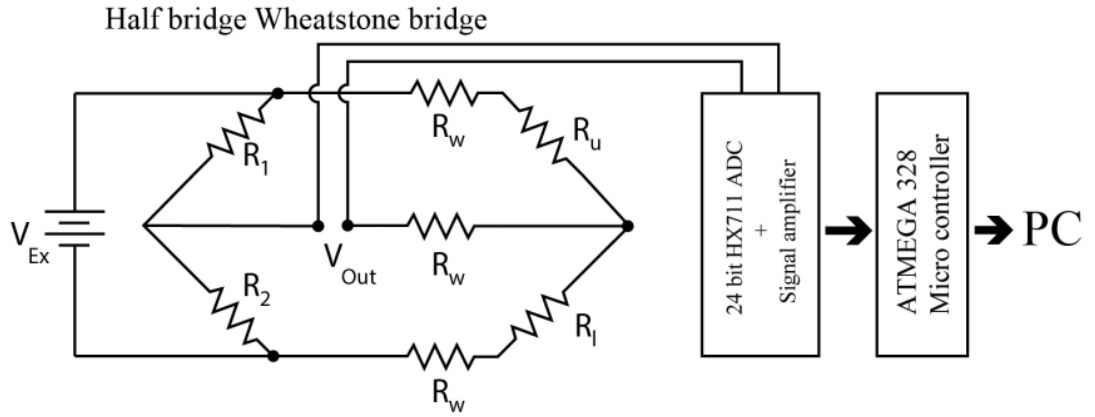
Figure 6-8: schematic of connection of strain gauges and sensor circuit

In cases **B** the axial component of the force generating axial strain in X axis will be ignored on each membrane due to half bridge configuration of the bridge while the strain created by bending around Y in right and left membranes will cancel out each other as they have the same value with opposite signs. Respectively in case **C**, strain created by the bending along Y and moment around X will be ignored on each membrane as both upper and lower gauges sense the same strain. In case **A**, The strain generated by applied force causes to resistance variation of strain gauges as written below:

$$GF = \frac{\Delta R_g / R_g}{\epsilon} \quad \text{(eq.1)}$$

Where GF is the gauge factor of the strain gauge; ϵ is strain in x direction; and R_g is resistance of strain gauge. As the adhesion between strain gauges and the load membranes is solid, longitudinal strain (X direction) of the membranes will affect change of resistance in strain gauges known as ϵ_l while transversal strains (ϵ_t) will not cause any resistance variation in strain gauges:

$$GF = \frac{\Delta R_l / R_l}{\epsilon_l} , GF = \frac{\Delta R_t / R_t}{\epsilon_t} \quad \text{(eq.2)}$$

Where R_l and R_t are longitudinal and transversal components of resistance respectively. As the strain gauges are sensitive to longitudinal components of the strain hence here ϵ represents longitudinal strain only.

Voltage ratio (V_r) is defined as below:

$$V_r = \left[\left(\frac{V_{out}}{V_{Ex}} \right)_{strained} - \left(\frac{V_{out}}{V_{Ex}} \right)_{unstrained} \right] \quad \text{(eq.3)}$$

Wheatstone bridge:

$$V_r = \frac{R_1}{R_1 + R_2} - \frac{R_u}{R_u + R_l} \quad \text{(eq.4)}$$

If R_l and R_u vary, the voltage ratio of the bridge can be written as:

$$V_r = \frac{R_1}{R_1 + R_2} - \frac{R_u - \Delta R_u}{(R_u - \Delta R_u) + (R_l + \Delta R_l)} \quad \text{(eq.5)}$$

$$R_u = R_l = R_g \ , R_1 = R_2$$

$$V_r = \frac{\Delta R_g}{2 R_g} \quad \text{(eq.6)}$$

Where ΔR_i represents resistance ith variation.

In case of half bridge, while R_l and R_u represent strain gauges mounted below and on top of the bending membranes respectively, actual strain can be calculated using the equation below:

$$\epsilon = \frac{2 V_r}{GF} \quad \text{(eq.7)}$$

The developed software in MATLAB allowed two types of operation:

- Sensor calibration by inputting known dead weights as input and measured output voltage
- Data processing by monitoring calibrated values

6.4.4 FEA analysis

To investigate stress and strain distribution in the sensor, Finite Element Analysis (FEA) is used. Using FEA helps to conclude optimum structural design, strain gauge placement on the sensor as well as the maximum load the sensor can bear. A precise CAD model of all components of DELTA Xtend implant was developed using reverse engineering measurements. The 3D CAD model of the sensor was designed based on the implant dimensions to replace polyethylene cup intraoperatively. 3D FEA model of the system was obtained using Autodesk Inventor (Autodesk, USA) commercial

software. The FEA model consists of two parts of sensor integrated as one piece, glenosphere and the humerus stem.
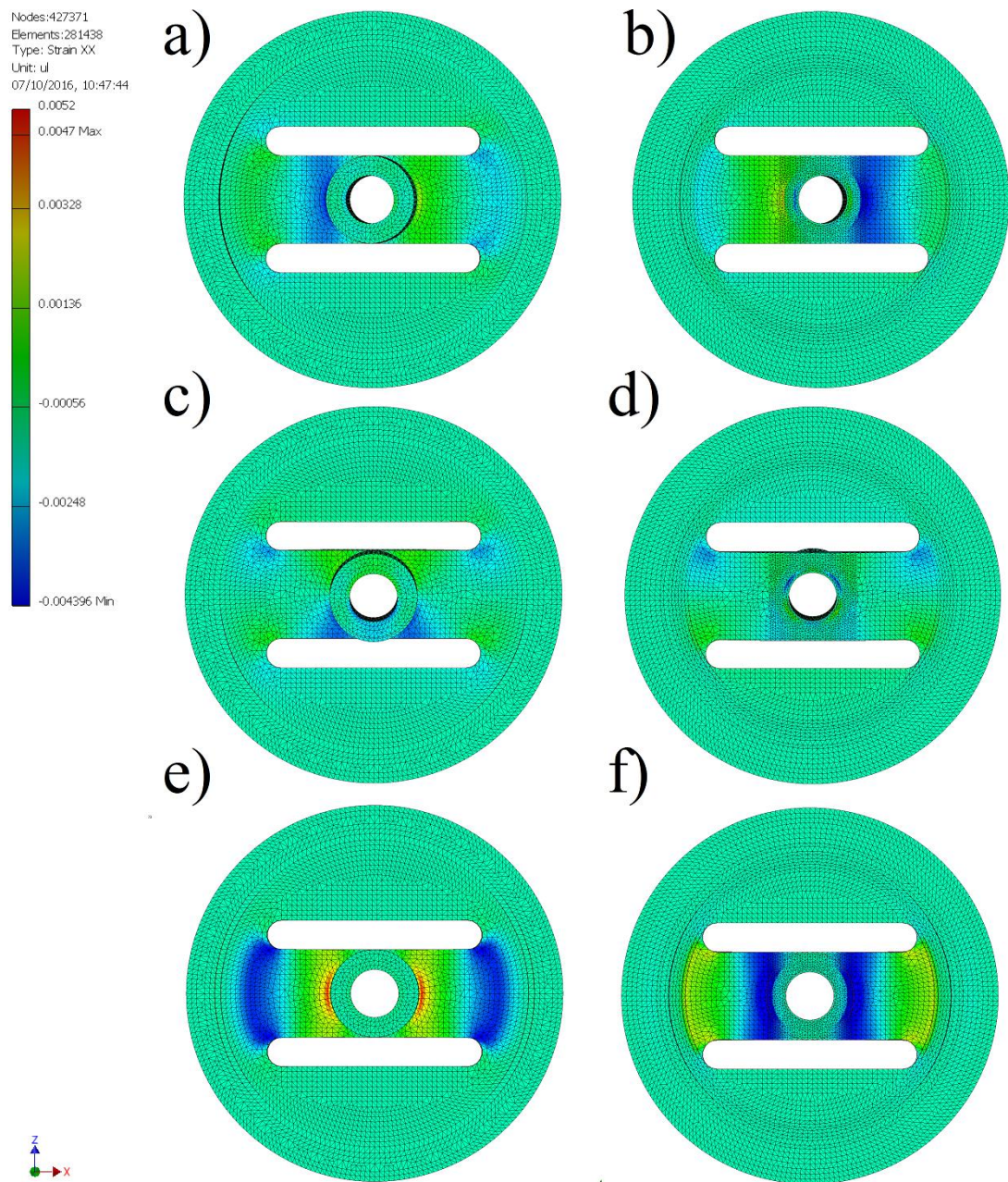
Figure 6-9: x-component strain distribution for different applied loads. a) bottom view of sensor for force in X direction; a) top view of sensor for force in X direction; a) bottom view of sensor for force in Y direction; a) top view of sensor for force in Y direction; a) bottom view of sensor for force in Z direction; a) top view of sensor for force in Z direction

FEA was implemented in finite element analysis feature of Autodesk Inventor in static mode assuming a linear elastic behavior of all implant and sensor parts. To define mechanical properties of FEA parts, Aluminum 7075-T651 was chosen as sensor material ($E = 71.7$GPa, $v = 0.33$) while prosthesis parts are made of Titanium alloy. The

humerus stem has a fixed constraint while a flat surface contact constraint is added between sensor sitting ring and humerus stem and a spherical contact constrain between glenosphere ball and sensor force bearing surface as boundary conditions. Uniaxial load varying between 0N and 245N is applied on center of the glenosphere and force is transferred to sensor through the contact between glenosphere and bearing spherical surface. A fine triangular meshing with average element size of 0.018 (fraction of model diameter) is applied to sensor forming 138780 tetrahedral elements.

X-component strain, in xy plane are visualized in Figure 6-9 by color palette while negative strain values are associated with compressive strain and positive strain values are associeted with tensile strain in x direction. Based on location of high strain regions, the most suitable place for 9mm strain guages are chosen to be located 9 mm far from the centre where 4 strain gauges are installed on sensor wings.

6.4.5   Sensor design and fabrication

Aluminum 7075-T651 was chosen as sensor material and all the pieces including sensor load bearing plate, sensor wing and adjusting spacers are made using high precision CNC machine tool to tolerance of 0.01mm. Four 320Ω foil strain gauges (Appendix A.XV) which are aluminum alloy temperature compensated are mounted precisely on regions with high strain in direction of X. and each two strain gauges form a half Wheatstone bridge configuration using two external resistors and powered with regulated 3.5V DC. The bridges are then connected to an ATMEGA 328 micro controller through a high resolution ADC (24 bit HX711) with the gain of 128 (Appendix A.XVI) (Figure 6-8). Two output signals are displayed and recorded in MATLAB (Appendix A.XVII). Output voltage of the each Wheatstone bridge is associated with measured strains are used to calibrate the sensor.

6.4.6   Joint simulator

A custom joint gimbal like joint simulator was designed, fabricated and used to both calibrate and to evaluate the sensor performance, repeatability, accuracy and reliability. As shown in (Figure 6-10) the simulator consist of two rotating beds articulated by two high torque servo motors, sensor gripper and adjustable weight on top of a sliding rod whose motion is constrained along z axis only using a linear bearing. The bottom of the load carrying rod sits on top of a 42 mm diameter steel ball that is in contact with the sensor. Centre of steel ball is aligned with the centre of rotation of both degrees of

freedom. The sensor was placed in a gripper in its neutral position and different known calibrated static weights are placed on top of the sliding rod.
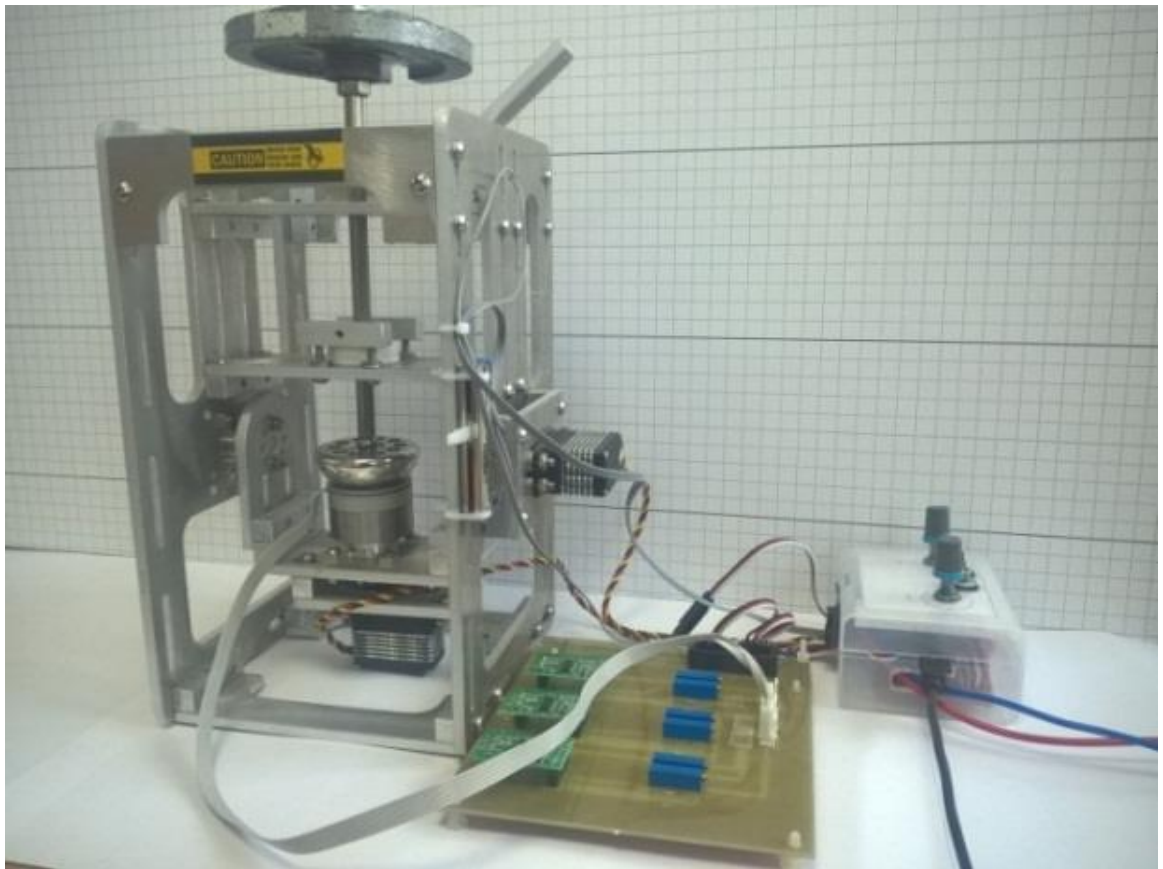
Figure 6-10: Setup to test performance of the sensor in joint simulator test rig

6.4.7 Results

The sensor was tested in the custom-built test rig using static weights. The force is provided by commercially available dead weights with relative error of 0.5% for 25Kg. The sensor demonstrated linear behavior and was able to measure force accurately within the designated range of between 0 and 245N.

To create the calibration curve, sensor signal is measured and compared with standard weights used in the test rig.

Calibration curves were obtained by fixing the force sensor in the gimbal carrier of the test rig and loaded by placing known static weights on top of the sensor throught the push bar. Load was increasing from 0 to 15kg (147N) in 1kg (9.8N) interval and then every 5kg (49N) up to maximum of 25kg (245N). The sensor was calibrated using a

simple linear regression shown in (Figure 6-11). The sensor structural integrity can be adjusted for higher maximum contact load with similar ease.
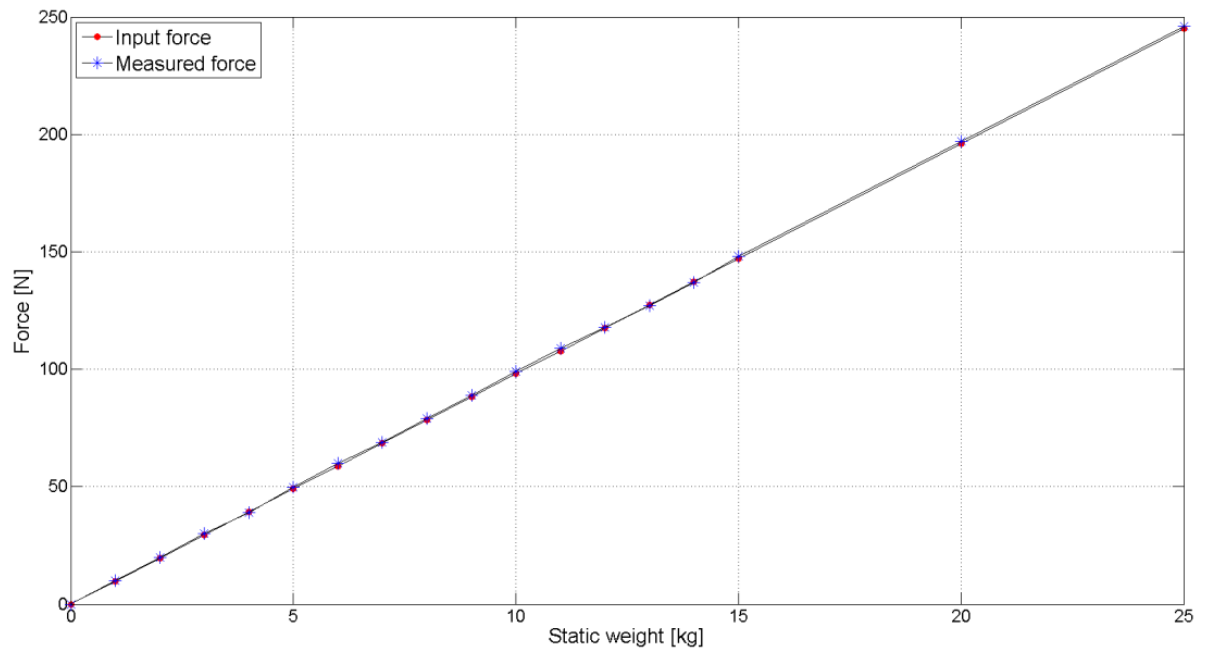
Figure 6-11: Measured force in Z direction as a function of input weight in case A

To test accuracy of the sensor, known weights placed on top of the push bar in all three scenarios of loading are compared to measured loads. A maximum error of 0.4% was recorded by comparing magnitude of externally applied load with measured load for the case A, in which resultant force in Z direction is applied. In case B and C where sensor was tilted 30 degree around Y and X, maximum error of 2.3% and 3.3% were recorded respectively as shown in (Figure 6-12). Sensitivity of 38 strain/Kg for normal force in Z was observed.
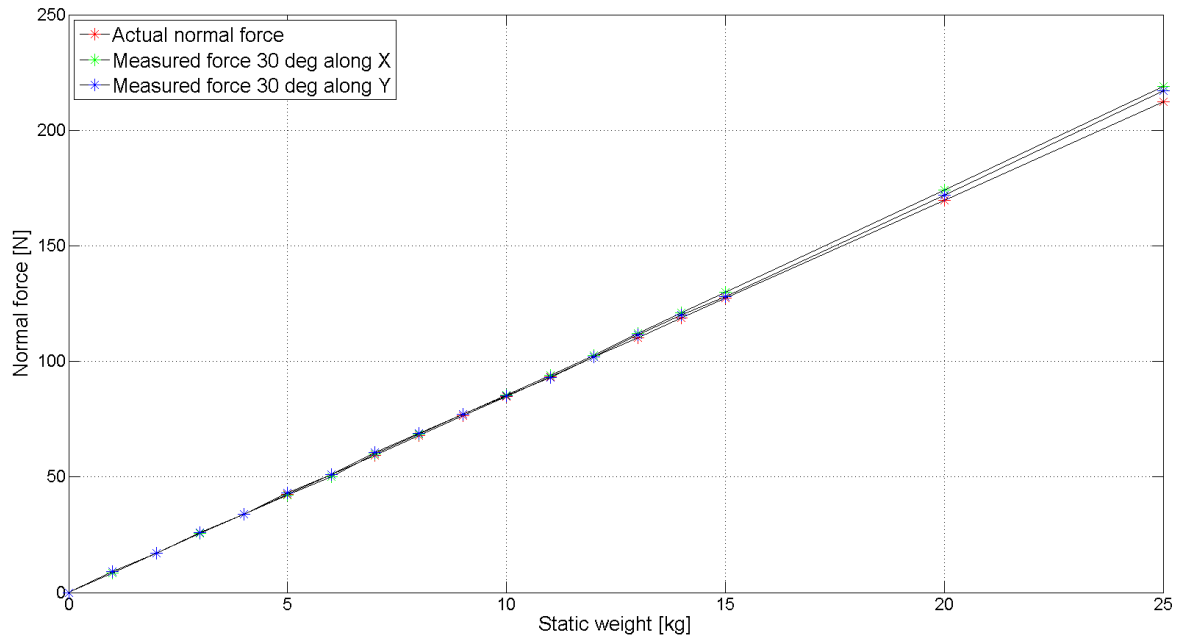
Figure 6-12: Measured force in Z direction as a function of input weight in case B and C

As shown in (Figure 6-13) creep behaviour of the sensor both in loading and unloading cases were really small both in primary creep phase (loading and unloading) and secondary creep phase (steady-state) resulting in a better stability and repeatability of the sensor. The sensor responses well to dynamic loading.
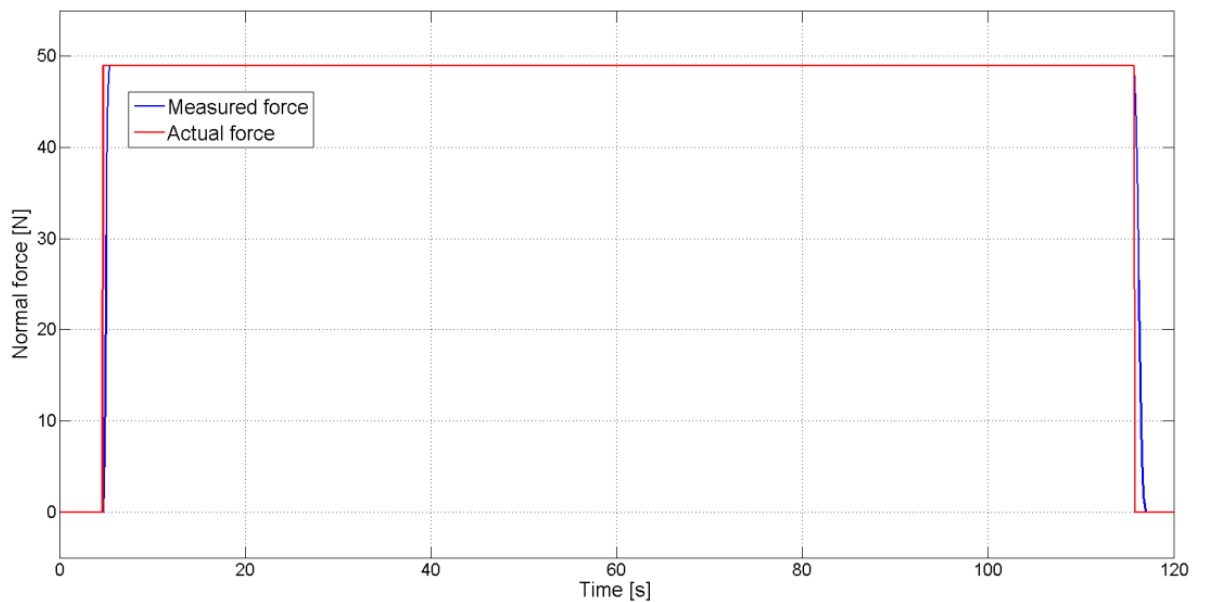
Figure 6-13: Sensor response to force step between 0N and 49N (5Kg) in case A

The best possible strain gauge to fit dimensions of the high strained region detected by FEA was chosen. Strain gauges are mounted 6mm from the centre of the sensor and in

X direction. As both ends of each strain gauge is located at 9mm and 12.2 mm from the centre of the force sensor, average of axial strains (X direction) in these two points is considered as FEA strain. The results indicate that FEA strain and measured strain have 36.6% of difference which could be due to mismatch of the strain gauges, real life loading, circuit parameters and structural complexity of the sensor (Figure 6-14). While according to linear behavior of both the sensor reading and FEA strain the measured strain can be corrected to FEA strains.
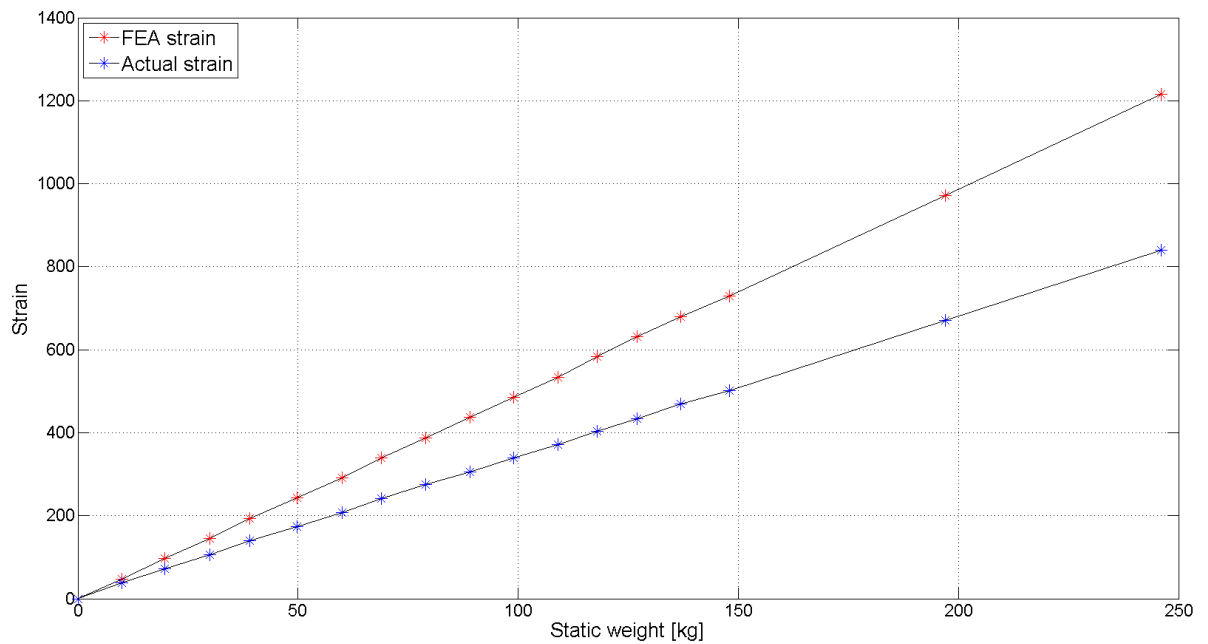
Figure 6-14: Comparison between read strain and x component of FEA strain in case A

Exact same results were obsereved while using the adjusting rings underneath the sensor as they only change the height of the sensor as the rings do not change any boundry condition in this test. The result was considered satisfactory.

6.4.8   Discussion

Different ways of measuring the force in glenohumeral joint, usually caused by passive muscle activities, were investigated and a more reliable method is proposed. It is concluded that direct force measurement on glenosphere using force sensors would be most effective if we are to reduce the number of revised surgery due to joints mechanical or kinematic failures.

A 3D model of the sensor considering limited space in humerus cup was developed including a load carrying beam divided into two separate membranes. FEA of the model

was conducted to find highly strained regions to place strain gauges on. 4 strain gauges were carefully placed on high strained regions of each membrane both on upper and lower surfaces. The sensor electronic setup is a Wheatstone bridge forming a separate half bridge on each membrane. The bridge is supplied with 3.5V through a voltage regulator. And sensor signals is amplified and then converted into digital signal using a high resolution ADC (24bit). A custom-built test rig consisting of a carrier with two degree of freedom and a push rod able to carry static load was developed to test the sensor with different static loads in different directions up to 245N. Data were analyzed to determine repeatability and linearity of the sensor. The sensitivity to axial loads in all directions was relatively high and linearity, sensitivity and repeatability are satisfactory. The effect of angular offset were explored and characterized.

Chapter 7   Outcomes and Future Works

7.1 Outcomes

A series of computer graphical user interfaces (GUI) was developed in collaboration with consultant surgeon from RBCH and based on information about his needs and advice on good practice. Every aspect of the assessment, from pre-operation to post operation are packed into the GUI capable of measuring and evaluating kinematics, range of motion, rate of rehabilitation and force measurements.

For ease of use every element of the work described in Chapters 4,5 and 6 are programed into a series of application packages that can be used for processing X-Ray images, to extract kinematic data; shoulder ROM and EMG assessment pre and post operatively; and finally joint contact force measurement using transducer.

The GUI packages developed in Matlab can be used independently or combined to form a complete shoulder assessment system that can be easily operated by a trained clinicians/operator pre, intra and post operatively.

A database of anatomical and prosthetic geometries, kinematics comparison in and between individuals before and after surgery as well as ROM and EMG combined with intraoperative force measurement, will make this a valuable system to objectively assess RSA which over time will enable surgeons to identify the ideal load intensity at the joint as a function of mentioned parameters.

The GUI includes three main sections: Imaging, Force Measurement and Range of Motion (ROM) assessment (Figure 7-1).
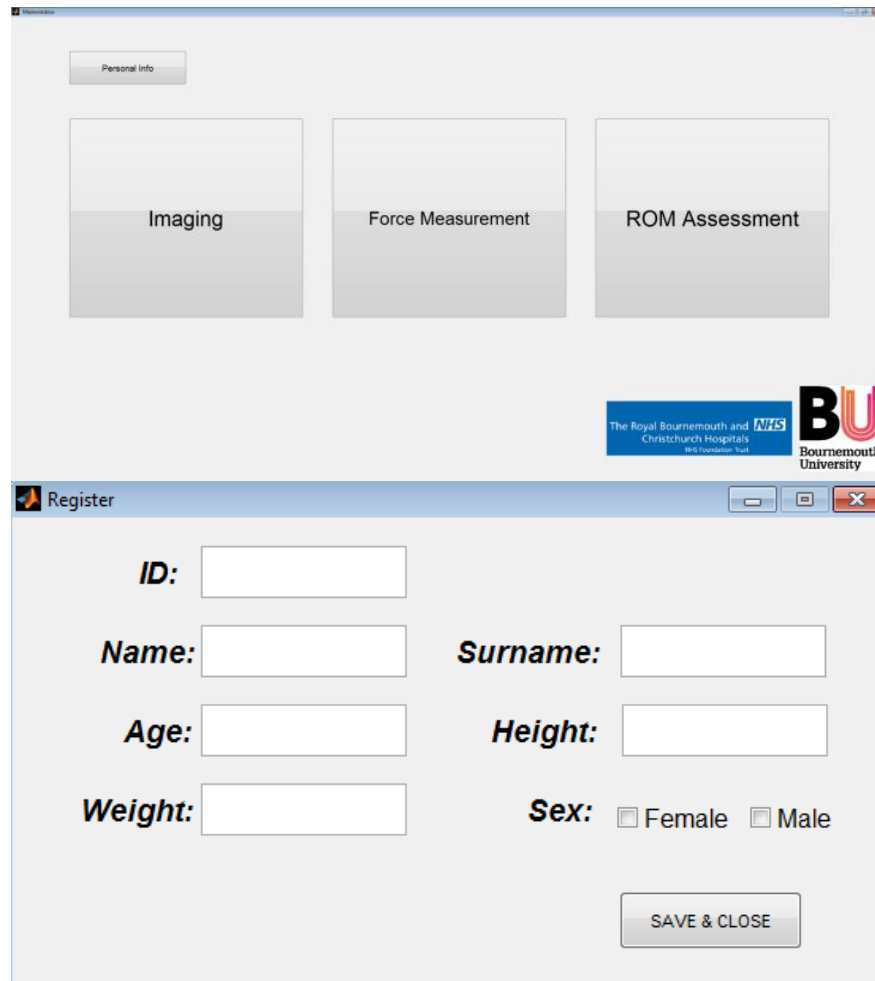
Figure 7-1: GUI developed in MATLAB

The software has the main front page which acts as shell covering all element of the shoulder assessment. Each application can then be individually executed and data extracted, presented or recorded depending on the requirement of the user by clicking the appropriate icon.

In the main window of GUI all the needed details of the patient (name, age, id no, etc) are recorded and securely stored, so later on individual's assessment results can be saved in main database identified by patients detail.

The GUI has been designed in a user friendly form and minimum amount of training is needed to be able to work with it. All the external devices (Force Sensor, IMU and EMG sensors) are easily connected to computer using serial USB ports. The developed platform can be simply modified to satisfy surgeon and operator's need. These are the first iteration of these interface and may require further development if they are to be

used commercially. These are here to show the scope, diversity and depth of the proposed system.

Imaging

In imaging section (Figure 7-2), X-ray or MRI images of patients are uploaded. These images must be taken in standard protocol developed as part of the research using calibrated spherical marker, standard and predefined positions and by expert radiologist in scapular plane of shoulder. The spherical marker with precise known diameter will be used to calibrate all the dimensions of each image. Key geometrical parameters are then selected by the operator and based on the kinematics graphs are provided.
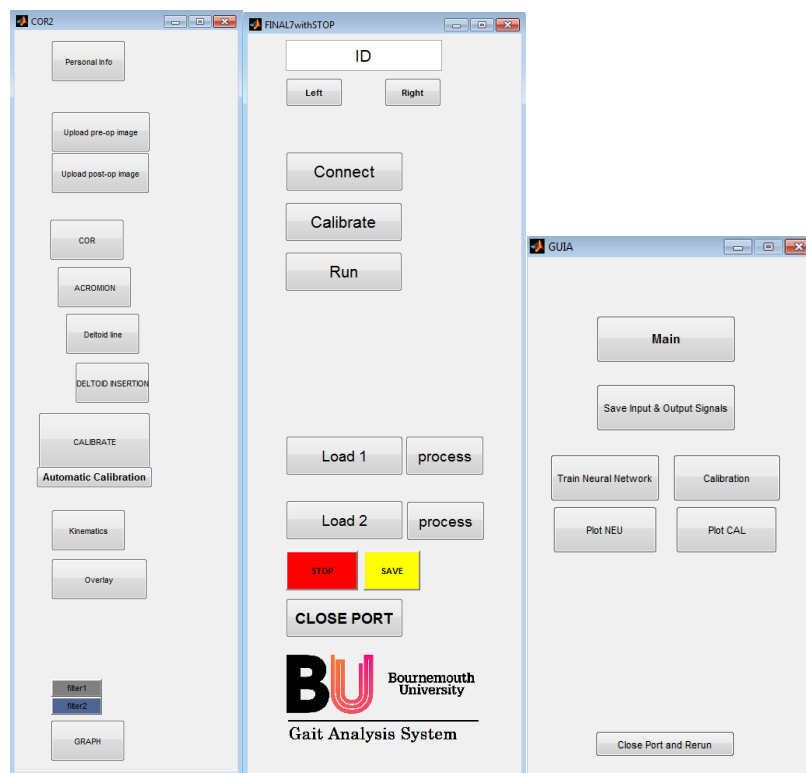
Figure 7-2: Left: Imaging   middle: ROM and EMG assessment   right: force measurement

Shoulder ROM and EMG assessment

Another key contribution from this study is the development of a strategy for the assessment of the performance before and after the operations. In this study we have proposed using an IMU (Inertial measurement Unit) sensor to measure maximum envelope of motion in 3D space before and after surgery to monitor precise comparison of ROM of individuals to be able to suggest the best possible physiotherapy after RSA.

Force Measurement

This window will allow the operator to first calibrate the sensor having known weights and then during surgery reads amplitude and direction of imposed force by deltoid on glenosphere.

7.2 Conclusion

A healthy shoulder is able to provide a range of motion equal to 2/3 of a sphere (Engin and Chen 1986) while in a shoulder suffering from deficient rotator cuff this range of motion is dramatically limited.

Review of shoulder anatomy and RSA, shows a gap in literature exists regarding the effect of initial geometrical (both anatomical and prosthetic) parameters on kinematics of shoulder both pre and post operation. This leaded to the development of a model to investigate the kinematics of native and reverse shoulders using simulated 3D models of shoulder using in MSC ADAMS.

Using the dynamic simulation, it was also possible to show the importance of the initial geometrical differences in individuals and how it can inform the placement of the implants. It also enables users to visualise the effect of lever arm beyond the range of motion possible by the deltoid contraction. This will have an effect on design of new implants glenoid to better control the lever arm length during abduction.

The musculoskeletal model was modelled using X-Ray and MRI images obtained from previous studies (Werner et al. 2008, Gutiérrez et al. 2009, Kircher et al. 2010, Saltzman et al. 2010, Lädermann et al. 2012, Gu and Yu 2013).

The musculoskeletal model then was validated against an adjustable mathematical model developed in MATLAB. It was concluded that to place the implant accurately, calibrated/standardise X-Ray images of individual's shoulder before the operation is needed. This was to extract individual geometrical measurements needed to calculate the various kinematic parameters.

This data provides a basis for developing an objective tool for pre and post op assessment of the kinematics of the shoulder. It can have other merits to it as it allows superposition of old and new shoulder to realise the effect of geometrical differences in kinematics, kinetics and moment arm and mechanical advantages they provide. The

ability to simulate the outcome before the operation will give surgeons more insight in to what can be expected or be achieved. The output can be recorded for reference and also provides insight into the mechanical advantage differences hence allowing for better surgical planning. Results from simulated model and mathematical model can also be used to validate each other. This is needed to ensure data integrity.

Using an image database of individuals' pre and post operatively, calculating the discussed kinematics parameters for each and correlating them with the outcome of surgery in long term, could inform surgeons intraoperatively about optimised placement of prosthesis to provide the maximum possible range of motion and least amount of pain.

Furthermore, development of a database informing the surgeon about the correlation between measured force and outcome of surgery could be a very useful tool and can have an impact on the training of new surgeons, outcome of the future surgeries. Better tool to quantify the forces will reduce the chances of premature failure and in the long terms will enable surgeons to adjust the correct tension first time and removing the need for revision surgeries due to mechanical failure.

In conclusion, regarding the fact that small differences in anatomic and prosthetic parameters can affect dramatically the outcome of RSA, the development of a structured approach/procedure for measurement is needed. This would enable all measurement on all patients to be taken on similar or identical planes to allow a more objective comparison of the Pre and post op range of motion to be conducted.

It is recommended as part of this research the need for setting up a national database of case studies that follow our protocol for imaging, placement and post operation assessment including the use of our force measurement system to allow better and more objective assessment of the whole episode.

It should be highlighted, that these models only consider geometrical and kinematics of the glenohumeral joint while there are many other patient characteristics such as muscle fibre type, muscle volume and bones shape which have not been taken into account in this study. Therefore, the prediction of subjective outcomes (pain relief and range of motion) needs more studies including mathematical and clinical approaches together.

While many of the parameters that are taken into account when designing and performing a restorative surgery are objective, there are some parameters that cannot be measured or quantified. This are usually felt and not precisely measured and their intensity or levels are at discretion of the surgeons and is based on their experience. For theses subjective measures, it is down to the surgeon's skill and experience to find the best prosthesis size and position during operation. The most important parameter, which is set by the surgeon during surgery, is the force applied to the contact area of glenohumeral joint during motion. This force is mostly generated by the passive reaction of the deltoid muscle on glenosphere within the glenohumeral joint and currently there is no mechanism except surgeons experience to measure and record this. This is achieved by moving patient's arm in different directions and feel this force using fingers natural haptic feedback and its intensity is judged adequate based on surgeon's experience. This force can be adjusted by placing different trial implants of various sizes to choose the best fit. This subjective ways of measuring the force in glenohumeral joint, usually caused by elastic properties of muscles are questioned in this thesis and a more objective method is proposed. This thesis criticizes these methods, concluding that direct force measurement on glenosphere using force sensors would be most effective if we are to reduce the number of revised surgery due to joints mechanical or kinematic failures. To be able to advise the surgeon regarding optimal deltoid tension while choosing implant size and positioning a force sensor measuring resultant of deltoid passive force on glenosphere can be used.

The biggest concern in development of force sensor for shoulder complex is validation of the sensors performance. Because it was not possible to directly put the sensor on a patient/cadaver's implanted shoulder hence an automatic joint simulator is designed and developed during this study to validate both force sensor and IMU for quantitative validations.

Accurate estimation of forces acting on glenosphere could be essential to improve outcome of surgery as well as implant design. The measure passive tension could be useful to advise the surgeon as to what implant size and positioning is the optimized one for individuals.

Shoulder disorders such as rotator cuff deficiency or glenohumeral/acromioclavicular joint problems - where the shoulder shows limited range of motion - can be assessed in terms of three dimensional ROM surface area and with EMG. It can also be used to

quantify and monitor progress of a rehabilitation program. In this study we have designed and developed a transducer using an IMU sensor combined with an EMG sensor to measure the maximum reachable envelope of motion in 3D space with simultaneous collection of deltoid activity.

7.3 Contribution to knowledge

New knowledge gained from simulated musculoskeletal model was used for development of a series of assessment tools. These tools are packed in a unique GUI associated with developed hardware enabling one to record all the mentioned parameters in a database to link them to outcome of RS.

Here are the contributions made in this dissertation:

- Expression of a musculoskeletal model of shoulder to study kinematics of shoulder before and after RSA. The Musculoskeletal model greatly reduces the complexity of real shoulder joint, resulting in an efficient comparison study of anatomic shoulder against reverse shoulder.
- The method proposed for X-ray processing to extract geometrical parameters and calculate kinematics based on them is new and innovative and constitute an additional contribution to knowledge.
- The proposed method for shoulder ROM and EMG assessment of itself is entirely novel and is therefore a further contribution to knowledge. This tool could quantify level of improvement of shoulder in terms of ROM and EMG.
- We have also developed an objective assessment tool that will give us knowledge of the exact initial contact force in shoulder joints. This knowledge never existed and until now it was impossible to obtain. This system will enable surgeons to set exact value of the contact force during the surgery and over time explore what should that force be.

7.4 Future Works

In this study a relatively small number of patients were recruited for X-Ray processing and shoulder ROM/EMG assessment. Regarding the force sensor, further validation on cadavers is needed. Below are proposed work packages, deliverables and milestones for future work:

Work Package	Deliverable	Milestone
Develop dedicated assessment software to calibrate, measure, quantify and extract all kinematic data needed to determine the true position of the implant and its center of rotations	Obtain ethics approval; Design and develop smart GUI; Design and develop imaging protocol to extract 3D data from 2D images	Dedicated software and calibrated X-ray images that will inform the kinematics of shoulder pre and post operation. Predict mechanical advantages over the entire range of motion of the deltoid in 2-plane at a time.
Develop a low cost shoulder assessment transducer artifact, protocol and evaluation system that combines data from IMU, EMG and optical transducer	Monitor, track and record kinematics data to inform the database; Obtain ethics approval; Development of a working system ready to be tested on volunteers and patients	Obtain absolute and relative kinematic data using IMU and optical transducer that linked to muscle activity using EMG. Develop an assessment score point that gives information about the factors limiting the shoulder movement
Develop a strain gauge based load cell/force transducer artifact and the associated electronics, hardware and software for passive measurement of the deltoid overall tension.	Obtain ethics approval before being applied intra operatively; Development of a transducer ready to be tested on fresh cadavers; Development of a transducer ready to be tested on dry bone models	Design of passive deltoid tension or joint contact force transducer artifact. Design of additional calibrated gauge rings to adjust pre-setting residual tension at shoulder joint
Create a database that includes anonymized patient data/information to find correlations between measured and calculated parameters and the outcome of surgery in the long term.	Develop relational database software to store and compare data or conduct more research; Create kinematics database of pre and post operation to store key biomechanics data; Create search engine to investigate the link between residual deltoid tension, kinematics parameters and joint functional outcome	Storing quantitative data from patients in a single database under a global network of database to allow sharing of information among scientists
Public engagement and dissemination	Advisory group meetings; Research report generation; Public seminars, focus group workshop, technical training; Introduction sessions through conferences, exhibitions; Journals publication	Knowledge and technology transfer. Application of technology in RSA

Table 7-1. Work packages, deliverables and milestones

References

Ackland, D. C., Roshan-Zamir, S., Richardson, M., and Pandy, M. G., 2011. Muscle and joint-contact loading at the glenohumeral joint after reverse total shoulder arthroplasty. *Journal of orthopaedic research : official publication of the Orthopaedic Research Society* [online], 29 (12), 1850–8. Available from: http://www.ncbi.nlm.nih.gov/pubmed/21567454 [Accessed 13 May 2014].

Alentorn-Geli, E., Guirro, P., and Santana, F., 2014. Treatment of fracture sequelae of the proximal humerus: comparison of hemiarthroplasty and reverse total shoulder arthroplasty. *Archives of Orthopaedic & Trauma Surgery*.

Anglin, C., Wyss, U. P., and Pichora, D. R., 2000. Shoulder prosthesis subluxation: Theory and experiment. *Journal of Shoulder and Elbow Surgery* [online], 9 (2), 104–114. Available from: http://linkinghub.elsevier.com/retrieve/pii/S1058274600900387 [Accessed 28 May 2014].

Anon., 2007. Surgical Technique + Design Rationale Delta Xtend.

Aslani, N., Noroozi, S., Hartley, R., Dupac, M., and Sewell, P., 2016. Assessment Of Key Parameters On The Performance Of The Deltoid Muscle In Reverse Shoulder Arthroplasty — A Modelling And Simulation-Based Study. *Journal of Mechanics in Medicine and Biology* [online], 1650072. Available from: http://dx.doi.org/10.1142/S021951941650072X.

Bergmann, G., Graichen, F., Bender, A., Kääb, M., Rohlmann, A., and Westerhoff, P., 2007. In vivo glenohumeral contact forces-Measurements in the first patient 7 months postoperatively. *Journal of Biomechanics* [online], 40 (10), 2139–2149. Available from: http://www.ncbi.nlm.nih.gov/pubmed/17169364 [Accessed 28 Apr 2014].

Berthonnaud, E., Morrow, M., Herzberg, G., An, K.-N., and Dimnet, J., 2010. Biomechanical Model Predicting Values of Muscle Forces in the Shoulder Girdle During Arm Elevation. *Journal of Mechanics in Medicine and Biology* [online], 10 (4), 643–666. Available from: http://www.worldscientific.com/doi/abs/10.1142/S0219519410003629 [Accessed 13 May 2014].

Boettcher, C. E., Ginn, K. A., and Cathers, I., 2008. Standard maximum isometric voluntary contraction tests for normalizing shoulder muscle EMG. *Journal of Orthopaedic Research*, 26 (12), 1591–1597.

Boileau, P., Melis, B., Duperron, D., Moineau, G., Rumian, A. P., and Han, Y., 2013. Revision surgery of reverse shoulder arthroplasty. *Journal of shoulder and elbow surgery / American Shoulder and Elbow Surgeons ... [et al.]* [online], 22 (10), 1359–70. Available from: http://www.ncbi.nlm.nih.gov/pubmed/23706884 [Accessed 13 May 2014].

Charlton, I. W., 2004. A model for the prediction of the forces at the glenohumeral joint. [online]. Available from: http://search.ebscohost.com/login.aspx?direct=true&db=edsble&AN=edsble.4078 67&site=eds-live&scope=site.

Chih-Chiang Chang A, 2013. Intraoperative Measurement Of Shoulder Joint Contact Forces. UNIVERSITY OF FLORIDA.

Crescini, D., Sardini, E., and Serpelloni, M., 2011. Design and test of an autonomous sensor for force measurements in human knee implants. *Sensors and Actuators A: Physical* [online], 166 (1), 1–8. Available from: http://linkinghub.elsevier.com/retrieve/pii/S092442471000508X [Accessed 7 Jan 2015].

Cristofolini, L., Marchetti, A., Cappello, A., and Viceconti, M., 2000. A novel transducer for the measurement of cement-prosthesis interface forces in cemented orthopaedic devices. *Medical engineering & physics* [online], 22 (7), 493–501. Available from: http://www.ncbi.nlm.nih.gov/pubmed/11165147.

Cta, D. and Prosthesis, R. S., 2004. Surgical Technique, Delta CTA.

Damm, P., Graichen, F., Rohlmann, A., Bender, A., and Bergmann, G., 2010. Total hip joint prosthesis for in vivo measurement of forces and moments. *Medical engineering & physics* [online], 32 (1), 95–100. Available from: http://www.ncbi.nlm.nih.gov/pubmed/19889565 [Accessed 13 May 2014].

Dinnes, J., Loveman, E., McIntyre, L., and Waugh, N., 2003. The effectiveness of diagnostic tests for the assessment of shoulder pain due to soft tissue disorders: a systematic review. *Health technology assessment (Winchester, England)*, 7 (29).

Djurić-Jovičić, M. D., Jovičić, N. S., and Popović, D. B., 2011. Kinematics of gait: New method for angle estimation based on accelerometers. *Sensors*, 11 (11), 10571–10585.

Doriot, N. and Wang, X., 2006. Effects of age and gender on maximum voluntary range of motion of the upper body joints. *Ergonomics*, 49 (3), 269–281.

Duncan, S., Sperling, J., and Kakinoki, Z., 2009. Resection arthroplasty of the shoulder. *MINERVA ORTOPEDICA E TRAUMATOLOGICA*.

Engin, A. E. and Chen, S.-M., 1986. Statistical Data Base for the Biomechanical Properties of the Human Shoulder Complex—II: Passive Resistive Properties Beyond the Shoulder Complex Sinus. *Journal of Biomechanical Engineering* [online], 108 (3), 222–227. Available from: http://dx.doi.org/10.1115/1.3138606.

Fässler, M., 2010. Force Sensing Technologies. *Studies on Mechatronics , ETH*, 1–49.

Favre, P., Sheikh, R., Fucentese, S. F., and Jacob, H. a C., 2005. An algorithm for estimation of shoulder muscle forces for clinical use. *Clinical biomechanics (Bristol, Avon)* [online], 20 (8), 822–33. Available from: http://www.ncbi.nlm.nih.gov/pubmed/15975696 [Accessed 13 May 2014].

Favre, P., Snedeker, J. G., and Gerber, C., 2009. Numerical modelling of the shoulder for clinical applications. *Philosophical transactions. Series A, Mathematical, physical, and engineering sciences*, 367, 2095–2118.

Flatow, E. L. and Harrison, A. K., 2011. A history of reverse total shoulder arthroplasty. *Clinical orthopaedics and related research* [online], 469 (9), 2432–9. Available from:

http://www.pubmedcentral.nih.gov/articlerender.fcgi?artid=3148354&tool=pmcen trez&rendertype=abstract [Accessed 13 May 2014].

Flavio Almeida Salles, A. Z. F., 2002. Isokinetic evaluation of eighteen male patients submitted to surgical corretion of acute acromioclavicular luxation with a minimum two-year follow-up. *ACTA ORTOP BRAS*, 10 (2), 19–24.

Flurin, H., Grey, S. G., Jones, R. B., Routman, H. D., Gilot, G. J., and Zuckerman, J. D., 2013. Scapular Notching in Reverse Shoulder Arthroplasty, 71 (4), 278–284.

Forchelet, D., Simoncini, M., Arami, A., Bertsch, A., Meurville, E., Aminian, K., Ryser, P., and Renaud, P., 2014. Enclosed electronic system for force measurements in knee implants. *Sensors (Basel, Switzerland)* [online], 14 (8), 15009–21. Available from: http://www.pubmedcentral.nih.gov/articlerender.fcgi?artid=4179003&tool=pmcen trez&rendertype=abstract [Accessed 4 Jan 2015].

Forte, F. C., de Castro, M. P., de Toledo, J. M., Ribeiro, D. C., and Loss, J. F., 2009. Scapular kinematics and scapulohumeral rhythm during resisted shoulder abduction--implications for clinical practice. *Physical therapy in sport : official journal of the Association of Chartered Physiotherapists in Sports Medicine* [online], 10 (3), 105–11. Available from: http://www.ncbi.nlm.nih.gov/pubmed/19616180 [Accessed 13 May 2014].

Frankle, M. a, Teramoto, A., Luo, Z.-P., Levy, J. C., and Pupello, D., 2009. Glenoid morphology in reverse shoulder arthroplasty: classification and surgical implications. *Journal of shoulder and elbow surgery / American Shoulder and Elbow Surgeons ... [et al.]* [online], 18 (6), 874–85. Available from: http://www.ncbi.nlm.nih.gov/pubmed/19482489 [Accessed 13 May 2014].

Fridén, J. and Lieber, R. L., 2001. Quantitative evaluation of the posterior deltoid to triceps tendon transfer based on muscle architectural properties. *The Journal of hand surgery* [online], 26 (1), 147–55. Available from: http://www.ncbi.nlm.nih.gov/pubmed/11172382 [Accessed 13 May 2014].

Grant, G. A., Goodkin, R., and Kliot, M., 1999. Evaluation and surgical management of peripheral nerve problems. *NEUROSURGERY* [online]. Available from: http://search.ebscohost.com/login.aspx?direct=true&db=edswsc&AN=000079368 700071&site=eds-live&scope=site.

Gritsenko, V., Dailey, E., Kyle, N., Taylor, M., Whittacre, S., and Swisher, A. K., 2015. Feasibility of Using Low-Cost Motion Capture for Automated Screening of Shoulder Motion Limitation after Breast Cancer Surgery. *PloS one* [online], 10 (6), e0128809. Available from: http://www.ncbi.nlm.nih.gov/pubmed/26076031%5Cnhttp://www.pubmedcentral. nih.gov/articlerender.fcgi?artid=PMC4468119.

Gu, G. and Yu, M. Y., 2013. Novel Physiotherapies Imaging Features and Clinical Significance of the Acromion Morphological Variations, 2–5.

Gupta, A. K., Chalmers, P. N., Rahman, Z., Bruce, B., Harris, J. D., McCormick, F., Abrams, G. D., and Nicholson, G. P., 2016. Reverse total shoulder arthroplasty in patients of varying body mass index. *Journal of Shoulder and Elbow Surgery*

[online], 23 (1), 35–42. Available from: http://dx.doi.org/10.1016/j.jse.2013.07.043.

Gutiérrez, S., Comiskey, C. a, Luo, Z.-P., Pupello, D. R., and Frankle, M. a, 2008. Range of impingement-free abduction and adduction deficit after reverse shoulder arthroplasty. Hierarchy of surgical and implant-design-related factors. *The Journal of bone and joint surgery. American volume* [online], 90 (12), 2606–15. Available from: http://www.ncbi.nlm.nih.gov/pubmed/19047705 [Accessed 13 May 2014].

Gutiérrez, S., Keller, T. S., Levy, J. C., Lee, W. E., and Luo, Z.-P., 2008. Hierarchy of stability factors in reverse shoulder arthroplasty. *Clinical orthopaedics and related research* [online], 466 (3), 670–6. Available from: http://www.pubmedcentral.nih.gov/articlerender.fcgi?artid=2505225&tool=pmcen trez&rendertype=abstract [Accessed 28 May 2014].

Gutiérrez, S., Luo, Z.-P., Levy, J., and Frankle, M. a, 2009. Arc of motion and socket depth in reverse shoulder implants. *Clinical biomechanics (Bristol, Avon)* [online], 24 (6), 473–9. Available from: http://www.ncbi.nlm.nih.gov/pubmed/19346036 [Accessed 13 May 2014].

Haering, D., Raison, M., and Begon, M., 2014. Measurement and description of three-dimensional shoulder range of motion with degrees of freedom interactions. *Journal of biomechanical engineering* [online], 136 (8), 1–6. Available from: http://europepmc.org/abstract/MED/24828544.

Han, J. J., Kurillo, G., Abresch, R. T., Nicorici, A., and Bajcsy, R., 2013. Validity , Reliability , and Sensitivity of a 3D Vision Sensor-based Upper Extremity Reachable Workspace Evaluation in Neuromuscular Diseases, 1–17.

Han JJ, de Bie E, Nicorici A, Abresch RT, Anthonisen C, Bajcsy R, Kurillo G, M. C., 2015. Reachable workspace and performance of upper limb (PUL) in Duchenne muscular dystrophy. *Neuromuscular Disorders* [online], 25 (April), S228. Available from: http://www.embase.com/search/results?subaction=viewrecord&from=export&id=L72163894%5Cnhttp://dx.doi.org/10.1016/j.nmd.2015.06.157.

Hodges, P. W., Gandevia, S. C., and Richardson, C. A., 1997. Contractions of specific abdominal muscles in postural tasks are affected by respiratory maneuvers. *Journal of Applied Physiology*, 83 (3), 753–760.

Hoenecke, H. R., Tibor, L. M., and D'Lima, D. D., 2012. Glenoid morphology rather than version predicts humeral subluxation: a different perspective on the glenoid in total shoulder arthroplasty. *Journal of shoulder and elbow surgery / American Shoulder and Elbow Surgeons ... [et al.]* [online], 21 (9), 1136–41. Available from: http://www.ncbi.nlm.nih.gov/pubmed/22079801 [Accessed 13 May 2014].

Hunt, A., Cross, A., Davis, J., Erdem, U., Herbert, A., Jenkins, R., Knott, A., Maclean, S., March, L., Tame, D., Thompson, G., Viney, D., Webb, J., and Wort, G., 2013. Guide to the Measurement of Force.

J.Tortora, G. and Derrickson, B. H., 2009. *Principles of Anatomy And Physiology (12th Edition)*.

Jacq, C., Meader, T., Emery, S., Simoncini, M., Meurville, E., and Ryser, P., 2014. Investigation of Polymer Thick-film Piezoresistors for Medical Wrist Rehabilitation and Artificial Knee Load Sensors. *Procedia Engineering* [online], 87, 1194–1197. Available from: http://linkinghub.elsevier.com/retrieve/pii/S1877705814024953 [Accessed 7 Jan 2015].

Jazayeri, R. and Kwon, Y. W., 2011. Evolution of the reverse total shoulder prosthesis. *Bulletin of the NYU hospital for joint diseases* [online], 69 (1), 50–5. Available from: http://www.ncbi.nlm.nih.gov/pubmed/21332439.

Jobin, C. M., Brown, G. D., Bahu, M. J., Gardner, T. R., Bigliani, L. U., Levine, W. N., and Ahmad, C. S., 2012. Reverse total shoulder arthroplasty for cuff tear arthropathy: the clinical effect of deltoid lengthening and center of rotation medialization. *Journal of shoulder and elbow surgery / American Shoulder and Elbow Surgeons ... [et al.]* [online], 21 (10), 1269–77. Available from: http://www.ncbi.nlm.nih.gov/pubmed/22056324 [Accessed 13 May 2014].

Johnson, G. R., Spalding, D., Nowitzke, A., and Bogdukt, N., 1996. MODELLING THE MUSCLES AND COORDINATE IMPLICATIONS OF THE SCAPULA DATA AND FUNCTIONAL. *Journal of biomechanics*, 29.

Jung, Y., Kang, D., and Kim, J., 2010. Upper body motion tracking with inertial sensors. *2010 IEEE International Conference on Robotics and Biomimetics* [online], (3), 1746–1751. Available from: http://ieeexplore.ieee.org/lpdocs/epic03/wrapper.htm?arnumber=5723595.

Kasman, G. and Wolf, S., 2002. SURFACE EMG MADE EASY : A Beginner ' s Guide for Rehabilitation Clinicians.

Kiet, T. K., Feeley, B. T., Naimark, M., Gajiu, T., Hall, S. L., Chung, T. T., and Ma, C. B., 2015. Shoulder: Outcomes after shoulder replacement: comparison between reverse and anatomic total shoulder arthroplasty. *Journal of Shoulder and Elbow Surgery*.

Kim, M.-S., Lim, K.-Y., Lee, D.-H., Kovacevic, D., and Cho, N.-Y., 2012. How does scapula motion change after reverse total shoulder arthroplasty? A preliminary report. *BMC musculoskeletal disorders* [online], 13 (1), 210. Available from: http://www.pubmedcentral.nih.gov/articlerender.fcgi?artid=3517751&tool=pmcentrez&rendertype=abstract [Accessed 13 May 2014].

Kircher, J., Morhard, M., Gavriilidis, I., Magosch, P., Lichtenberg, S., and Habermeyer, P., 2010. Is there an association between a low acromion index and osteoarthritis of the shoulder? *International orthopaedics* [online], 34 (7), 1005–10. Available from: http://www.pubmedcentral.nih.gov/articlerender.fcgi?artid=2989045&tool=pmcentrez&rendertype=abstract [Accessed 13 May 2014].

Klepps, S., Auerbach, J., Calhon, O., Lin, J., Cleeman, E., and Flatow, E., 2004. A cadaveric study on the anatomy of the deltoid insertion and its relationship to the deltopectoral approach to the proximal humerus. *Journal of Shoulder and Elbow Surgery* [online], 13 (3), 322–327. Available from: http://linkinghub.elsevier.com/retrieve/pii/S1058274603003288 [Accessed 13 May

2014].

Koh, K. H., Han, K. Y., Yoon, Y. C., Lee, S. W., and Yoo, J. C., 2013. True anteroposterior (Grashey) view as a screening radiograph for further imaging study in rotator cuff tear. *Journal of Shoulder and Elbow Surgery* [online], 22 (7), 901–907. Available from: http://dx.doi.org/10.1016/j.jse.2012.09.015.

Kolber, M. J., Salamh, P. A., Hanney, W. J., and Samuel Cheng, M., 2013. Clinimetric evaluation of the disabilities of the arm, shoulder, and hand (DASH) and Quick DASH questionnaires for patients with shoulder disorders. *Physical Therapy Reviews* [online], 19 (3), 163–173. Available from: http://www.tandfonline.com/doi/abs/10.1179/1743288X13Y.0000000125.

Kontaxis, a. and Johnson, G. R., 2009. The biomechanics of reverse anatomy shoulder replacement − A modelling study. *Clinical Biomechanics* [online], 24 (3), 254–260. Available from: http://linkinghub.elsevier.com/retrieve/pii/S0268003308003525 [Accessed 13 May 2014].

Kuechle, D. K., Newman, S. R., Itoi, E., Niebur, G. L., Morrey, B. F., and An, K. N., 2000. The relevance of the moment arm of shoulder muscles with respect to axial rotation of the glenohumeral joint in four positions. *Clinical biomechanics (Bristol, Avon)* [online], 15 (5), 322–9. Available from: http://www.ncbi.nlm.nih.gov/pubmed/10758292.

Kwon, Y. W., Forman, R. E., Walker, P. S., and Zuckerman, J. D., 2010. Analysis of reverse total shoulder joint forces and glenoid fixation. *Bulletin of the NYU hospital for joint diseases* [online], 68 (4), 273–80. Available from: http://www.ncbi.nlm.nih.gov/pubmed/21162705.

Lädermann, A., Walch, G., Lubbeke, A., Drake, G. N., Melis, B., Bacle, G., Collin, P., Edwards, T. B., and Sirveaux, F., 2012. Influence of arm lengthening in reverse shoulder arthroplasty. *Journal of shoulder and elbow surgery / American Shoulder and Elbow Surgeons ... [et al.]* [online], 21 (3), 336–41. Available from: http://www.ncbi.nlm.nih.gov/pubmed/21816632 [Accessed 13 May 2014].

Lee, S. H., Yoon, C., Chung, S. G., Kim, H. C., Kwak, Y., Park, H. W., and Kim, K., 2015. Measurement of shoulder range of motion in patients with adhesive capsulitis using a Kinect. *PLoS ONE*, 10 (6).

Lin, C.-J., Lin, P.-C., Guo, L.-Y., and Su, F.-C., 2011. Prediction of applied forces in handrim wheelchair propulsion. *Journal of biomechanics* [online], 44 (3), 455–60. Available from: http://www.ncbi.nlm.nih.gov/pubmed/20980008 [Accessed 13 May 2014].

Ludewig, P. M., Hassett, D. R., Laprade, R. F., Camargo, P. R., and Braman, J. P., 2010. Comparison of scapular local coordinate systems. *Clinical biomechanics* [online], 25 (5), 415–21. Available from: http://www.pubmedcentral.nih.gov/articlerender.fcgi?artid=2862764&tool=pmcentrez&rendertype=abstract [Accessed 13 May 2014].

Maier, M. W., Niklasch, M., Dreher, T., Zeifang, F., Rettig, O., Klotz, M. C., Wolf, S. I., and Kasten, P., 2014. Motion patterns in activities of daily living: 3- year

longitudinal follow-up after total shoulder arthroplasty using an optical 3D motion analysis system. *BMC Musculoskeletal Disorders* [online], 15 (1) (no (244), 1–8. Available from: http://ovidsp.ovid.com/ovidweb.cgi?T=JS&CSC=Y&NEWS=N&PAGE=fulltext& D=emed12&AN=2014516214%5Cnhttp://nt2yt7px7u.search.serialssolutions.com/ ?sid=OVID:Embase&genre=article&id=pmid:&id=doi:10.1186/1471-2474-15-244&issn=1471-2474&volume=15&issue=1&spage=no+pag.

Mansat, P., Coutié, A.-S., Bonnevialle, N., Rongières, M., Mansat, M., and Bonnevialle, P., 2013. Shoulder: Resurfacing humeral prosthesis: do we really reconstruct the anatomy? *Journal of Shoulder and Elbow Surgery*.

Matsuki, K., Matsuki, K. O., Yamaguchi, S., Ochiai, N., Sasho, T., Sugaya, H., Toyone, T., Wada, Y., Takahashi, K., and Banks, S. a, 2012. Dynamic in vivo glenohumeral kinematics during scapular plane abduction in healthy shoulders. *The Journal of orthopaedic and sports physical therapy* [online], 42 (2), 96–104. Available from: http://www.ncbi.nlm.nih.gov/pubmed/22030448 [Accessed 12 May 2014].

McClure, P. W. and Michener, L. A., 2014. Staged Approach for Rehabilitation Classification: Shoulder Disorders (STAR-Shoulder). *Physical therapy* [online], 95 (5), 791–800. Available from: http://ptjournal.apta.org/content/95/5/791.full.

Meyer, D. C., Rahm, S., Farshad, M., Lajtai, G., and Wieser, K., 2013. Deltoid muscle shape analysis with magnetic resonance imaging in patients with chronic rotator cuff tears. *BMC Musculoskelet Disord*, 14, 247.

Millard, M., Uchida, T., Seth, A., and Delp, S. L., 2013. Flexing computational muscle: modeling and simulation of musculotendon dynamics. *Journal of biomechanical engineering* [online], 135 (2), 21005. Available from: http://www.pubmedcentral.nih.gov/articlerender.fcgi?artid=3705831&tool=pmcen trez&rendertype=abstract [Accessed 30 Apr 2014].

Mimata, Y., Nishida, J., Sato, K., Suzuki, Y., and Doita, M., 2015. Shoulder: Glenohumeral arthrodesis for malignant tumor of the shoulder girdle. *In Journal of Shoulder and Elbow Surgery*.

Mitchell, C., 2008. Management of shoulder disorders in primary care. *Hands on-Arthritis Research Campaign-* [online], (207711). Available from: http://gptt.com.au/Exam preparation CK Khong/RACGP/Check/MS hot topics/Shoulder problems.pdf.

Do Moon, G., Lim, J. Y., Kim, D. Y., and Kim, T. H., 2015. Comparison of Maitland and Kaltenborn mobilization techniques for improving shoulder pain and range of motion in frozen shoulders. *Journal of physical therapy science* [online], 27 (5), 1391–5. Available from: http://www.pubmedcentral.nih.gov/articlerender.fcgi?artid=4483405&tool=pmcen trez&rendertype=abstract.

Moser, T., Lecours, J., Michaud, J., Bureau, N. J., Guillin, R., and Cardinal, É., 2013. The deltoid, a forgotten muscle of the shoulder. *Skeletal radiology* [online], 42 (10), 1361–75. Available from: http://www.ncbi.nlm.nih.gov/pubmed/23784480 [Accessed 13 May 2014].

Nagai, K., Tateuchi, H., Takashima, S., Miyasaka, J., Hasegawa, S., Arai, R., Tsuboyama, T., and Ichihashi, N., 2013. Effects of trunk rotation on scapular kinematics and muscle activity during humeral elevation. *Journal of electromyography and kinesiology : official journal of the International Society of Electrophysiological Kinesiology* [online], 23 (3), 679–87. Available from: http://www.ncbi.nlm.nih.gov/pubmed/23428332 [Accessed 13 May 2014].

Nam, D., Kepler, C. K., Neviaser, a S., Jones, K. J., Wright, T. M., Craig, E. V, and Warren, R. F., 2010. Reverse total shoulder arthroplasty: current concepts, results, and component wear analysis. *The Journal of bone and joint surgery. American volume* [online], 92 Suppl 2, 23–35. Available from: http://www.ncbi.nlm.nih.gov/pubmed/21189245 [Accessed 8 May 2014].

Naveed, M. a, Kitson, J., and Bunker, T. D., 2011. The Delta III reverse shoulder replacement for cuff tear arthropathy: a single-centre study of 50 consecutive procedures. *The Journal of bone and joint surgery. British volume* [online], 93 (1), 57–61. Available from: http://www.ncbi.nlm.nih.gov/pubmed/21196544 [Accessed 10 May 2014].

Neer, C. S. 2nd, Craig, E. V, and Fukuda, H., 1983. Cuff-tear arthropathy. *The Journal of bone and joint surgery. American volume*, 65 (9), 1232–1244.

Nikooyan, a a, Veeger, H. E. J., Westerhoff, P., Graichen, F., Bergmann, G., and van der Helm, F. C. T., 2010. Validation of the Delft Shoulder and Elbow Model using in-vivo glenohumeral joint contact forces. *Journal of biomechanics* [online], 43 (15), 3007–14. Available from: http://www.ncbi.nlm.nih.gov/pubmed/20655049 [Accessed 29 Apr 2014].

Nusser, M., Fehle, A., and Senner, V., 2012. Preliminary Studies for Validation of a Novel Sensor Fiber to Measure Forces in Artificial Knee Ligaments. *Procedia Engineering* [online], 34, 236–241. Available from: http://linkinghub.elsevier.com/retrieve/pii/S1877705812018401 [Accessed 7 Jan 2015].

Onstot, B. R., Jacofsky, M. C., and Hansen, M. L., 2013. Muscle force and excursion requirements and moment arm analysis of a posterior-superior offset reverse total shoulder prosthesis. *Bulletin of the Hospital for Joint Disease (2013)* [online], 71 Suppl 2 (Suppl 2), S25-30. Available from: http://www.ncbi.nlm.nih.gov/pubmed/24328576.

Palermo, E., Rossi, S., Marini, F., Patanè, F., and Cappa, P., 2014. Experimental evaluation of accuracy and repeatability of a novel body-to-sensor calibration procedure for inertial sensor-based gait analysis. *Measurement: Journal of the International Measurement Confederation* [online], 52, 145–155. Available from: http://dx.doi.org/10.1016/j.measurement.2014.03.004.

Pearl, M. L., Sidles, J. A., Lippitt, S. B., Harryman II, D. T., and Matsen III, F. A., 1992. Codman's paradox: Sixty years later. *Journal of Shoulder and Elbow Surgery* [online], 1 (4), 219–225. Available from: http://dx.doi.org/10.1016/1058-2746(92)90017-W.

Permeswaran, V. N., 2014. Understanding mechanical trade-offs in changing centers of rotation for reverse shoulder arthroplasty design. [online]. Available from:

http://ir.uiowa.edu/etd/4716/%5Cnhttp://files/821/viewcontent.pdf%5Cnhttp://ir.ui owa.edu/cgi/viewcontent.cgi?article=5232&context=etd.

Post, M. and Jablon, M., 1983. Constrained total shoulder arthroplasty. Long-term follow-up observations. *Clinical Orthopaedics and Related Research.*

Reinold, M. M., Macrina, L. C., Wilk, K. E., Fleisig, G. S., Dun, S., Barrentine, S. W., Ellerbusch, M. T., and Andrews, J. R., 2007. Electromyographic Analysis of the Supraspinatus and Deltoid Muscles During 3 Common Rehabilitation Exercises. *Journal of athletic training*, 42 (4), 464–469.

Reinold, M. M., Wilk, K. E., Fleisig, G. S., Zheng, N., Barrentine, S. W., Chmielewski, T., Cody, R. C., Jameson, G. G., and Andrews, J. R., 2004. Electromyographic analysis of the rotator cuff and deltoid musculature during common shoulder external rotation exercises. *The Journal of orthopaedic and sports physical therapy*, 34, 385–394.

Rettig, O., Krautwurst, B., Maier, M. W., and Wolf, S. I., 2015. Definition of anatomical zero positions for assessing shoulder pose with 3D motion capture during bilateral abduction of the arms. *BMC musculoskeletal disorders* [online], 16, 383. Available from: http://www.pubmedcentral.nih.gov/articlerender.fcgi?artid=4673792&tool=pmcen trez&rendertype=abstract.

Ribeiro, D. C., de Toledo, J. M., Krug, R. C., and Loss, J. F., 2009. A comparison between two models of shoulder muscle force estimation. *Journal of applied biomechanics* [online], 25 (1), 43–53. Available from: http://www.ncbi.nlm.nih.gov/pubmed/19299829.

Roche, C. P., Diep, P., Hamilton, M. a, Flurin, P.-H., and Routman, H. D., 2013. Comparison of bone removed with reverse total shoulder arthroplasty. *Bulletin of the Hospital for Joint Disease (2013)* [online], 71 Suppl 2 (Suppl 2), S36-40. Available from: http://www.ncbi.nlm.nih.gov/pubmed/24328578.

Sakaki, Y., Kaneko, F., Watanabe, K., Kobayashi, T., Katayose, M., Aoki, N., Shibata, E., and Yamashita, T., 2013. Effects of different movement directions on electromyography recorded from the shoulder muscles while passing the target positions. *Journal of Electromyography and Kinesiology* [online], 23 (6), 1362–1369. Available from: http://www.ncbi.nlm.nih.gov/pubmed/24113424 [Accessed 13 May 2014].

Sakoma, Y., Sano, H., Shinozaki, N., Itoigawa, Y., Yamamoto, N., Ozaki, T., and Itoi, E., 2011. Anatomical and functional segments of the deltoid muscle. *Journal of anatomy* [online], 218 (2), 185–190. Available from: http://www.pubmedcentral.nih.gov/articlerender.fcgi?artid=3042752&tool=pmcen trez&rendertype=abstract [Accessed 13 May 2014].

Saltzman, M. D., Mercer, D. M., Warme, W. J., Bertelsen, A. L., and Matsen, F. a, 2010. A method for documenting the change in center of rotation with reverse total shoulder arthroplasty and its application to a consecutive series of 68 shoulders having reconstruction with one of two different reverse prostheses. *Journal of shoulder and elbow surgery / American Shoulder and Elbow Surgeons ... [et al.]* [online], 19 (7), 1028–33. Available from:

http://www.ncbi.nlm.nih.gov/pubmed/20435489 [Accessed 13 May 2014].

Sanchez-Sotelo, J., 2011. Total shoulder arthroplasty. *The open orthopaedics journal* [online], 5, 106–14. Available from: http://www.pubmedcentral.nih.gov/articlerender.fcgi?artid=3093753&tool=pmcen trez&rendertype=abstract.

Schamblin, M., Gupta, R., Yang, B. Y., McGarry, M. H., McMaster, W. C., and Lee, T. Q., 2009. In vitro quantitative assessment of total and bipolar shoulder arthroplasties: a biomechanical study using human cadaver shoulders. *Clinical biomechanics (Bristol, Avon)* [online], 24 (8), 626–31. Available from: http://www.ncbi.nlm.nih.gov/pubmed/19501938 [Accessed 13 May 2014].

Schwartz, D. G., Kang, S. H., Lynch, T. S., Edwards, S., Nuber, G., Zhang, L.-Q., and Saltzman, M., 2013. The anterior deltoid's importance in reverse shoulder arthroplasty: a cadaveric biomechanical study. *Journal of shoulder and elbow surgery / American Shoulder and Elbow Surgeons ... [et al.]* [online], 22 (3), 357–64. Available from: http://www.ncbi.nlm.nih.gov/pubmed/22608931 [Accessed 13 May 2014].

Seminati, E., Marzari, A., Vacondio, O., and Minetti, A. E., 2015. Shoulder 3D range of motion and humerus rotation in two volleyball spike techniques: injury prevention and performance. *Sports Biomechanics* [online], 14 (July), 1–16. Available from: http://www.tandfonline.com/doi/full/10.1080/14763141.2015.1052747.

Sharma, S. P., Bærheim, A., and Kvåle, A., 2015. Passive range of motion in patients with adhesive shoulder capsulitis, an intertester reliability study over eight weeks. *BMC musculoskeletal disorders* [online], 16, 37. Available from: http://www.pubmedcentral.nih.gov/articlerender.fcgi?artid=4340115&tool=pmcen trez&rendertype=abstract.

Steenbrink, F., de Groot, J. H., Veeger, H. E. J., van der Helm, F. C. T., and Rozing, P. M., 2009. Glenohumeral stability in simulated rotator cuff tears. *Journal of biomechanics* [online], 42 (11), 1740–5. Available from: http://www.ncbi.nlm.nih.gov/pubmed/19450803 [Accessed 13 May 2014].

Terrier, A., Aeberhard, M., Michellod, Y., Mullhaupt, P., Gillet, D., Farron, A., and Pioletti, D. P., 2010. A musculoskeletal shoulder model based on pseudo-inverse and null-space optimization. *Medical engineering & physics* [online], 32 (9), 1050–6. Available from: http://www.ncbi.nlm.nih.gov/pubmed/20709589 [Accessed 13 May 2014].

Terrier, A., Vogel, A., Capezzali, M., and Farron, A., 2008. An algorithm to allow humerus translation in the indeterminate problem of shoulder abduction. *Medical engineering & physics* [online], 30 (6), 710–6. Available from: http://www.ncbi.nlm.nih.gov/pubmed/17826295 [Accessed 13 May 2014].

Terrier, a, Reist, A., Merlini, F., and Farron, A., 2008. Simulated joint and muscle forces in reversed and anatomic shoulder prostheses. *The Journal of bone and joint surgery. British volume* [online], 90 (6), 751–6. Available from: http://www.ncbi.nlm.nih.gov/pubmed/18539668 [Accessed 13 May 2014].

Thelen, D. G., 2003. Adjustment of muscle mechanics model parameters to simulate

dynamic contractions in older adults. *Journal of biomechanical engineering* [online], 125 (1), 70–77. Available from: http://biomechanical.asmedigitalcollection.asme.org/article.aspx?articleid=1409437 [Accessed 8 May 2014].

Valenti, R., Dryanovski, I., and Xiao, J., 2015. Keeping a Good Attitude: A Quaternion-Based Orientation Filter for IMUs and MARGs. *Sensors* [online], 15 (8), 19302–19330. Available from: http://www.mdpi.com/1424-8220/15/8/19302/.

Veeger, H. E. J., Rozendaal, L. a, and van der Helm, F. C. T., 2002. Load on the shoulder in low intensity wheelchair propulsion. *Clinical biomechanics (Bristol, Avon)* [online], 17 (3), 211–8. Available from: http://www.ncbi.nlm.nih.gov/pubmed/11937259.

Walker, M., Brooks, J., Willis, M., and Frankle, M., 2011. How reverse shoulder arthroplasty works. *Clinical orthopaedics and related research* [online], 469 (9), 2440–51. Available from: http://www.pubmedcentral.nih.gov/articlerender.fcgi?artid=3148368&tool=pmcentrez&rendertype=abstract [Accessed 28 May 2014].

Werner, B. S., Daggett, M., Carrillon, Y., and Walch, G., 2015. Evaluation of lengthening in reverse shoulder arthroplasty comparing X-rays and computerised tomography. *International Orthopaedics*, 39 (12), 2389–2394.

Werner, C. M. L., Conrad, S. J., Meyer, D. C., Keller, A., Hodler, J., and Gerber, C., 2008. Intermethod agreement and interobserver correlation of radiologic acromiohumeral distance measurements. *Journal of shoulder and elbow surgery / American Shoulder and Elbow Surgeons ... [et al.]* [online], 17 (2), 237–40. Available from: http://www.ncbi.nlm.nih.gov/pubmed/18162412 [Accessed 13 May 2014].

Westerhoff, P., Graichen, F., Bender, A., Halder, A., Beier, A., Rohlmann, A., and Bergmann, G., 2009. In vivo measurement of shoulder joint loads during activities of daily living. *Journal of biomechanics* [online], 42 (12), 1840–9. Available from: http://www.ncbi.nlm.nih.gov/pubmed/19643418 [Accessed 13 May 2014].

Wickham, J. B. and Brown, J. M. M., 2012. The function of neuromuscular compartments in human shoulder muscles. *Journal of Neurophysiology*, 107 (1), 336–345.

Wierks, C., Skolasky, R. L., Ji, J. H., and McFarland, E. G., 2009. Reverse total shoulder replacement: Intraoperative and early postoperative complications. *Clinical Orthopaedics and Related Research*, 467, 225–234.

De Wilde, L., Audenaert, E., Barbaix, E., Audenaert, A., and Soudan, K., 2002. Consequences of deltoid muscle elongation on deltoid muscle performance: a computerised study. *Clinical biomechanics* [online], 17 (7), 499–505. Available from: http://www.ncbi.nlm.nih.gov/pubmed/12206940.

Wolf, S. I., Fradet, L., and Rettig, O., 2009. Conjunct rotation: Codman's paradox revisited. *Medical {&} Biological Engineering {&} Computing* [online], 47 (5), 551–556. Available from: http://dx.doi.org/10.1007/s11517-009-0484-6.
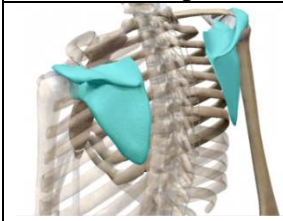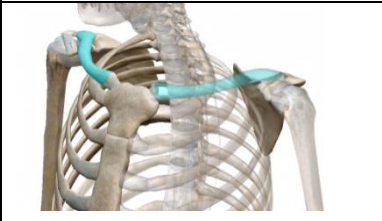
Wright, T., Samitier, G., Alentorn-Geli, E., and Torrens, C., 2015. Reverse shoulder arthroplasty. Part 1: Systematic review of clinical and functional outcomes. *International Journal of Shoulder Surgery* [online], 9 (1), 24. Available from: http://www.internationalshoulderjournal.org/text.asp?2015/9/1/24/150226.
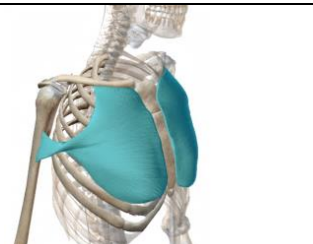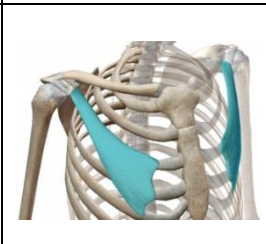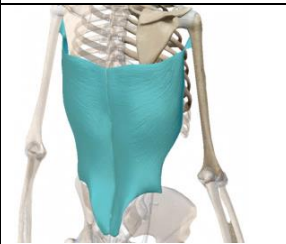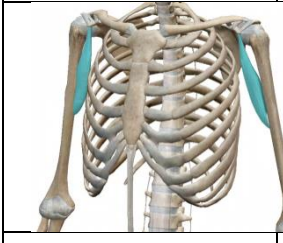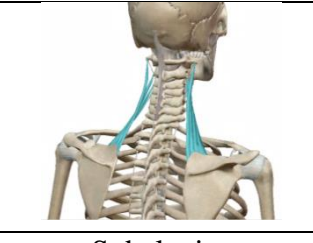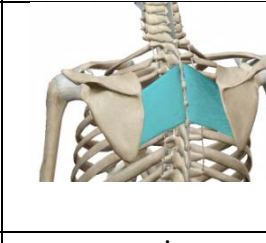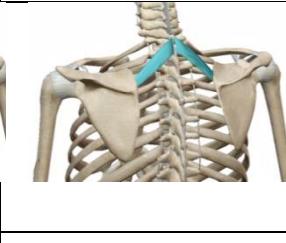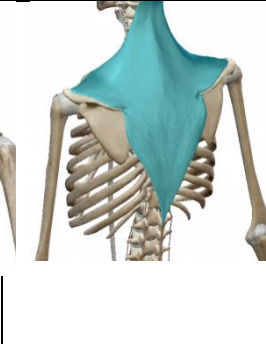
Yu, J. H. and Lee, G. C., 2013. Comparison of shoulder range of motion, strength, and endurance in amateur pitchers practicing repetitive overhead throwing. *Isokinetics and Exercise Science*, 21 (2), 135–140.
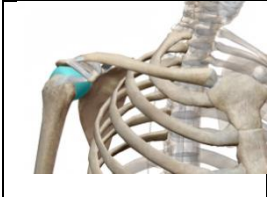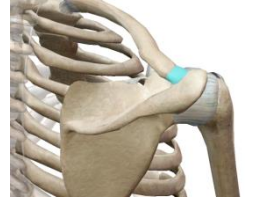
Appendix

A.I. Shoulder bones, muscles and ligaments

Bones		
scapula	clavicle	Humerus

Other Muscles			
Teres Major	Pectoralis Major	Pectoralis Minor	Latissimus dorsi
coracobrachialis	levator scapula	Rhomboid major	Rhomboid minor
serratus	Subclavius	trapezius	

Ligaments			
Capsular Ligament Superior Glenohumeral Ligament Middle Glenohumeral Ligament Inferior Glenohumeral Ligament	Coracohumeral Ligament	Coracoacromial Ligament	Coracoclavicular Ligament (Trapezoid Portion)
Coracoclavicular Ligament (Conoid Portion)	Acromioclavicular Ligament	Superior transverse Scapular Ligament	Sternoclavicular Ligament

A.II. X-ray ethical approval

The Royal Bournemouth and **NHS**
Christchurch Hospitals
NHS Foundation Trust

The Royal Bournemouth Hospital
Castle Lane East
Bournemouth
Dorset
United Kingdom
BH7 7DW

Tel: 01202 303626
www.rbch.nhs.uk

Mr Navid Aslani
Bournemouth University
Fern Barrow
Poole
BH12 5BB
Dorset

23/11/2015

Dear Mr Aslani,

Reference: Investigation of deltoid kinematics and pretension in Reverse Shoulder Arthroplasty (RSA)
REC reference: N/A
IRAS Project ID: N/A

I am pleased to inform you that this project has now received approvals from all parties and that you now have formal permission to start.

Please see the Terms and Conditions for undertaking research at the Trust at:
http://dorsetresearch.org/docs/rbh/TC_for_research_at_RBCH.pdf.

In accordance with NIHR 70 day recruitment targets, the first patient should be recruited by 31/01/2016.

Please let me know when you officially start and I would be grateful for a progress report annually.

Good luck with the study,

Caroline Jamieson-Leadbitter
Head of Research

116

Research Ethics Checklist

Reference Id	8845
Status	Approved
Date Approved	05/01/2017

Researcher Details

Name	Navid Aslani
School	Faculty of Science & Technology
Status	Postgraduate Research (MRes, MPhil, PhD, DProf, DEng)
Course	Postgraduate Research
Have you received external funding to support this research project?	No
Please list any persons or institutions that you will be conducting joint research with, both internal to BU as well as external collaborators.	siamak noroozi

Project Details

Title	Investigating the Ideal Deltoid Kinematics and Tension in Reverse Shoulder Arthroplasty (RSA)
Proposed Start Date of Data Collection	18/08/2015
Proposed End Date of Project	08/01/2017
Original Supervisor	Siamak Noroozi
Approver	Sarah Bell

117

A.III. X-ray patient's consent form

Bournemouth University

Patient Informed Consent Form

Full title of project: Investigating the Ideal Deltoid Kinematics and Tension in Reverse Shoulder Arthroplasty (RSA)
Name, position and contact details of researcher:
Navid Aslani. PhD Researcher in Biomechanical Engineering in Bournemouth University.
Poole House P517, Talbot Campus ,Fern Barrow, Poole, Dorset BH12 5BB
Name, position and contact details of supervisor:
Professor Siamak Noroozi
Poole House P124, Talbot Campus, Fern Barrow, Poole, BH12 5BB

Please initial all boxes

I confirm that I have read and understood the participant information sheet for the above research project. I have had the opportunity to consider the information, ask questions and have had these answered satisfactorily.

I understand that my participation is voluntary and that I am free to withdraw up to the point where the data is anonymised, without giving reason and without there being any negative consequences. In addition, should I not wish to answer any particular question(s), complete a test or give a sample, I am free to decline.

I give permission for members of the research team to have access to my anonymised responses. I understand that my name will not be linked with the research materials, and I will not be identified or identifiable in the report or reports that result from the research.

I understand that relevant sections of my medical notes and data collected during the study

I agree to images taken of myself being used in the publication of scientific papers, providing they are anonymised. I understand that once published these images could be seen by anyone, and that they may be published on the internet. I also understand that once published neither I nor the authors of the publication will have control over who may view these images.

I agree to take part in the above research project.

_____   _____
_____
Name of Participant Date   Signature

Name of Researcher   Date   Signature

118

A.IV. X-ray processing Matlab code

```matlab
function varargout = COR2(varargin)
% COR2 MATLAB code for COR2.fig
%      COR2, by itself, creates a new COR2 or raises the existing
%      singleton*.
%
%      H = COR2 returns the handle to a new COR2 or the handle to
%      the existing singleton*.
%
%      COR2('CALLBACK',hObject,eventData,handles,...) calls the local
%      function named CALLBACK in COR2.M with the given input
arguments.
%
%      COR2('Property','Value',...) creates a new COR2 or raises the
%      existing singleton*.  Starting from the left, property value
pairs are
%      applied to the GUI before COR2_OpeningFcn gets called.  An
%      unrecognized property name or invalid value makes property
application
%      stop.  All inputs are passed to COR2_OpeningFcn via varargin.
%
%      *See GUI Options on GUIDE's Tools menu.  Choose "GUI allows
only one
%      instance to run (singleton)".
%
% See also: GUIDE, GUIDATA, GUIHANDLES

% Edit the above text to modify the response to help COR2

% Last Modified by GUIDE v2.5 04-May-2016 14:32:29

% Begin initialization code - DO NOT EDIT
gui_Singleton = 1;
gui_State = struct('gui_Name',       mfilename, ...
                   'gui_Singleton',  gui_Singleton, ...
                   'gui_OpeningFcn', @COR2_OpeningFcn, ...
                   'gui_OutputFcn',  @COR2_OutputFcn, ...
                   'gui_LayoutFcn',  [] , ...
                   'gui_Callback',   []);
if nargin && ischar(varargin{1})
    gui_State.gui_Callback = str2func(varargin{1});
end

if nargout
    [varargout{1:nargout}] = gui_mainfcn(gui_State, varargin{:});
else
    gui_mainfcn(gui_State, varargin{:});
end
% End initialization code - DO NOT EDIT

% --- Executes just before COR2 is made visible.
function COR2_OpeningFcn(hObject, eventdata, handles, varargin)
% This function has no output args, see OutputFcn.
% hObject    handle to figure
% eventdata  reserved - to be defined in a future version of MATLAB
% handles    structure with handles and user data (see GUIDATA)
% varargin   command line arguments to COR2 (see VARARGIN)

% Choose default command line output for COR2
```

```matlab
handles.output = hObject;

% Update handles structure
guidata(hObject, handles);

% UIWAIT makes COR2 wait for user response (see UIRESUME)
% uiwait(handles.figure1);


% --- Outputs from this function are returned to the command line.
function varargout = COR2_OutputFcn(hObject, eventdata, handles)
% varargout  cell array for returning output args (see VARARGOUT);
% hObject    handle to figure
% eventdata  reserved - to be defined in a future version of MATLAB
% handles    structure with handles and user data (see GUIDATA)

% Get default command line output from handles structure
varargout{1} = handles.output;

%UPLOADING IMAGE PRE-OP
% --- Executes on button press in pushbutton1.
function pushbutton1_Callback(hObject, eventdata, handles)
% hObject    handle to pushbutton1 (see GCBO)
% eventdata  reserved - to be defined in a future version of MATLAB
% handles    structure with handles and user data (see GUIDATA)
global imag selectz
imag=uigetfile({'*.jpg';'*.bmp'},'File Selector');

imag=imread(imag);
axes(handles.axes1);
cla reset

imshow(imag);
selectz=1;
assignin('base','selectz',selectz);
assignin('base','imag',imag);
%UPLOADING IMAGE POST-OP
% --- Executes on button press in pushbutton16.
function pushbutton16_Callback(hObject, eventdata, handles)
% hObject    handle to pushbutton16 (see GCBO)
% eventdata  reserved - to be defined in a future version of MATLAB
% handles    structure with handles and user data (see GUIDATA)
global imag2 selectz
imag2=uigetfile({'*.jpg';'*.bmp'},'File Selector');

imag2=imread(imag2);
axes(handles.axes1);
cla reset

imshow(imag2);
selectz=2;
assignin('base','selectz',selectz);
assignin('base','imag2',imag2);


%FINDING COR
% --- Executes on button press in pushbutton2.
function pushbutton2_Callback(hObject, eventdata, handles)
% hObject    handle to pushbutton2 (see GCBO)
% eventdata  reserved - to be defined in a future version of MATLAB
```

```matlab
% handles    structure with handles and user data (see GUIDATA)
global xo1 yo1 xo2 yo2 xo3 yo3 xcor_pre ycor_pre xx_pre yy_pre selectz
xcor_post ycor_post xx_post yy_post
[xo1,yo1]=ginput(1);
hold on
axes(handles.axes1);
plot(xo1,yo1 , '.r', 'MarkerSize',20);
grid on

[xo2,yo2]=ginput(1);
hold on
axes(handles.axes1);
plot(xo2,yo2, '.r', 'MarkerSize',20);
grid on

[xo3,yo3]=ginput(1);
hold on
axes(handles.axes1);
plot(xo3,yo3, '.r', 'MarkerSize',20);
grid on

xm1=(xo2+xo1)/2;
ym1=(yo2+yo1)/2;

xm2=(xo3+xo2)/2;
ym2=(yo3+yo2)/2;

ma=(yo2-yo1)/(xo2-xo1);
mb=(yo3-yo2)/(xo3-xo2);

mar=-1/ma;
mbr=-1/mb;

xcor=(mar*xm1-mbr*xm2+ym2-ym1)/(mar-mbr);
ycor=mar*(xcor-xm1)+ym1;
% axes(handles.axes1);
plot(xcor,ycor, '.black', 'MarkerSize',30);
plot([xcor-100 xcor+100], [ycor ycor],'LineWidth',3);

%CIRCLE
r=sqrt((xcor-xo1)^2+(ycor-yo1)^2);

zz=0:0.1:2*pi;
xx=r*cos(zz)+xcor;
yy=r*sin(zz)+ycor;
plot(xx,yy)

if selectz ==1
    xcor_pre=xcor;
    ycor_pre=ycor;
    xx_pre=xx;
    yy_pre= yy;
assignin('base','xcor_pre',xcor_pre);
assignin('base','ycor_pre',ycor_pre);
assignin('base','xx_pre',xx_pre);
assignin('base','yy_pre',yy_pre);
end

if selectz ==2
```

```matlab
    xcor_post=xcor;
    ycor_post=ycor;
    xx_post=xx;
    yy_post= yy;
assignin('base','xcor_post',xcor_post);
assignin('base','ycor_post',ycor_post);
assignin('base','xx_post',xx_post);
assignin('base','yy_post',yy_post);
end


%ACROMION
% --- Executes on button press in pushbutton3.
function pushbutton3_Callback(hObject, eventdata, handles)
% hObject    handle to pushbutton3 (see GCBO)
% eventdata  reserved - to be defined in a future version of MATLAB
% handles    structure with handles and user data (see GUIDATA)
global xo yo selectz xo_pre yo_pre xo_post yo_post
[xo,yo]=ginput(1);
hold on
axes(handles.axes1);
plot(xo,yo , '.y', 'MarkerSize',20);
plot([xo-100 xo+100], [yo yo],'LineWidth',3);
grid on


if selectz ==1
    xo_pre=xo;
    yo_pre=yo;
assignin('base','xo_pre',xo_pre);
assignin('base','yo_pre',yo_pre);
end

if selectz ==2
    xo_post=xo;
    yo_post=yo;
assignin('base','xo_post',xo_post);
assignin('base','yo_post',yo_post);
end

%DELTOID INSERTION
% --- Executes on button press in pushbutton4.
function pushbutton4_Callback(hObject, eventdata, handles)
% hObject    handle to pushbutton4 (see GCBO)
% eventdata  reserved - to be defined in a future version of MATLAB
% handles    structure with handles and user data (see GUIDATA)
global xd yd selectz
[xd,yd]=ginput(1);
hold on
axes(handles.axes1);
plot(xd,yd , '.y', 'MarkerSize',20);
plot([xd-100 xd+100], [yd yd],'LineWidth',3);
grid on

if selectz ==1
    xd_pre=xd;
    yd_pre=yd;
assignin('base','xd_pre',xd_pre);
assignin('base','yd_pre',yd_pre);
end
```

```matlab
if selectz ==2
    xd_post=xd;
    yd_post=yd;
assignin('base','xd_post',xd_post);
assignin('base','yd_post',yd_post);
end


%CALIBRATE
% --- Executes on button press in pushbutton5.
function pushbutton5_Callback(hObject, eventdata, handles)
% hObject    handle to pushbutton5 (see GCBO)
% eventdata  reserved - to be defined in a future version of MATLAB
% handles    structure with handles and user data (see GUIDATA)
global lfactor imag yd xd selectz
[xc,yc]=ginput(2);
hold on
axes(handles.axes1);
plot(xc,yc,'linewidth',2);
lc=sqrt((xc(1)-xc(2))^2+(yc(1)-yc(2))^2);
lconstant=26; %the indx has a length equal to 26mm
%TTTTTTTTTTTTTTTTTTTTTTTTTTTTTTTTTTTTTTTTTTTTTTTTTTTTTTTTTTTTTTTT
lfactor=lconstant/lc;

%one centimeter is:
onecm=lc/(lconstant/10);
for iii=yd-10000:onecm:10000
    plot([-10000 10000], [iii iii],'r:');
     plot([iii iii], [-10000 10000],'r:');

    hold on
end


if selectz ==1
    lfactor_pre=lfactor;
%     centers_pre=centers;
assignin('base','lfactor_pre',lfactor_pre);
% assignin('base','centers_pre',centers_pre);
end

if selectz ==2
    lfactor_post=lfactor;
%     centers_post=centers;
assignin('base','lfactor_post',lfactor_post);
% assignin('base','centers_post',centers_post);
end

%%%%%%%%%%%%%%%%%%%%%%%%%%%%%%%%%%%%%%%%%%
%%%%%%%%%%%%%%%%%%%%%%%%%%%%%%%%%%%%%%%%%%
%%%%%%%%%%%%%%%%%%%%%%%%%%%%%%%%%%%%%%%%%

%GRAPH
% --- Executes on button press in pushbutton6.
function pushbutton6_Callback(hObject, eventdata, handles)
% hObject    handle to pushbutton6 (see GCBO)
% eventdata  reserved - to be defined in a future version of MATLAB
% handles    structure with handles and user data (see GUIDATA)
```

```
global xcor ycor yd xd xo yo lfactor L LLL kuku NAME SURNAME AGE
HEIGHT WEIGHT ID a b LL e
phi=0;
c=10;
muscleoffset=5;
LLL=(ycor)-yd;
ee=(xcor)-xd;
aa=(xcor)-xo;
bb=(ycor)-yo;
L=lfactor*abs(LLL);
e=lfactor*abs(ee);
a=lfactor*abs(aa);
b=lfactor*abs(bb);
%===================================
%===================================
tetha=0:1:130;
tethar=tetha*pi/180;
phi=phi*pi/180;
gama=atan(e/L);
LL=sqrt(L^2+e^2);

ni=LL*sin(tethar+gama)-a*cos(phi)-c*sin(phi);
di=b+LL*cos(tethar+gama);
wi=ni./di;
betar=tethar+gama-atan(wi);
beta=180*betar/pi;
%-------------------------------------------------------
x=-LL*sin(tethar+gama)*cos(phi)+a;
y=+b+LL*cos(tethar+gama);
z=c+LL*sin(tethar+gama)*sin(phi);
q=sqrt(x.^2+y.^2+z.^2);

figure
%kuku=subplot('position',[0.03 0.72 ,0.45 0.24]);
subplot(3,2,1);
plot(tetha,q,'linewidth',2);
xlabel('Abduction');
ylabel('Muscle Length');
set(gca,'xtick',[0:10:1000]);
set(gca,'ytick',[0:20:1000]);
grid on

betar=tethar+gama-atan(wi);
sinb=abs(sin(betar));

hold on
%subplot('position',[0.03 0.07 0.45 0.24]);
subplot(3,2,3);
plot(tetha,LL*sinb,'linewidth',2);
xlabel('Abduction');
ylabel('Lever Arm=L*Sin(B)');
set(gca,'xtick',[0:10:1000]);
set(gca,'ytick',[0:10:100]);
grid on

Lp=diff(q)./diff(tetha);

hold on
%subplot('position',[0.03 0.4 0.45 0.24]);
subplot(3,2,5);
```

```matlab
plot(tetha(2:end),Lp,'linewidth',2);
xlabel('Abduction');
ylabel('Muscle Length Change Rate');
set(gca,'xtick',[0:10:1000]);
set(gca,'ytick',[-100:0.2:100]);
grid on

hold on
%subplot('position',[0.53 0.065 0.45 0.6]);
subplot(3,2,[2 4 6]);
imread('blank.jpg');
imshow('blank.jpg')

text(10,50,'Patient Detail:','FontSize',20);
text(10,100,'ID: ','FontSize',15);
text(135,100,ID,'FontSize',15);
text(10,150,'NAME: ','FontSize',15);
text(165,150,NAME,'FontSize',15);
text(300,150,'SURNAME: ','FontSize',15);
text(550,150,SURNAME,'FontSize',15);
text(10,200,'AGE: ','FontSize',15);
text(150,200,AGE,'FontSize',15);
text(300,200,'HEIGHT: ','FontSize',15);
text(500,200,HEIGHT,'FontSize',15);
text(700,200,'WEIGHT: ','FontSize',15);
text(900,200,WEIGHT,'FontSize',15);
text(10,350,'Dimensions:','FontSize',20);
text(50,450,'m=             mm','FontSize',20);
a=round(a*100)/100;
a=num2str(a);
text(150,450,a,'FontSize',20);
text(50,500,'n =             mm','FontSize',20);
b=round(b*100)/100;
b=num2str(b);
text(150,500,b,'FontSize',20);
text(50,550,'d =             mm','FontSize',20);
LL=round(LL*100)/100;
LL=num2str(LL);
text(150,550,LL,'FontSize',20);
text(50,600,'e =             mm','FontSize',20);
e=round(e*100)/100;
e=num2str(e);
text(150,600,e,'FontSize',20);
text(10,900,'Sensor Reading:','FontSize',20);
text(50,1050,'F=   N','FontSize',20);
text(10,1200,'Note:','FontSize',20);


%PERSONAL INFO
% --- Executes on button press in pushbutton7.
function pushbutton7_Callback(hObject, eventdata, handles)
% hObject    handle to pushbutton7 (see GCBO)
% eventdata  reserved - to be defined in a future version of MATLAB
% handles    structure with handles and user data (see GUIDATA)
pushbutton7_Callback(Register);

%FILTER1
% --- Executes on button press in pushbutton8.
function pushbutton8_Callback(hObject, eventdata, handles)
% hObject    handle to pushbutton8 (see GCBO)
```

```matlab
% eventdata  reserved - to be defined in a future version of MATLAB
% handles    structure with handles and user data (see GUIDATA)
global imag
RGBa = imadjust(imag,[.1 .1 0; .9 .9 1],[]);
hold on
axes(handles.axes1);
imshow(RGBa);



%FILTER2
% --- Executes on button press in pushbutton9.
function pushbutton9_Callback(hObject, eventdata, handles)
% hObject    handle to pushbutton9 (see GCBO)
% eventdata  reserved - to be defined in a future version of MATLAB
% handles    structure with handles and user data (see GUIDATA)
global imag
RGBa2 = imadjust(imag,[.2 .2 0; .7 .7 1],[]);
hold on
axes(handles.axes1);
imshow(RGBa2);



%EXCEL
% --- Executes on button press in pushbutton12.
function pushbutton12_Callback(hObject, eventdata, handles)
% hObject    handle to pushbutton12 (see GCBO)
% eventdata  reserved - to be defined in a future version of MATLAB
% handles    structure with handles and user data (see GUIDATA)
global a b LL e NAME SURNAME ID
filename = 'MAIN.xlsx';
AAA = {a b LL e};
BBB = {ID NAME SURNAME};
sheet = 1;
xlRange1 = 'D3';
xlRange2 = 'A3';
xlswrite(filename,AAA,sheet,xlRange1);
xlswrite(filename,BBB,sheet,xlRange2);
%winopen('MAIN.xlsx')

%AUTOMATIC CALIBRATION
% --- Executes on button press in pushbutton13.
function pushbutton13_Callback(hObject, eventdata, handles)
% hObject    handle to pushbutton13 (see GCBO)
% eventdata  reserved - to be defined in a future version of MATLAB
% handles    structure with handles and user data (see GUIDATA)

global  imag lfactor xd yd centers lfactor_post lfactor_pre selectz
centers_pre centers_post

[centers, radii] = imfindcircles(imag,[20
1000],'ObjectPolarity','dark','Sensitivity',0.92);
hold on
h=viscircles(centers,radii);

%%%%%%%%%%%%%%%%%%%%%%%%%%%%%%%%%%%%%%%%%
axes(handles.axes1);
text(700,570,'Calibrated','FontSize',20,'color','r');
```

```matlab
lc=radii*2;
lconstant=25; %the indx has a length equal to 38 mm
%TTTTTTTTTTTTTTTTTTTTTTTTTTTTTTTTTTTTTTTTTTTTTTTTTTTTTTTTTTTTTTTT
lfactor=lconstant/lc;

%one centimeter is:
onecm=lc/(lconstant/10);
for iii=centers(1,2)-1000:onecm:10000
    plot([-100 1000], [iii iii],'r:');
     plot([iii iii], [-1000 1000],'r:');

    hold on
end



if selectz ==1
    lfactor_pre=lfactor;
    centers_pre=centers;
assignin('base','lfactor_pre',lfactor_pre);
assignin('base','centers_pre',centers_pre);
end

if selectz ==2
    lfactor_post=lfactor;
    centers_post=centers;
assignin('base','lfactor_post',lfactor_post);
assignin('base','centers_post',centers_post);
end

%PERSONAL INFO
% --- Executes on button press in pushbutton14.
function pushbutton14_Callback(hObject, eventdata, handles)
% hObject    handle to pushbutton14 (see GCBO)
% eventdata  reserved - to be defined in a future version of MATLAB
% handles    structure with handles and user data (see GUIDATA)
run('Register.m')

% --- Executes on button press in pushbutton18.
function pushbutton18_Callback(hObject, eventdata, handles)
% hObject    handle to pushbutton18 (see GCBO)
% eventdata  reserved - to be defined in a future version of MATLAB
% handles    structure with handles and user data (see GUIDATA)

run('KinematicsGraphs.m');

%OVERLAY
% --- Executes on button press in pushbutton19.
function pushbutton19_Callback(hObject, eventdata, handles)
% hObject    handle to pushbutton19 (see GCBO)
% eventdata  reserved - to be defined in a future version of MATLAB
% handles    structure with handles and user data (see GUIDATA)
global imag2 imag xo_pre xo_post yo_pre yo_post xx_pre yy_pre xx_post
yy_post
global xd_pre yd_pre xd_post yd_post xcor_pre ycor_pre xcor_post
ycor_post
global lfactor_pre lfactor_post

xo_pre=evalin('base','xo_pre');
yo_pre=evalin('base','yo_pre');
```

127

```matlab
xo_post=evalin('base','xo_post');
yo_post=evalin('base','yo_post');
xd_pre=evalin('base','xd_pre');
yd_pre=evalin('base','yd_pre');
xd_post=evalin('base','xd_post');
yd_post=evalin('base','yd_post');
lfactor_pre=evalin('base','lfactor_pre');
lfactor_post=evalin('base','lfactor_post');
% centers_pre=evalin('base','centers_pre');
% centers_post=evalin('base','centers_post');


imag2 = imtranslate(imag2,[(-xo_post+xo_pre), (-yo_post+yo_pre)]);
%%%%%%
%scaling images relative to eachother
if lfactor_post>lfactor_pre
    sc=lfactor_post/lfactor_pre;
imag2 = imresize(imag2,sc)   ;
end


if lfactor_post<lfactor_pre
    sc=lfactor_pre/lfactor_post;
imag2 = imresize(imag2,sc)   ;
end
%%%%%%

C =
imfuse(imag,imag2,'falsecolor','Scaling','joint','ColorChannels',[1 2
0]);
axes(handles.axes1);
imshow(C);
%humerus circle
plot(xx_pre,yy_pre,'color','r','linewidth',2)
hold on
 plot(sc*xx_post+(-sc*xo_post+xo_pre),sc*yy_post+(-
sc*yo_post+yo_pre),'color','g','linewidth',2)
 hold on
  %humerus centre
 plot(xcor_pre,ycor_pre,'.r','MarkerSize',40)
hold on
 plot(sc*xcor_post+(-sc*xo_post+xo_pre),sc*ycor_post+(-
sc*yo_post+yo_pre),'.g','MarkerSize',40)
 hold on
 %deltoid insertion
 plot(xd_pre,yd_pre,'.r','MarkerSize',40)
 hold on
 plot(sc*xd_post+(-sc*xo_post+xo_pre),sc*yd_post+(-
sc*yo_post+yo_pre),'.g','MarkerSize',40)
  %Acromion
 plot(xo_pre,yo_pre,'.r','MarkerSize',40)
 hold on
 plot(sc*xo_post+(-sc*xo_post+xo_pre),sc*yo_post+(-
sc*yo_post+yo_pre),'.g','MarkerSize',40)
 %lines connecting points
 plot([xcor_pre xd_pre xo_pre xcor_pre],[ycor_pre yd_pre yo_pre
ycor_pre],'color','r','linewidth',2);
 hold on
 plot([sc*xcor_post+(-sc*xo_post+xo_pre) sc*xd_post+(-
sc*xo_post+xo_pre) sc*xo_post+(-sc*xo_post+xo_pre) sc*xcor_post+(-
sc*xo_post+xo_pre)],[sc*ycor_post+(-sc*yo_post+yo_pre) sc*yd_post+(-
sc*yo_post+yo_pre) sc*yo_post+(-sc*yo_post+yo_pre) sc*ycor_post+(-
sc*yo_post+yo_pre)],'color','g','linewidth',2);
```

```matlab
%DO THE DRAWINGS

%Deltoid Line
% --- Executes on button press in pushbutton20.
function pushbutton20_Callback(hObject, eventdata, handles)
% hObject    handle to pushbutton20 (see GCBO)
% eventdata  reserved - to be defined in a future version of MATLAB
% handles    structure with handles and user data (see GUIDATA)
[xdt1,ydt1]=ginput(1);
hold on
axes(handles.axes1);
plot(xdt1,ydt1, '.r', 'MarkerSize',20);
[xdt2,ydt2]=ginput(1);
hold on
axes(handles.axes1);
plot(xdt2,ydt2, '.r', 'MarkerSize',20);
[xdt3,ydt3]=ginput(1);
hold on
axes(handles.axes1);
plot(xdt3,ydt3, '.r', 'MarkerSize',20);
[xdt4,ydt4]=ginput(1);
hold on
axes(handles.axes1);
plot(xdt4,ydt4, '.r', 'MarkerSize',20);
[xdt5,ydt5]=ginput(1);
hold on
axes(handles.axes1);
plot(xdt5,ydt5, '.r', 'MarkerSize',20);

hold on
axes(handles.axes1);
x = [xdt1,xdt2,xdt3,xdt4,xdt5];
y = [ydt1,ydt2,ydt3,ydt4,ydt5];
xx = ydt1-10:1:ydt5+10;
xy=[x;y];
yy = spline(y,x,xx);
plot(yy,xx,'color','b','linewidth',4)
% xi = xdt1-5000:1:xdt3+5000;
% y1 = interp1(x,y,xi);
% y2 = interp1(x,y,xi,'spline');
% plot(xi,y1,'r');

hold on
fnplt(cscvn(xy),'r',2)
```

A.V.   BNO055

Data sheet

BNO055
Intelligent 9-axis absolute orientation sensor

Bosch Sensortec

BOSCH
Invented for life

User Motion →
- Quaternion
- Linear Acceleration
- Rotation
- Gravity
- Robust Heading

BNO055: data sheet

Document revision	1.2
Document release date	November 2014
Document number	BST-BNO055-DS000-12
Technical reference code(s)	0 273 141 209
Notes	Data in this document are subject to change without notice. Product photos and pictures are for illustration purposes only and may differ from the real product's appearance.

.

A.VI. MyoWare EMG sensor

3-lead Muscle / Electromyography Sensor for Microcontroller Applications

MyoWare™ Muscle Sensor (AT-04-001)   **DATASHEET**

FEATURES
- *NEW* - Wearable Design
- *NEW* - Single Supply
  - +2.9V to +5.7V
  - Polarity reversal protection
- *NEW* - Two Output Modes
  - EMG Envelope
  - Raw EMG
- *NEW* - Expandable via Shields
- *NEW* - LED Indicators
- Specially Designed For Microcontrollers
- Adjustable Gain

APPLICATIONS
- Video games
- Robotics
- Medical Devices
- Wearable/Mobile Electronics
- Prosthetics/Orthotics
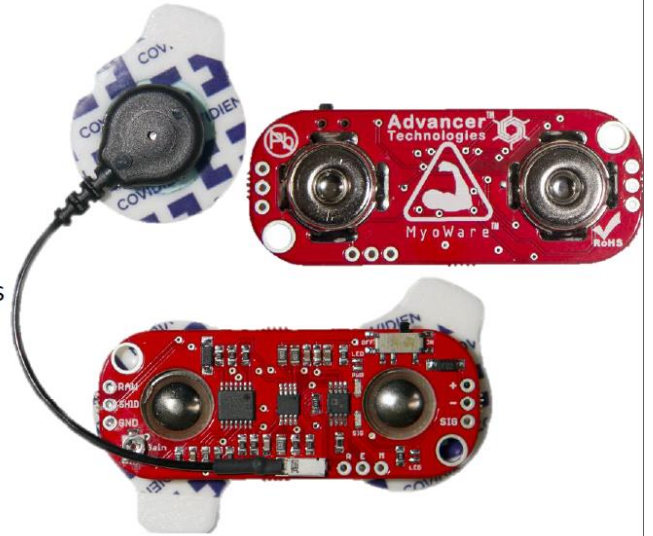
What is electromyography?

Measuring muscle activation via electric potential, referred to as electromyography (EMG), has traditionally been used for medical research and diagnosis of neuromuscular disorders. However, with the advent of ever shrinking yet more powerful microcontrollers and integrated circuits, EMG circuits and sensors have found their way into prosthetics, robotics and other control systems.

Sensor Layout

Mid Muscle Electrode Snap
Power Switch

Raw EMG Signal - 7
Shield Power (output) - 8
GND - 9

1 - Power Supply, +Vs
2 - Power Supply, GND
3 - Output Signal, SIG

Adjustable Gain
End Muscle Electrode Snap

Reference Electrode Cable

4 - Mid Muscle Electrode Pin
5 - End Muscle Electrode Pin
6 - Reference Electrode Pin
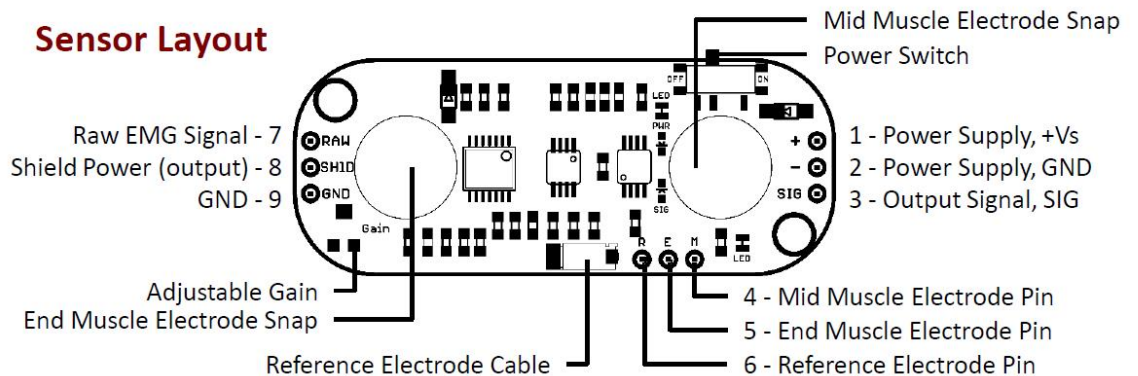
EMAIL: support@advancer.co   **Advancer™ Technologies**   www.AdvancerTechnologies.com

A.VII. Assessment tool circuit
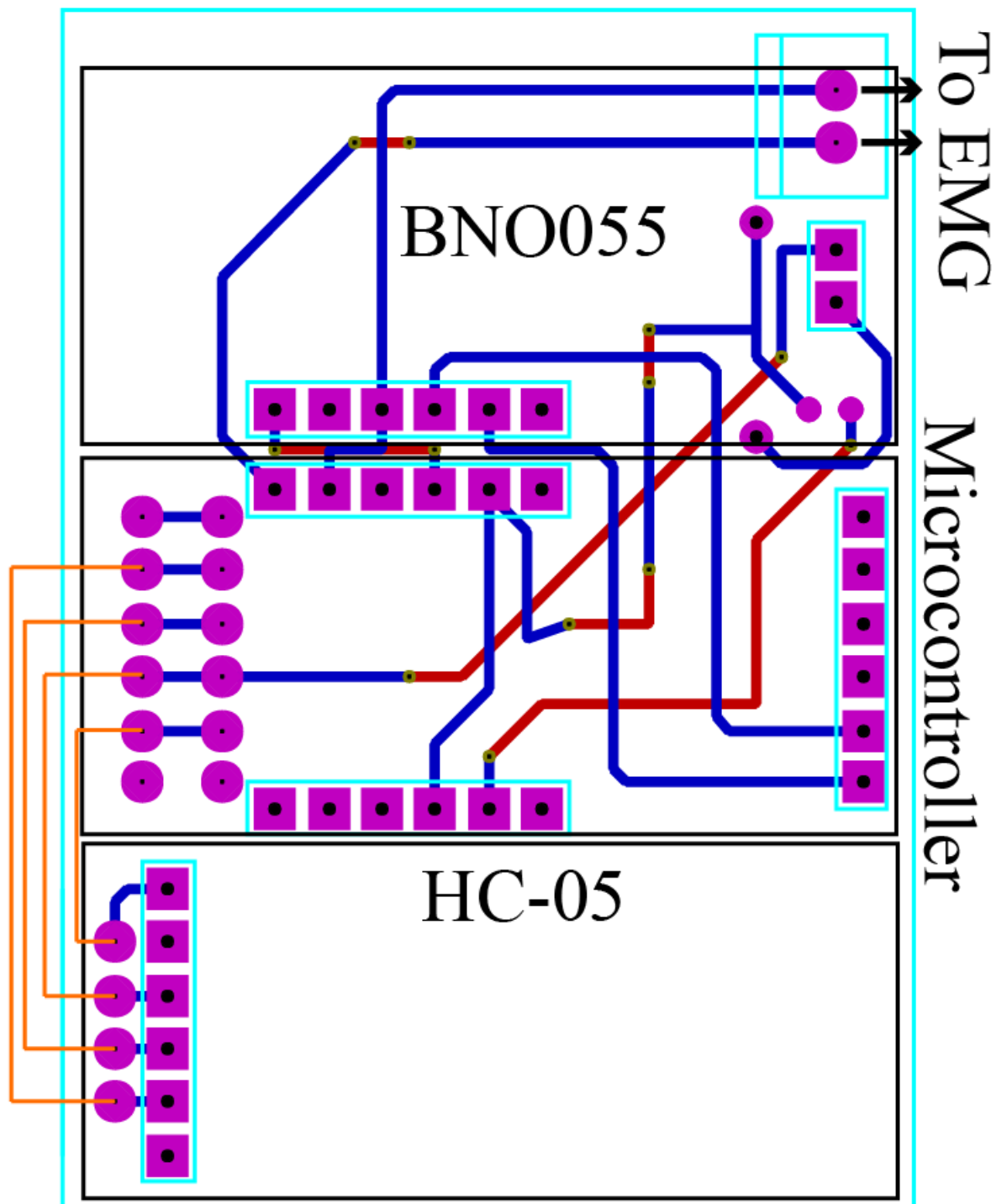
A.VIII. Assessment tool Arduino code

```cpp
#include <Wire.h>
#include <Adafruit_Sensor.h>
#include <Adafruit_BNO055.h>
#include <utility/imumaths.h>

/* This driver uses the Adafruit unified sensor library
(Adafruit_Sensor),
   which provides a common 'type' for sensor data and some helper
functions.

   To use this driver you will also need to download the
Adafruit_Sensor
   library and include it in your libraries folder.

   You should also assign a unique ID to this sensor for use with
   the Adafruit Sensor API so that you can identify this particular
   sensor in any data logs, etc.  To assign a unique ID, simply
   provide an appropriate value in the constructor below (12345
   is used by default in this example).

   Connections
   ===========
   Connect SCL to analog 5
   Connect SDA to analog 4
   Connect VDD to 3-5V DC
   Connect GROUND to common ground

   History
   =======
   2015/MAR/03  - First release (KTOWN)
   2015/Mar/12  - Dave's mod - calibration
*/

/* Set the delay between fresh samples */
#define BNO055_SAMPLERATE_DELAY_MS (50)

Adafruit_BNO055 bno = Adafruit_BNO055(55);

/**********************************************************************
*****/
/*
    Displays some basic information on this sensor from the unified
    sensor API sensor_t type (see Adafruit_Sensor for more
information)
*/
/**********************************************************************
*****/
void displaySensorDetails(void)
{
  sensor_t sensor;
  bno.getSensor(&sensor);
 // Serial.println("------------------------------------");
 // Serial.print  ("Sensor:       "); Serial.println(sensor.name);
 // Serial.print  ("Driver Ver:   "); Serial.println(sensor.version);
 // Serial.print  ("Unique ID:    ");
Serial.println(sensor.sensor_id);
  //Serial.print  ("Max Value:    "); Serial.print(sensor.max_value);
Serial.println(" xxx");
```

```
  //Serial.print  ("Min Value:     "); Serial.print(sensor.min_value);
Serial.println(" xxx");
 // Serial.print  ("Resolution:   "); Serial.print(sensor.resolution);
Serial.println(" xxx");
 // Serial.println("------------------------------------");
 // Serial.println("");
  //delay(500);
}

/************************************************************************
*****/
/*
    Arduino setup function (automatically called at startup)
*/
/************************************************************************
*****/
void setup(void)
{
  Serial.begin(38400);
  //Serial.println("Orientation Sensor Test"); Serial.println("");


 pinMode(2, OUTPUT);


  /* Initialise the sensor */
  if(!bno.begin())
  {
    /* There was a problem detecting the BNO055 ... check your
connections */
    Serial.print("Ooops, no BNO055 detected ... Check your wiring or
I2C ADDR!");
    while(1);
  }
setCal();        // Set Calibration Values - Comment out to read
calibration values
  delay(10);

  /* Display some basic information on this sensor */
  displaySensorDetails();

  bno.setExtCrystalUse(true);

}

/************************************************************************
*****/
/*
    Arduino loop function, called once 'setup' is complete (your own
code
    should go here)
*/
/************************************************************************
*****/
void loop(void)
{
  /* Get a new sensor event */
  sensors_event_t event;
  bno.getEvent(&event);
//getCalStat();                      // Uncomment to get calibration
values
```

```
int sensorvalue = analogRead (A3);
int EMG = analogRead (A0);
  Serial.print(sensorvalue);
    Serial.print("\t");
  /* Display the floating point data */
  //Serial.print("X: ");
  Serial.print(event.orientation.x, 4);
  Serial.print("\t");
  //Serial.print("\tY: ");
  Serial.print(event.orientation.y, 4);
  Serial.print("\t");
  //Serial.print("\tZ: ");
  Serial.print(event.orientation.z, 4);
   Serial.print("\t");
    Serial.println(EMG);

  //Serial.println("");

  delay(BNO055_SAMPLERATE_DELAY_MS);

digitalWrite(2, HIGH);   // turn the LED on (HIGH is the voltage
level)
  delay(5);               // wait for a second
  digitalWrite(2, LOW);    // turn the LED off by making the voltage
LOW
  delay(5);



}
void setCal(){
  // DAVES MOD - Writes calibration data to sensor//
  byte calData;
  bno.setMode( bno.OPERATION_MODE_CONFIG );    // Put into CONFIG_Mode
  delay(25);

  calData = bno.setCalvalARL(232);

  calData = bno.setCalvalARM(3);

  calData = bno.setCalvalMRL(220);

  calData = bno.setCalvalMRM(2);

  calData = bno.setCalvalAOXL(244);

  calData = bno.setCalvalAOXM(255);

  calData = bno.setCalvalAOYL(5);

  calData = bno.setCalvalAOYM(0);

  calData = bno.setCalvalAOZL(254);

  calData = bno.setCalvalAOZM(255);

  calData = bno.setCalvalMOXL(181);

  calData = bno.setCalvalMOXM(255);

  calData = bno.setCalvalMOYL(202);
```

```
    calData = bno.setCalvalMOYM(0);

    calData = bno.setCalvalMOZL(155);

    calData = bno.setCalvalMOZM(255);

    calData = bno.setCalvalGOXL(254);

    calData = bno.setCalvalGOXM(255);

    calData = bno.setCalvalGOYL(255);

    calData = bno.setCalvalGOYM(255);

    calData = bno.setCalvalGOZL(255);

    calData = bno.setCalvalGOZM(255);

  bno.setMode( bno.OPERATION_MODE_NDOF );    // Put into NDOF Mode
  delay(25);
}

void getCal(){
  // Dave's Mod - Reads Calibration Data when sensors are calibrated
  byte calData;
  bno.setMode( bno.OPERATION_MODE_CONFIG );    // Put into CONFIG_Mode

  calData = bno.getCalvalARL();
  Serial.println(calData);

  calData = bno.getCalvalARM();
  Serial.println(calData);

  calData = bno.getCalvalMRL();
  Serial.println(calData);

  calData = bno.getCalvalMRM();
  Serial.println(calData);

  calData = bno.getCalvalAOXL();
  Serial.println(calData);

  calData = bno.getCalvalAOXM();
  Serial.println(calData);

  calData = bno.getCalvalAOYL();
  Serial.println(calData);

  calData = bno.getCalvalAOYM();
  Serial.println(calData);

  calData = bno.getCalvalAOZL();
  Serial.println(calData);

  calData = bno.getCalvalAOZM();
  Serial.println(calData);

  calData = bno.getCalvalMOXL();
  Serial.println(calData);
```

```
    calData = bno.getCalvalMOXM();
    Serial.println(calData);

    calData = bno.getCalvalMOYL();
    Serial.println(calData);

    calData = bno.getCalvalMOYM();
    Serial.println(calData);

    calData = bno.getCalvalMOZL();
    Serial.println(calData);

    calData = bno.getCalvalMOZM();
    Serial.println(calData);

    calData = bno.getCalvalGOXL();
    Serial.println(calData);

    calData = bno.getCalvalGOXM();
    Serial.println(calData);

    calData = bno.getCalvalGOYL();
    Serial.println(calData);

    calData = bno.getCalvalGOYM();
    Serial.println(calData);

    calData = bno.getCalvalGOZL();
    Serial.println(calData);

    calData = bno.getCalvalGOZM();
    Serial.println(calData);

    while(1){                               // Stop
      delay(10);
    }


}
void getCalStat(){
  // Dave's Mod - Move sensor to calibrate, when status shows
calibration, read values
byte cal = bno.getCalib();
  byte calSys = (0xC0 & cal) >> 6;
  byte calGyro = (0x30 & cal) >> 4;
  byte calAccel = (0x0C & cal) >> 2;
  byte calMag = (0x03 & cal) >> 0;

  Serial.println(cal);
  Serial.print("System calibration status "); Serial.println(calSys);
  Serial.print("Gyro   calibration status "); Serial.println(calGyro);
  Serial.print("Accel  calibration status ");
Serial.println(calAccel);
  Serial.print("Mag    calibration status "); Serial.println(calMag);

  delay(10);
  if (cal==255){
    getCal();
  }
}
```

A.IX.   Assessment tool Matlab code

```matlab
function varargout = FINAL3(varargin)
% FINAL3 MATLAB code for FINAL3.fig
%      FINAL3, by itself, creates a new FINAL3 or raises the existing
%      singleton*.
%
%      H = FINAL3 returns the handle to a new FINAL3 or the handle to
%      the existing singleton*.
%
%      FINAL3('CALLBACK',hObject,eventData,handles,...) calls the
local
%      function named CALLBACK in FINAL3.M with the given input
arguments.
%
%      FINAL3('Property','Value',...) creates a new FINAL3 or raises
the
%      existing singleton*.  Starting from the left, property value
pairs are
%      applied to the FINAL3 before FINAL3_OpeningFcn gets called.  An
%      unrecognized property name or invalid value makes property
application
%      stop.  All inputs are passed to FINAL3_OpeningFcn via varargin.
%
%      *See FINAL3 Options on GUIDE's Tools menu.  Choose "FINAL3
allows only one
%      instance to run (singleton)".
%
% See also: GUIDE, GUIDATA, GUIHANDLES

% Edit the above text to modify the response to help FINAL3

% Last Modified by GUIDE v2.5 05-Jul-2016 12:31:48

% Begin initialization code - DO NOT EDIT
gui_Singleton = 1;
gui_State = struct('gui_Name',       mfilename, ...
                   'gui_Singleton',  gui_Singleton, ...
                   'gui_OpeningFcn', @FINAL3_OpeningFcn, ...
                   'gui_OutputFcn',  @FINAL3_OutputFcn, ...
                   'gui_LayoutFcn',  [] , ...
                   'gui_Callback',   []);
if nargin && ischar(varargin{1})
    gui_State.gui_Callback = str2func(varargin{1});
end

if nargout
    [varargout{1:nargout}] = gui_mainfcn(gui_State, varargin{:});
else
    gui_mainfcn(gui_State, varargin{:});
end
% End initialization code - DO NOT EDIT

% --- Executes just before FINAL3 is made visible.
function FINAL3_OpeningFcn(hObject, eventdata, handles, varargin)
% This function has no output args, see OutputFcn.
% hObject    handle to figure
% eventdata  reserved - to be defined in a future version of MATLAB
% handles    structure with handles and user data (see GUIDATA)
% varargin   command line arguments to FINAL3 (see VARARGIN)
```

```matlab
% Choose default command line output for FINAL3
handles.output = hObject;

%SHOW LOGO ON MAIN GUI
WINDOW)))))))))))))))))))))))))))))))))))))))))))))))))))))
axes(handles.axes10)
imshow('BUlogo.png')


% Update handles structure
guidata(hObject, handles);
global flag;
flag=1;
% UIWAIT makes FINAL3 wait for user response (see UIRESUME)
% uiwait(handles.figure1);

% --- Outputs from this function are returned to the command line.
function varargout = FINAL3_OutputFcn(hObject, eventdata, handles)
% varargout  cell array for returning output args (see VARARGOUT);
% hObject    handle to figure
% eventdata  reserved - to be defined in a future version of MATLAB
% handles    structure with handles and user data (see GUIDATA)

% Get default command line output from handles structure
varargout{1} = handles.output;

%CONNECT
% --- Executes on button press in pushbutton1.
function pushbutton1_Callback(hObject, eventdata, handles)
% hObject    handle to pushbutton1 (see GCBO)
% eventdata  reserved - to be defined in a future version of MATLAB
% handles    structure with handles and user data (see GUIDATA)
% clear all
% close all
% clc
 axes(handles.axes1);
text(0.1,0.1,0,'Connecting...
','VerticalAlignment','bottom','FontSize',30,'color','black');
drawnow
%arduin=serial('COM14','BaudRate',38400); % create serial
communication object on port COM18
global arduin
arduin = Bluetooth('NAVID-A',1);
% arduin=serial('COM41','BaudRate',38400);

fopen(arduin); % initiate arduino communication
% msgbox('Sensor is Connected!','Connection');

% pause(1)
axes(handles.axes1);
cla
text(0.1,0.1,0,'Connected','VerticalAlignment','bottom','FontSize',30,
'color','g');
```

```matlab
 %RUN MAIN CODE
% --- Executes on button press in pushbutton3.
function pushbutton3_Callback(hObject, eventdata, handles)
% hObject    handle to pushbutton3 (see GCBO)
% eventdata  reserved - to be defined in a future version of MATLAB
% handles    structure with handles and user data (see GUIDATA)
global arduin firsta0 firsta1 firsta2 firsta3 firsta4 firsta5 ROT0 pp
pp1 aa0 aa1 aa2 aa3 aa5 aa6 gen genz2 arm XS YS ZS abd habd
global flag;

%%%%%%%%%%%%%%%%%
lenn1=2000;
lenn2=2000;
lenn3=2;
index1=1:lenn1;
gg=zeros(lenn1,1);
ff=zeros(lenn2,1);
aa0=zeros(lenn2,1);
aa1=zeros(lenn2,1);
aa2=zeros(lenn2,1);
aa3=zeros(lenn2,1);
aa5=zeros(lenn2,1);
aa6=zeros(lenn2,1);
tt=zeros(lenn3,1);

%XYZ COORDINATE OF RIGHT ARM
XS=zeros(lenn2,1);
YS=zeros(lenn2,1);
ZS=zeros(lenn2,1);

%SPHERICAL COORDINATE ANGLES COORDINATE OF RIGHT ARM
abd=zeros(lenn2,1);
habd=zeros(lenn2,1);

%STRAIN GAUGE FILTER PARAMETERS
stfilt=0;
filtvalue=0.4;


%INITAIL COORDINATE OF RIGHT ARM
xxo=0;
yyo=-600;
zzo=0;
%%%%%%%%%%%%%%%%%
%CIRCULAT GAUGE CIRCLE
[xp yp] = circus(1,0,0);
%Gage Sign
xq = [0.05 -0.05 0];
yq = [0 0 -1];
xq2 = [0.05 -0.05 0];
yq2 = [0 0 1];


%%%%%%%%%%%%%%%%%%%%%%%%%
%%%%%%%%%%%%%%%%%%%%%%%%%

tic
% % tocv=102.5;
```

```matlab
tocv=62.5;

 while toc<=tocv
  if flag==1
      readz3=fscanf(arduin,'%f');
%          strV2 = num2str(tocv-(round(toc*100)/100));
        if toc<2
           text(-
700,700,0,'WAIT','VerticalAlignment','bottom','FontSize',50,'color','r
');


        end
        if (2.5>toc)&&(toc>=2)
 text(-
700,700,0,'GO!','VerticalAlignment','bottom','FontSize',50,'color','g'
);
        end

   %readz1=fscanf(arduin,'%f');
   %readz2=fscanf(arduin,'%f');

%STRAIN
a0=readz3(1);
%IMU
a1=readz3(2);
a2=readz3(3);
a3=readz3(4);
a4=readz3(5);
%EMG
a5=readz3(6);
a0=a0-firsta0;
% a1=a1-firsta1;
% a2=a2-firsta2;
% a3=a3-firsta3;
% a4=a4-firsta4;
a5=a5-firsta5;

aw=a1;
ax=a2;
ay=a3;
az=a4;
a0(a0<5)=0;
a5(a5<5)=0;

%BODY PARTS

%Hip BONE
y0=[-100+200 100+200];x0=[0 0];z0=[0-800 0-800];
%%%
%LEFT LEG (FEMUR)
y1=[100+200 100+200];x1=[0 100];z1=[0-800 -500-800];
%%%%
%RIGHT LEG (FEMUR)
y2=[-100+200 -100+200];x2=[0 100];z2=[0-800 -500-800];
%%%
%LEFT LEG (TIBIA)
y11=[100+200 100+200];x11=[100 0];z11=[-500-800 -1000-800];
%%%%
%RIGHT LEG (TIBIA)
```

```matlab
y22=[-100+200 -100+200];x22=[100 0];z22=[-500-800 -1000-800];
%%%
%LEFT FOOT
y111=[100+200 100+200];x111=[0 150];z111=[-1000-800 -1000-800];
%%%%
%RIGHT FOOT
y222=[-100+200 -100+200];x222=[0 150];z222=[-1000-800 -1000-800];
%%%%
%SPINE
y3=[0+200 0+200];x3=[0 0];z3=[0-800 800-800];
%%%%
%SHOULDER
y4=[-200+200 200+200];x4=[0 0];z4=[800-800 800-800];
%%%%
%NECK
y7=[0+200 0+200];x7=[0 0];z7=[800-800 1000-800];


%%%%
%LEFT HAND(RADIUS)
x66=[0 0];y66=[400 400];z66=[0 -600];
%ROTATION MATRIX
ROT=[aw^2+ax^2-ay^2-az^2,2*ax*ay-2*aw*az,2*ax*az+2*aw*ay;
    2*ax*ay+2*aw*az,aw^2-ax^2+ay^2-az^2,2*ay*az-2*aw*ax;
    2*ax*az-2*aw*ay,2*ay*az+2*aw*ax,aw^2-ax^2-ay^2+az^2];

%Cancel for Initials
ROT=inv(ROT0)*ROT;
%NEW COORDINATE
newcor=ROT*[xxo;yyo;zzo];
xxn=newcor(1,1);
yyn=newcor(3,1);
zzn=newcor(2,1);

%SAVE X<Y<Z COORDINATES
% XS = [XS(2:end) ; xxn];
% YS = [YS(2:end) ; yyn];
% ZS = [ZS(2:end) ; zzn];

figure(3)
% axes(handles.axes1);
% subplot(3,2,[1 5])
subtightplot(3,2,[1 5], [0.01 0.05], [0.1 0.01], [0.1 0.01])
%PLOT RIGHT HAND MOVING
X=[0,xxn];
Y=[0,yyn];
Z=[0,zzn];
plot3(X,Y,Z,'linewidth',2);
xlabel('X')
ylabel('Y')
zlabel('Z')

%PLOT THE REST OF BODY
hold on
line(x0,y0,z0,'linewidth',2);
hold on
line(x1,y1,z1,'linewidth',2);
hold on
line(x2,y2,z2,'linewidth',2);
hold on
```

```matlab
line(x11,y11,z11,'linewidth',2);
hold on
line(x22,y22,z22,'linewidth',2);
hold on
line(x111,y111,z111,'linewidth',2);
hold on
line(x222,y222,z222,'linewidth',2);
hold on
line(x3,y3,z3,'linewidth',2);
hold on
line(x4,y4,z4,'linewidth',2);
hold on
line(x7,y7,z7,'linewidth',2);
hold on
line(x66,y66,z66,'linewidth',2);

%Abduction
VEC1=[xxn;yyn;zzn];
vec1=[0;0;-600];

VEC2=[xxn;yyn];
vec2=[600;0];

%Horizontal ABDUCTION
habduct = atan2(VEC2(1)*vec2(2)-
vec2(1)*VEC2(2),VEC2(1)*vec2(1)+VEC2(2)*vec2(2));
habduct = habduct*180/pi;
%MODIFICATION FOR SMALL ANGLES
threshold=sqrt(xxn^2+yyn^2);

%ABDUCTION
abduct = atan2(norm(cross(VEC1,vec1)), dot(VEC1,vec1));
abduct=abduct*180/pi;
%MODIFICATION FOR FULL MOTION??????????????????????????????

abd = [abd(2:end) ; abduct];
habd = [habd(2:end) ; habduct];

hold on
% %FSR PAIN BAR CHART
% py=[-110 -110 -110 -110];
% px=[150 150 250 250];
% pz=[-1000 -1000+(a0/2)+1 -1000+(a0/2)+1 -1000];
% % ((1000-a0)/1000)
% fill3(px, py, pz,[1,0.3,0]);
% text(250,-50,-1020,'PAIN (%)
:','VerticalAlignment','bottom','FontSize',10,'color','r');

%EMG BAR CHART
pyy=[-110 -110 -110 -110];
pxx=[300 300 400 400];
pzz=[-1000 -1000+(a5/2)+1 -1000+(a5/2)+1 -1000];
% ((1000-a0)/1000)
fill3(pxx, pyy, pzz,[1,0.3,0]);
text(400,-50,-1020,'EMG
:','VerticalAlignment','bottom','FontSize',10,'color','g');
%%%%%%%%%%%%%%%%%%%%%%%%%%%%%%
%%%%%%%%%%%%%%%%%%%%%%%%%%%%%%
%%%%%%%%%%%%%%%%%%%%%%%%%%%%%%%%%%
%%%%%%%%%%%%%%%%%%%%%%%%%%%%%%%%%%%%
```

143

```matlab
strValuesQ = num2str(abduct);
text(400,-50,-500,strValuesQ,'FontSize',12,'color','black');
strValuesQz = num2str(habduct);
text(400,-50,-300,strValuesQz,'FontSize',12,'color','black');
%%%%%%%%%%%%%%%%%%%
%%%%%%%%%%%%%%%%%%%%%%%%%%%%%
%%%%%%%%%%%%%%%%%%%%%%%%%%%%
%%%%%%%%%%%%%%%%%%%%%%%%%%%%%

% hold on
axis equal
axis off
view(-45,135);


%%%%%%%%%%%%%%%


%-------------------------------------------------------------
%-------------------------------------------------------------
strValues1 = num2str(a0);
 strValues2 = num2str(a1);
 strValues3 = num2str(a2);
 strValues4 = num2str(a3);
 strValues5 = num2str(a4);
 strValues6 = num2str(a5);
%
% text(0,360,-170,'EMG
:','VerticalAlignment','bottom','FontSize',12,'color','b');
%  text(0,360,-
240,strValues6,'VerticalAlignment','bottom','FontSize',12,'color','b')
;
% %
%  text(0,360,-40,'Pain
:','VerticalAlignment','bottom','FontSize',10,'color','r');
%  text(0,360,-
110,strValues1,'VerticalAlignment','bottom','FontSize',10,'color','r')
;
% %
%  text(0,360,90,'Alpha (deg)
:','VerticalAlignment','bottom','FontSize',10,'color','black');
%
text(0,360,20,strValues2,'VerticalAlignment','bottom','FontSize',10,'c
olor','black');
% %
%  text(0,360,220,'Beta (deg)
:','VerticalAlignment','bottom','FontSize',10,'color','black');
%
text(0,360,150,strValues3,'VerticalAlignment','bottom','FontSize',10,'
color','black');
% %
%  text(0,360,350,'Gamma (deg)
:','VerticalAlignment','bottom','FontSize',10,'color','black');
%
text(0,360,280,strValues4,'VerticalAlignment','bottom','FontSize',10,'
color','black');

 %%%%%%%%%%%
 if toc>=2.5
  strV = num2str(tocv-(round(toc*100)/100));
      fprintf('elapsed time is: %.2f seconds. \n',toc)
```

```matlab
text(-
700,700,0,strV,'VerticalAlignment','bottom','FontSize',50,'color','bla
ck');
 end
 %%%%%%%%%%
drawnow
cla

%ANGLES
%%%%%%%%%%%%%%%%%%%%%%%%%%%%%%%%%%%%%%%%%%%%
%%%%%%%%%%%%%%%%%%%%%%%%%%%%%%%%%%%%%%%%%%
%%%%%%%%%%%%%%%%%%%%%%%%%%%%%%%%%%%%%%%%%

% hold on
%%%%%%%%%%%%%%%%%%%%%%%%%%%%%%%%%%%%%%%%%%%%%%
%%%%%%%%%%%%%%%%%%%%%%%%%%%%%%%%%%%%%%%%%%%%%%
% GAUGES
% AXIS for Gauges
% axes(handles.axes11);
% subplot(3,2,4)
% subtightplot(3,2,2, [0.01 0.05], [0.1 0.01], [0.1 0.01])
% %SHOWING ROTATION IN GAUGE1
% % cla
% % khat1=fill(xq,yq,'r');
% % % hold on
% % rotate(khat1,[0 0 1],abduct,[0,0,0]);
% % hold on
% % %CIRCULAT GAUGE
% % plot(xp,yp,'color','black','linewidth',2);
% % hold on
% % plot(xp/2,yp/2,'--','color','black');
% % %CIRCULAT GAUGE LINES
% % plot([0 0],[-1 1],'--','color','black');
% % hold on
% % plot([-1 1],[0 0],'--','color','black');
% % hold on
% % plot([-cosd(45) cosd(45)],[-sind(45) sind(45)],'--
','color','black');
% % hold on
% % plot([-cosd(135) cosd(135)],[-sind(135) sind(135)],'--
','color','black');
% strValuesQ = num2str(abduct);
% text(0,0.2,strValuesQ,'FontSize',12,'color','black');
% % ylabel('Abduction', 'FontWeight', 'bold', 'FontSize', 12)
% hold off
% axis equal
%  axis off
%
% xlim([-1.1 1.1]);
% ylim([-1.1 1.1]);
% drawnow
% cla
% drawnow
% cla
% hold on
% axis equal
% hold off
% drawnow
% cla
%SHOWING ROTATION IN GAUGE2
% axes(handles.axes12);
```

```matlab
% subplot(3,2,6)
% subtightplot(3,2,4, [0.01 0.05], [0.1 0.01], [0.1 0.01])
% % khat2=fill(xq2,yq2,'b');
% % hold on
% % rotate(khat2,[0 0 1],habduct,[0,0,0]);
% % hold on
% % %CIRCULAT GAUGE
% % plot(xp,yp,'color','black','linewidth',2);
% % hold on
% % plot(xp/2,yp/2,'--','color','black');
% % %CIRCULAT GAUGE LINES
% % plot([0 0],[-1 1],'--','color','black');
% % hold on
% % plot([-1 1],[0 0],'--','color','black');
% % hold on
% % plot([-cosd(45) cosd(45)],[-sind(45) sind(45)],'--
% ','color','black');
% % hold on
% % plot([-cosd(135) cosd(135)],[-sind(135) sind(135)],'--
% ','color','black');
%
% strValuesQz = num2str(habduct);
% text(0,0.2,strValuesQz,'FontSize',12,'color','black');
%
% hold off
% axis equal
% axis off
% % ylabel('Horizontal Abduction', 'FontWeight', 'bold', 'FontSize',
12)
% xlim([-1.1 1.1]);
% ylim([-1.1 1.1]);
%
% % hold off
% drawnow
% cla
% hold on
%%%%%%%%%%%%%%%%%%%%%%%%%%%%%%%%%%%%%%%%%%%
%%%%%%%%%%%%%%%%%%%%%%%%%%%%%%%%%%%%%%%%%%%
%%%%%%%%%%%%%%%%%%%%%%%%%%%%%%%%%%%%%%%%%%%
% %%%%%%%%%%%%%%%%%%%%%%%%%%%%%%%%%%%%%%%
 %ANGLES TREND
aa0 = [aa0(2:end) ; a0];
%%%
% aa1 = [aa1(2:end) ; a1];
% aa2 = [aa2(2:end) ; a2];
% aa3 = [aa3(2:end) ; a3];
% aa5 = [aa5(2:end) ; a4];
%%%
aa6 = [aa6(2:end) ; a5];
  else
      break;
  end
  end
% gen=[aa0 abd  habd  aa6];
% assignin('base','gen',gen);
% FileName = genz2;
% assignin('base','gen',FileName);
% AAA = gen;
% xlswrite(FileName,AAA);
%
% fclose(arduin); % end communication with arduino
```

```matlab
%LOAD FILE-1
% --- Executes on button press in pushbutton4.
function pushbutton4_Callback(hObject, eventdata, handles)
% hObject    handle to pushbutton4 (see GCBO)
% eventdata  reserved - to be defined in a future version of MATLAB
% handles    structure with handles and user data (see GUIDATA)
global FileName pathname
[FileName,pathname] = uigetfile('*.xls','Select the MATLAB code
file','C:\Users\NAslani\Google Drive\AAA\RSA ASSESSMENT\')
assignin('base','pathname',pathname);
assignin('base','FileName',FileName);


%LOAD FILE-2
% --- Executes on button press in pushbutton5.
function pushbutton5_Callback(hObject, eventdata, handles)
% hObject    handle to pushbutton5 (see GCBO)
% eventdata  reserved - to be defined in a future version of MATLAB
% handles    structure with handles and user data (see GUIDATA)
global FileName1 pathname1
[FileName1,pathname1] = uigetfile('*.xls','Select the MATLAB code
file','C:\Users\NAslani\Google Drive\AAA\RSA ASSESSMENT\')
assignin('base','pathname1',pathname1);
assignin('base','FileName1',FileName1);


%PROCESS-1
% --- Executes on button press in pushbutton6.
function pushbutton6_Callback(hObject, eventdata, handles)
% hObject    handle to pushbutton6 (see GCBO)
% eventdata  reserved - to be defined in a future version of MATLAB
% handles    structure with handles and user data (see GUIDATA)
global FileName pathname num1 k xlmin ylmin xlmax ylmax
num1 = xlsread(FileName);
% num1=round(num1)
%delet all zeroz
num1( ~any(num1,2), : ) = [];   %rows

%delet first 5 and last 5
num1 = num1(5:end,:);
num1 = num1(1:end-5,:);


%Convert horizontal abduction values from negative to positive
for ii = 1:length(num1)
    if num1(ii,3)<-100
        num1(ii,3) = 360+num1(ii,3);
    end
end

%eliminate horizontal abduction values bigger than 180
num1(num1(:, 3)>220, :)= [];
%delet elements with abduction below 5 degrees
num1(num1(:, 2)<5, :)= [];

% num1=round(num1);
% Kim=find(num1(:, 2)<3.5 );
% min(num1(:, 3)))

a=num1(:,1);
x=num1(:,3);
y=num1(:,2);
emg=num1(:,4);
```

```matlab
%delet PAIN noises
a(a<5)=0;

%PAIN
%%%%%%%%%%%%%%%%%%%%%%%%%%%%%%%%%%%%%%%%
%%%%%%%%%%%%%%%%%%%%%%%%%%%%%%%%%%%%%%%%
figure(4)
% axes(handles.axes3);
subplot(3,2,1)
assignin('base','num1',num1);
%MOTION ENVELOPE

[k ar] = convhull(x,y);
fill(x(k),y(k),'g','facealpha', 0.1 );
xt=(min(x));
yt=(max(y));
% aaa=text(xt,yt-4,num2str(ar));
% set(aaa, 'FontName', 'Arial', 'FontWeight', 'bold', 'FontSize',
12,'Color', 'black');
%  text(xt,yt,'Area(deg^2):','FontName', 'Arial', 'FontWeight',
'bold', 'FontSize', 12,'Color', 'black');
hold on

%PAIN MARKERS
paincord=num1(num1(:,1)>0,:);
aa=paincord(:,1);
xx=paincord(:,3);
yy=paincord(:,2);
sz=size(paincord);


%%%%%%%%%%%%%%%%%%%%%%%%%%%%%%
stepsize=0.4;
stepx = min(x)-2:stepsize:max(x)+2;
stepy = min(y)-2:stepsize:max(y)+2;
[XI,YI] = meshgrid(stepx, stepy);

ZIp = griddata(x,y,a,XI, YI);
% surf(XI,YI,ZIp);
% shading interp
trs=2;

xlmin=round(min(x)-trs);
xlmax=round(max(x)+trs);
ylmin=round(min(y)-trs);
ylmax=round(max(y)+trs);

set(gca,'XTick',xlmin:30:xlmax);
set(gca,'YTick',ylmin:30:ylmax);
grid on
title('Pain Distribution', 'FontWeight', 'bold', 'FontSize', 12)
 xlabel('Azimuthal angle (deg)', 'FontWeight', 'bold', 'FontSize',
12);
 ylabel('Elevation angle (deg)', 'FontWeight', 'bold', 'FontSize',
12);
%%%%%%%%%%%%%%%%%%%%%%%%%%%%%%%%%%%%%%%%%%%
%%%%%%%%%%%%%%%%%%%%%%%%%%%%%%%%%%%%%%%%%%%
hold on
scatter(x,y,40,'filled','MarkerEdgeColor','black','MarkerFaceColor','g
','LineWidth',1);
```

```matlab
%%%%%%%%%%%%%%%%%%%%%
%NEUTRAL AXES

plot3([0 0],[-180 220],[1024 1024],'linewidth',2,'color','black');
hold on
plot3([90 90],[-180 180],[1024 1024],'linewidth',2,'color','black');
hold on
plot3([-220 220],[90 90],[1024 1024],'linewidth',2,'color','black');
hold on
plot3([180 180],[-180 180],[1024 1024],'linewidth',2,'color','black');
hold on
%%%%%%%%%%%%%%%%%%%%%%%%%%%%%%%
xlim([xlmin xlmax]);
ylim([ylmin ylmax]);
%EMG
%%%%%%%%%%%%%%%%%%%%%%%%%%%%%%%%%%%%%%%%%%%%%%
%%%%%%%%%%%%%%%%%%%%%%%%%%%%%%%%%%%%%%%%%%%%%%

% axes(handles.axes5);
subplot(3,2,3)
assignin('base','num1',num1);
%MOTION ENVELOPE
[k ar] = convhull(x,y);
fill(x(k),y(k),'g','facealpha', 0.5 );
xt=(min(x));
yt=(max(y));
% aaa=text(xt,yt-4,num2str(ar));
% set(aaa, 'FontName', 'Arial', 'FontWeight', 'bold', 'FontSize',
12,'Color', 'black');
%  text(xt,yt,'Area(deg^2):','FontName', 'Arial', 'FontWeight',
'bold', 'FontSize', 12,'Color', 'black');
hold on

%EMG MARKERS
emgcord=num1(num1(:,1)>0,:);
ee=emgcord(:,4);
xx=emgcord(:,3);
yy=emgcord(:,2);
sz=size(emgcord);

%%%%%%%%%%%%%%%%%%%%%%%%
%NEUTRAL AXES

plot3([0 0],[-180 220],[1024 1024],'linewidth',2,'color','black');
hold on
plot3([90 90],[-180 180],[1024 1024],'linewidth',2,'color','black');
hold on
plot3([-220 220],[90 90],[1024 1024],'linewidth',2,'color','black');
hold on
plot3([180 180],[-180 180],[1024 1024],'linewidth',2,'color','black');
hold on
%%%%%%%%%%%%%%%%%%%%%%%%%%%%%%%%
ZIe = griddata(x,y,emg,XI, YI);
surf(XI,YI,ZIe);
shading interp

xlim([xlmin xlmax]);
ylim([ylmin ylmax]);
set(gca,'XTick',xlmin:30:xlmax);
```

```matlab
set(gca,'YTick',ylmin:30:ylmax);
grid on
title('EMG Distribution', 'FontWeight', 'bold', 'FontSize', 12)
 xlabel('Azimuthal angle (deg)', 'FontWeight', 'bold', 'FontSize',
12);
 ylabel('Elevation angle (deg)', 'FontWeight', 'bold', 'FontSize',
12);
   hold on
% scatter(x,y);
%Information
% axes(handles.axes7);
subplot(3,2,5)
aaa=text(0.1,0.8,num2str(ar));
set(aaa, 'FontName', 'Arial', 'FontWeight', 'bold', 'FontSize',
12,'Color', 'black');
 text(0.1,0.9,'Area(deg * deg) = ','FontName', 'Arial', 'FontWeight',
'bold', 'FontSize', 10,'Color', 'black');

 aay=text(0.1,0.5,num2str(max(y)));
set(aay, 'FontName', 'Arial', 'FontWeight', 'bold', 'FontSize',
12,'Color', 'black');
 text(0.1,0.6,'Maximum Flexion (deg) = ','FontName', 'Arial',
'FontWeight', 'bold', 'FontSize', 10,'Color', 'black');

 aax=text(0.1,0.2,num2str(max(x)));
set(aax, 'FontName', 'Arial', 'FontWeight', 'bold', 'FontSize',
12,'Color', 'black');
 text(0.1,0.3,'Maximum Horizontal Flexion (deg) = ','FontName',
'Arial', 'FontWeight', 'bold', 'FontSize', 10,'Color', 'black');

 axis off
%%%%%%%%%%%%%%%%%%%%
 %%%%%%%%%%%%%%%%%%%%%%%
 colorDepth = 1000;
colormap(jet(colorDepth));
figure(10)
hold on;
pcolor(XI,YI,ZIe); shading flat;

[C,hfigc] = contour(XI, YI, ZIe,[0:0.1:1]);
set(hfigc, ...
    'LineWidth',1.0, ...
    'Color', [1 1 1]);
hold off;
hcb = colorbar('location','EastOutside');

 %%%%%%%%%%%%%%%%%%%%%%%
 %%%%%%%%%%%%%%%%%%%%%%%

  axis off
%PROCESS-2
% --- Executes on button press in pushbutton7.
function pushbutton7_Callback(hObject, eventdata, handles)
% hObject    handle to pushbutton7 (see GCBO)
% eventdata  reserved - to be defined in a future version of MATLAB
% handles    structure with handles and user data (see GUIDATA)
global FileName1 pathname1 num2 k1 xlmin ylmin xlmax ylmax
num2 = xlsread(FileName1);

%delet all zeroz
```

```matlab
num2( ~any(num2,2), : ) = [];   %rows


%delet first 5 and last 5
num2 = num2(5:end,:);
num2 = num2(1:end-5,:);

%Convert horizontal abduction values from negative to positiove
for ii = 1:length(num2)
    if num2(ii,3)<-90
        num2(ii,3) = 360+num2(ii,3);
    end
end


%eliminate horizontal abduction values bigger than 180
num2(num2(:, 3)>180, :)= [];
%delet elements with abduction below 5 degrees
num2(num2(:, 2)<3, :)= [];


a1=num2(:,1);
x1=num2(:,3);
y1=num2(:,2);
emg1=num2(:,4);

% for ii = 1:length(x1)
%     if x1(ii)<0
%         x1(ii) = 360+x1(ii);
%     end
% end

a1(a1<5)=0;
figure(4)
% axes(handles.axes4);
subplot(3,2,2)
assignin('base','num2',num2);
%MOTION ENVELOPE

[k1 ar1] = convhull(x1,y1);
fill(x1(k1),y1(k1),'g','facealpha', 0.5 );
xt1=(min(x1));
yt1=(max(y1));
% aaa1=text(xt1,yt1-4,num2str(ar1));
% set(aaa1, 'FontName', 'Arial', 'FontWeight', 'bold', 'FontSize',
12,'Color', 'black');
%  text(xt1,yt1,'Area(deg^2):','FontName', 'Arial', 'FontWeight',
'bold', 'FontSize', 12,'Color', 'black');
hold on


%PAIN MARKERS
%%%%%%%%%%%%%%%%%%%%%%%%%%%%%%%%%%%%%%%%%%%%%%%
%%%%%%%%%%%%%%%%%%%%%%%%%%%%%%%%%%%%%%%%%%%%%%%
paincord1=num2(num2(:,1)>0,:);
aa1=paincord1(:,1);
xx1=paincord1(:,3);
yy1=paincord1(:,2);
sz1=size(paincord1);
```

```matlab
% for ii = 1:length(xx1)
%     if xx1(ii)<0
%         xx1(ii) = 360+xx1(ii);
%     end
% end
%%%%%%%%%%%%%%%%%%%%%%%%%%%%
stepsize=0.4;
stepx1 = min(x1)-2:stepsize:max(x1)+2;
stepy1 = min(y1)-2:stepsize:max(y1)+2;
[XI1,YI1] = meshgrid(stepx1, stepy1);

ZI1 = griddata(x1,y1,a1,XI1, YI1);
surf(XI1,YI1,ZI1);
shading interp
trs1=2;
xlmin1=min(x1)-trs1;
xlmax1=max(x1)+trs1;
ylmin1=min(y1)-trs1;
ylmax1=max(y1)+trs1;

xlim([xlmin1 xlmax1]);
ylim([ylmin1 ylmax1]);
set(gca,'XTick',xlmin1:45:xlmax1, 'XMinorTick','on');
set(gca,'YTick',ylmin1:45:ylmax1, 'YMinorTick','on');
grid on
title('Pain Distribution', 'FontWeight', 'bold', 'FontSize', 12)
 xlabel('Horizontal Flexion (deg)');
 ylabel('Flexion (deg)');
 hold on
 scatter(x1,y1);
%%%%%%%%%%%%%%%%%%%%%%%%%%%%%%%%%%%%%%%%%%%%%%%
%%%%%%%%%%%%%%%%%%%%%%%%%%%%%%%%%%%%%%%%%%%%%%%
%EMG
%%%%%%%%%%%%%%%%%%%%%%%%%%%%%%%%%%%%%%%%%%%
%%%%%%%%%%%%%%%%%%%%%%%%%%%%%%%%%%%%%%%%%%%

% axes(handles.axes6);
subplot(3,2,4)
assignin('base','num2',num2);
%MOTION ENVELOPE
scatter(x1,y1);
[k1 ar1] = convhull(x1,y1);
fill(x1(k1),y1(k1),'g','facealpha', 0.5 );
xt1=(min(x1));
yt1=(max(y1));
% aaa1=text(xt1,yt1-4,num2str(ar1));
% set(aaa1, 'FontName', 'Arial', 'FontWeight', 'bold', 'FontSize',
12,'Color', 'black');
%  text(xt1,yt1,'Area(deg^2):','FontName', 'Arial', 'FontWeight',
'bold', 'FontSize', 12,'Color', 'black');
hold on

%EMG MARKERS
emgcord1=num2(num2(:,1)>0,:);
ee1=emgcord1(:,4);
xx1=emgcord1(:,3);
yy1=emgcord1(:,2);
sz1=size(emgcord1);
```

```matlab
        for ii = 1:length(xx1)
            if xx1(ii)<0
                xx1(ii) = 360+xx1(ii);
            end
        end
        %%%%%%%%%%%%%%%%%%%%%%%%%%%%

        ZIe1 = griddata(x1,y1,emg1,XI1, YI1);
        surf(XI1,YI1,ZIe1);
        shading interp

        trs1=2;
        xlmin1=round(min(x1)-trs1);
        xlmax1=round(max(x1)+trs1);
        ylmin1=round(min(y1)-trs1);
        ylmax1=round(max(y1)+trs1);


        xlim([xlmin1 xlmax1]);
        ylim([ylmin1 ylmax1]);
        set(gca,'XTick',xlmin1:30:xlmax1, 'XMinorTick','on');
        set(gca,'YTick',ylmin1:30:ylmax1, 'YMinorTick','on');
        grid on
        title('EMG Distribution', 'FontWeight', 'bold', 'FontSize', 12)
         xlabel('Horizontal Flexion (deg)');
         ylabel('Flexion (deg)');
          hold on
         scatter(x1,y1);
        %Information
        % axes(handles.axes8);
        subplot(3,2,6)
        aaa11=text(0.1,0.8,num2str(ar1));
        set(aaa11, 'FontName', 'Arial', 'FontWeight', 'bold', 'FontSize',
        12,'Color', 'black');
         text(0.1,0.9,'Area(deg * deg) = ','FontName', 'Arial', 'FontWeight',
        'bold', 'FontSize', 10,'Color', 'black');

         aay1=text(0.1,0.5,num2str(max(y1)));
        set(aay1, 'FontName', 'Arial', 'FontWeight', 'bold', 'FontSize',
        12,'Color', 'black');
         text(0.1,0.6,'Maximum Flexion (deg) = ','FontName', 'Arial',
        'FontWeight', 'bold', 'FontSize', 10,'Color', 'black');

         aax1=text(0.1,0.2,num2str(max(x1)));
        set(aax1, 'FontName', 'Arial', 'FontWeight', 'bold', 'FontSize',
        12,'Color', 'black');
         text(0.1,0.3,'Maximum Horizontal Flexion (deg) = ','FontName',
        'Arial', 'FontWeight', 'bold', 'FontSize', 10,'Color', 'black');
         axis off


        % --- Executes when figure1 is resized.
        function figure1_ResizeFcn(hObject, eventdata, handles)
        % hObject    handle to figure1 (see GCBO)
        % eventdata  reserved - to be defined in a future version of MATLAB
        % handles    structure with handles and user data (see GUIDATA)


        function edit1_Callback(hObject, eventdata, handles)
        % hObject    handle to edit1 (see GCBO)
```

```matlab
% eventdata  reserved - to be defined in a future version of MATLAB
% handles    structure with handles and user data (see GUIDATA)


% Hints: get(hObject,'String') returns contents of edit1 as text
%        str2double(get(hObject,'String')) returns contents of edit1
as a double
global genz genz2 a b
genz = get(handles.edit1, 'string');
a = genz;
b = 'xlsx';
genz2 = strjoin(cellstr(a),b);
%   namez = 'genz.xlsx';
%   genzz=('%03d',icl) '.xlsx';
% xlswrite(genzz,genz);



% --- Executes during object creation, after setting all properties.
function edit1_CreateFcn(hObject, eventdata, handles)
% hObject    handle to edit1 (see GCBO)
% eventdata  reserved - to be defined in a future version of MATLAB
% handles    empty - handles not created until after all CreateFcns
called

% Hint: edit controls usually have a white background on Windows.
%       See ISPC and COMPUTER.
if ispc && isequal(get(hObject,'BackgroundColor'),
get(0,'defaultUicontrolBackgroundColor'))
    set(hObject,'BackgroundColor','white');
end

%CALIBRATE
% --- Executes on button press in pushbutton8.
function pushbutton8_Callback(hObject, eventdata, handles)
% hObject    handle to pushbutton8 (see GCBO)
% eventdata  reserved - to be defined in a future version of MATLAB
% handles    structure with handles and user data (see GUIDATA)
global arduin  firsta1 firsta2 firsta3 firsta4 firsta0 firsta5 ROT0
firsta6 pp pp1 gen genz

%INITIAL RIGHT HAND POSITION
xxo0=0;
yyo0=-600;
zzo0=0;

tic
tocvv=5;

 while toc<=tocvv

     axes(handles.axes1);
     strV = num2str(tocvv-(round(toc*100)/100));
%        fprintf('elapsed time is: %.2f seconds. \n',toc');

     text(0.1,0.4,0,'Please Do Not Move for 5
Seconds','VerticalAlignment','bottom','FontSize',10,'color','r');


text(0.1,0,0,strV,'VerticalAlignment','bottom','FontSize',40,'color','
r');
drawnow
```

154

```matlab
cla

%      firstread1=fscanf(arduin,'%f');
firstread2=fscanf(arduin,'%f');
    firstread3=fscanf(arduin,'%f');
 a0=firstread3(1);
 a1=firstread3(2);
 a2=firstread3(3);
 a3=firstread3(4);
 a4=firstread3(5);
 a5=firstread3(6);

aw0=a1;
ax0=a2;
ay0=a3;
az0=a4;

ROT0=[aw0^2+ax0^2-ay0^2-az0^2,2*ax0*ay0-2*aw0*az0,2*ax0*az0+2*aw0*ay0;
    2*ax0*ay0+2*aw0*az0,aw0^2-ax0^2+ay0^2-az0^2,2*ay0*az0-2*aw0*ax0;
    2*ax0*az0-2*aw0*ay0,2*ay0*az0+2*aw0*ax0,aw0^2-ax0^2-ay0^2+az0^2];
newcor0=ROT0*[xxo0;yyo0;zzo0];
xxn0=newcor0(1,1);
yyn0=newcor0(2,1);
zzn0=newcor0(3,1);

firsta0=a0;
firsta1=a1;
firsta2=a2;
firsta3=a3;
firsta4=a4;
firsta5=a5;
  %----------------------------------
 end

text(0.1,0,0,'Calibrated','VerticalAlignment','bottom','FontSize',40,'
color','g');
% msgbox('Sensor is calibrated','Calibration');

%Left arm selection
% --- Executes on button press in pushbutton9.
function pushbutton9_Callback(hObject, eventdata, handles)
% hObject    handle to pushbutton9 (see GCBO)
% eventdata  reserved - to be defined in a future version of MATLAB
% handles    structure with handles and user data (see GUIDATA)
global arm
arm=1;
axes(handles.axes9);

scatter(0.2,0,150,'MarkerEdgeColor',[0 .1 .5],...
            'MarkerFaceColor',[0 .3 .8],...
            'LineWidth',2);
xlim([0 1]);
axis off

%Right arm selection
% --- Executes on button press in pushbutton10.
function pushbutton10_Callback(hObject, eventdata, handles)
% hObject    handle to pushbutton10 (see GCBO)
% eventdata  reserved - to be defined in a future version of MATLAB
% handles    structure with handles and user data (see GUIDATA)
```

```matlab
global arm
arm=2;
axes(handles.axes9);

scatter(0.8,0,150,'MarkerEdgeColor',[0 .1 .5],...
              'MarkerFaceColor',[0 .3 .8],...
              'LineWidth',2);
xlim([0 1]);
axis off

%Close Port
% --- Executes on button press in pushbutton11.
function pushbutton11_Callback(hObject, eventdata, handles)
% hObject    handle to pushbutton11 (see GCBO)
% eventdata  reserved - to be defined in a future version of MATLAB
% handles    structure with handles and user data (see GUIDATA)
clc
clear all
if ~isempty(instrfind)
    fclose(instrfind);
    delete(instrfind);
end
close all
clc
disp('Serial Port Closed')
run('FINAL7');

% --- Executes on button press in pushbutton13.
function pushbutton13_Callback(hObject, eventdata, handles)
% hObject    handle to pushbutton13 (see GCBO)
% eventdata  reserved - to be defined in a future version of MATLAB
% handles    structure with handles and user data (see GUIDATA)
global flag arduin;
flag=0;
fclose(arduin); % end communication with arduino

% --- Executes on button press in pushbutton14.
function pushbutton14_Callback(hObject, eventdata, handles)
% hObject    handle to pushbutton14 (see GCBO)
% eventdata  reserved - to be defined in a future version of MATLAB
% handles    structure with handles and user data (see GUIDATA)

global gen aa0 abd habd aa6 genz2;
gen=[aa0 abd  habd  aa6];
assignin('base','gen',gen);
FileName = genz2;
assignin('base','gen',FileName);
AAA = gen;
xlswrite(FileName,AAA);
```

156

A.X. Joint simulator CAD models
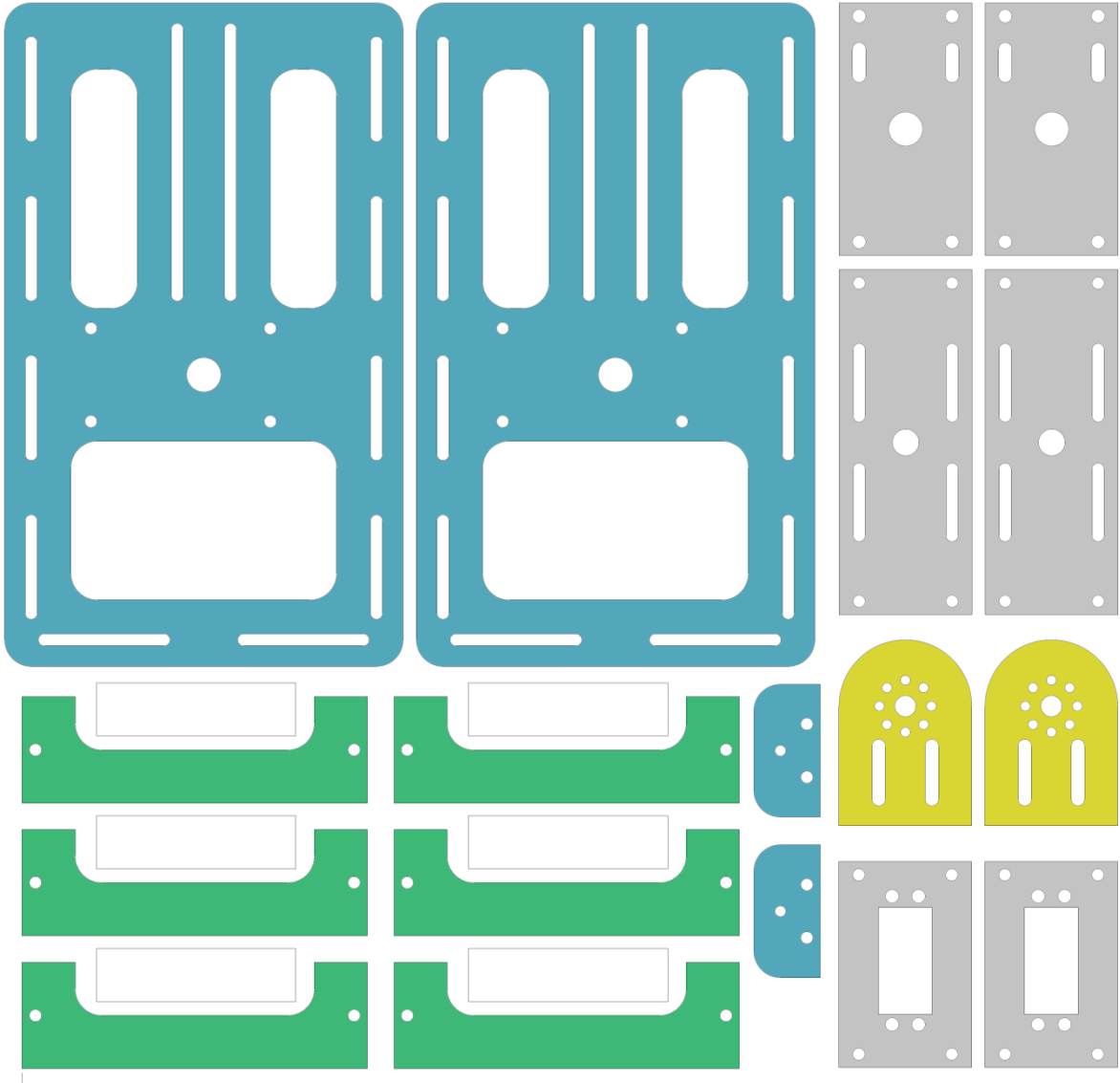
A.XI.   Joint simulator Arduino code

```
#include <Servo.h>
#include "HX711.h"
//{FORCE SENSOR
HX711 scale(A3, A2);
HX711 scale1(A5, A4);
//}FORCE SENSOR
Servo myservo1;
Servo myservo2;

int potpin1 = 0;
int potpin2 = 1;
int potread1;
int pos1;

int potread2;
int pos2;

int vala;
int valb;
long pot1 = 0;
long pot2 = 0;

//CONTACT and MASS
const int buttonPin = 5;
int buttonState = 0;
int potpin3 = 6;
long pot3 = 0;
int mass;


void setup()
{
  //{FORCE SENSOR
float cal1=0;
float cal2=0;
//}FORCE SENSOR

//{FORCE SENSOR
scale.set_gain(128);
scale1.set_gain(128);
//}FORCE SENSOR
  myservo1.attach(3);
  myservo2.attach(4);
    Serial.begin(9600);
    pinMode(buttonPin, INPUT);
}

void loop()
{
//in general
//pot = (analogRead(pin) * alpha + pot * beta) / (alpha + beta);  // a
& b are adjustable weights.

vala = analogRead(potpin1);
  vala = map(vala, 0, 1023, 0, 180);
pot1 = (vala  + 5 * pot1)/6;  // new value only counts for 16%
  myservo1.write(vala);
  delay(15);
```

```
  valb = analogRead(potpin2);
  valb = map(valb, 0, 1023, 0, 180);
pot2 = (valb  + 5 * pot2)/6;  // new value only counts for 16%

  myservo2.write(valb);
  delay(15);

buttonState = digitalRead(buttonPin);
mass = analogRead(potpin3);
  mass = map(mass, 0, 1023, 0, 112);
pot3 = (mass  + 5 * pot3)/6;



Serial.print(pot1);
    Serial.print("\t");
Serial.print(pot2);


  //{FORCE SENSOR
    Serial.print("\t");
Serial.print(scale.read());        // print a raw reading from the
ADC
  Serial.print("\t");
//Serial.print("read scale 1: \t\t");
Serial.print(scale1.read());
Serial.print("\t");
Serial.print(buttonState);
Serial.print("\t");
Serial.println(pot3);
//}FORCE SENSOR
}
```

A.XII. Servo Motor

Product Description

Hitec's strongest servo period, the "Ultra Torque" HS-7950TH is designed to operate on a two cell LiPo Pack. Featuring our high resolution "G2" second generation programmable digital circuit and our indestructible Titanium gears, the HS-7950TH has the performance and durability you've come to expect from a Hitec servo. Other features in the HS-7950TH include a 7.4V optimized coreless motor, integrated heat sink case, and a top case with two hardened steel gear pins supported by axial brass bushing. The HS-7950TH has been designed for the most demanding hobby applications including the largest aircraft and monster trucks. Featuring a titanic 403 oz./in. of torque at 6.0 volts, while still maintaining a respectable 0.15 second transit time.

Features

•G2 Digital Circuit
•Titanium Gear Train (MK first gear)
•Ultra Performance Coreless Motor
•Heatsink Case
•(8) O-Rings for Water/Dust/Fuel protection
•Dual Ball Bearing Supported Output Shaft

Programmable Features

•Dead Band Width
•Direction of Rotation
•Speed of Rotation (slower)
•End Points
•Neutral Points
•Fail Safe On/Off
•Fail Safe Point
•Resolution* (default is high resolution)
•Overload Protection* (default is off)
*These features are only programmable with the HFP-20, HPP-20 or HPP-21 programmers.

Specifications

Motor Type:	Coreless
Bearing Type:	Dual Ball Bearing
Speed (6.0V/7.4V):	0.15 / 0.13
Torque oz./in. (6.0V/7.4V):	403 / 486
Torque kg./cm. (6.0V/7.4V):	29.0 / 35.0
Size in Inches:	1.57 x 0.79 x 1.50
Size in Millimeters:	39.88 x 20.07 x 38.10
Weight oz.:	2.40
Weight g.:	68.04

A = .780" (19.82mm)
B = .547" (13.9mm)
C = 1.352" (34.35mm)
D = .394" (10mm)
E = .394" (10mm)
F = 1.181" (30mm)
G = .472" (12mm)
H = 1.102" (28mm)
J = 2.09" (53.1mm)
K = .384" (9.75mm)
L = .174" (4.42mm)
M = 1.575" (40mm)
X = .126" (3.2mm)
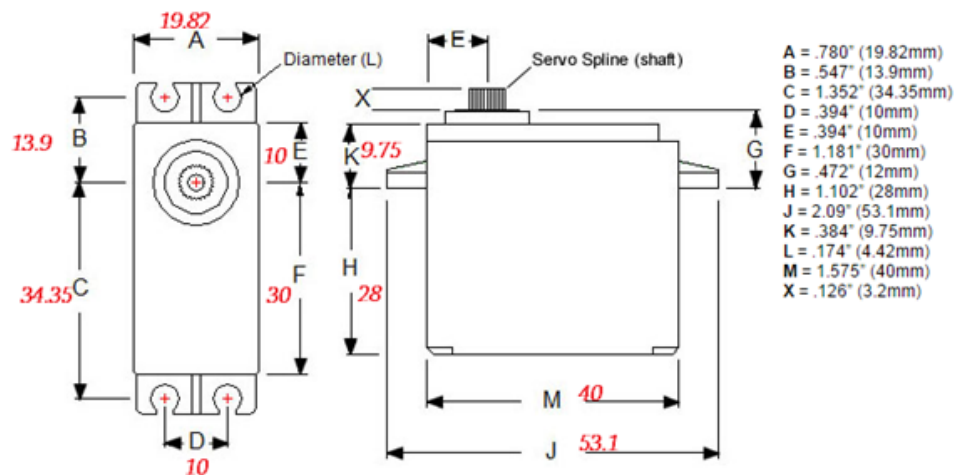
A.XIII. Shoulder assessment ethical approval

Research Ethics Checklist

Bournemouth University

Reference Id	12330
Status	Approved
Date Approved	27/06/2016

Researcher Details

Name	Navid Aslani
School	Faculty of Science & Technology
Status	Postgraduate Research (MRes, MPhil, PhD, DProf, DEng)
Course	Postgraduate Research
Have you received external funding to support this research project?	No
Please list any persons or institutions that you will be conducting joint research with, both internal to BU as well as external collaborators.	Bournemouth Hospital

Project Details

Title	Shoulder 3D range of motion assesment using IMU and EMG
Proposed Start Date of Data Collection	06/06/2016
Proposed End Date of Project	06/12/2016
Supervisor	Siamak Noroozi
Approver	Siamak Noroozi

A.XIV. Shoulder assessment consent form

Bournemouth University

Informed Consent Form

Full title of project: Shoulder 3D range of motion tracking using IMU and EMG sensors

Name, position and contact details of researcher:
Navid Aslani. PhD Researcher in Biomechanical Engineering in Bournemouth University.
Poole House P517, Talbot Campus ,Fern Barrow, Poole, Dorset BH12 5BB

Name, position and contact details of supervisor:
Professor Siamak Noroozi
Poole House P124, Talbot Campus, Fern Barrow, Poole, BH12 5BB

Please initial all boxes

I confirm that I have read and understood the participant information sheet for the above research project. I have had the opportunity to consider the information, ask questions and have had these answered satisfactorily.

☐

I understand that my participation is voluntary and that I am free to withdraw up to the point where the data is anonymised, without giving reason and without there being any negative consequences. In addition, should I not wish to answer any particular question(s), complete a test or give a sample, I am free to decline.

☐

I give permission for members of the research team to have access to my anonymised responses. I understand that my name will not be linked with the research materials, and I will not be identified or identifiable in the report or reports that result from the research.

☐

I understand that relevant sections of my medical notes and data collected during the study

☐

I agree to data recorded from my motion being used in the publication of scientific papers, providing they are anonymised. I understand that once published these images could be seen by anyone, and that they may be published on the internet. I also understand that once published neither I nor the authors of the publication will have control over who may view these data.

☐

I agree to take part in the above research project.

☐

_____   _____
_____
Name of Participant Date   Signature

Name of Researcher   Date   Signature

162

A.XV. Strain gauge

PRECISION STRAIN GAGE
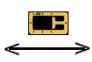## PRECISION LINEAR PATTERN FOR STATIC AND DYNAMIC APPLICATIONS

SGD Series

- Very Flexible, Mechanically Strong
- Small Bending Radius
- Broad Temperature Range
- Ribbon Leads or Solder Pads
- Clear Alignment Marks
- Affix with Cold or Hot Curing Adhesives

OMEGA® strain gages are available in a variety of models to cover most strain measurement applications. Their rugged construction and flexibility make them suitable for highly accurate static and dynamic measurement. The measuring grid is formed by etching constantan foil, which is then completely sealed in a carrier medium composed of polyimide film. The linear pattern strain gages are used to measure strain in a single direction. They are often used for experimental stress analysis applications. The strain gage pattern is shown on the left side of the table. Notice the "arrow" which indicates the principal stress direction.

The linear pattern strain gages are available in a variety or styles and sizes. OMEGA is offering miniature linear patterns for strain measurement of a stress concentration or high gradient areas. We also have wide or narrow grid patterns, and small, medium or large patterns. To determine if the strain gages have temperature characteristics matched to steel or aluminum, see the column labeled "COMP" short for compensation, "ST" indicates steel, "AL" indicates aluminum, "UNC" indicates uncompensated. See the column labeled "BTP" for accessory bondable terminal pad model numbers.

Dimensions are listed for pattern gage grid length (A) and width (B), and the matrix or carrier length (C) and width (D). The patterns include alignment triangles. The carrier or matrix material on the patterns may be trimmed in the field on all sides to within 0.25 mm of the foil grid with no effect on strain gage performance.

To Order

| GAGE PATTERN Leads not shown | MODEL NO. Pkg of 10 | NOM. RESIS-TANCE (Ω) | DIMENSIONS mm (inch)† GRID | | CARRIER | | MAX V* (Vrms) | TERMINATION | TEMP COMP | TERM PAD |
			A	B	C	D				
Shown actual size 4.70 mm	SGD-1.5/120-LY11	120	1.50 (0.059)	1.20 (0.047)	4.70 (0.185)	3.40 (0.134)	2.5	Ribbon Leads	ST	
	SGD-1.5/120-LY13	120	Miniature linear pattern Measurement of stress concentration 120 Ω				3.5	Ribbon Leads	AL	BTP-1
	SGD-1.5/120-LY41	120					2.5	Solder Pads	ST	
	SGD-1.5/120-LY43	120					3.5	Solder Pads	AL	
Shown actual size 7.60 mm	SGD-2/350-LY11	350	2.00 (0.079)	2.50 (0.098)	7.60 (0.299)	5.80 (0.228)	7.5	Ribbon Leads	ST	
	SGD-2/350-LY13	350	Miniature linear pattern Measurement of stress concentration, higher resistance reduced heat generation 350 Ω				10	Ribbon Leads	AL	BTP-1
	SGD-2/350-LY41	350					7.5	Solder Pads	ST	
	SGD-2/350-LY43	350					10	Solder Pads	AL	
Shown actual size 7.10 mm	SGD-2D/350-LY11	350	1.90 (0.075)	4.80 (0.189)	7.10 (0.280)	6.60 (0.260)	10	Ribbon Leads	ST	
	SGD-2D/350-LY13	350	Miniature linear pattern grid width, wide 350 Ω				14	Ribbon Leads	AL	BTP-2
	SGD-2D/350-LY41	350					10	Solder Pads	ST	
	SGD-2D/350-LY43	350					14	Solder Pads	AL	
Shown actual size 7.00 mm	SGD-3/350-LY11	350	3.20 (0.126)	2.50 (0.098)	7.00 (0.276)	4.00 (0.157)	9.5	Ribbon Leads	ST	
	SGD-3/350-LY13	350	linear pattern leads/ pads at on end of grid 350 Ω				13	Ribbon Leads	AL	BTP-3
	SGD-3/350-LY41	350					9.5	Solder Pads	ST	
	SGD-3/350-LY43	350					13	Solder Pads	AL	

Visit us online

A.XVI. Force sensor circuit
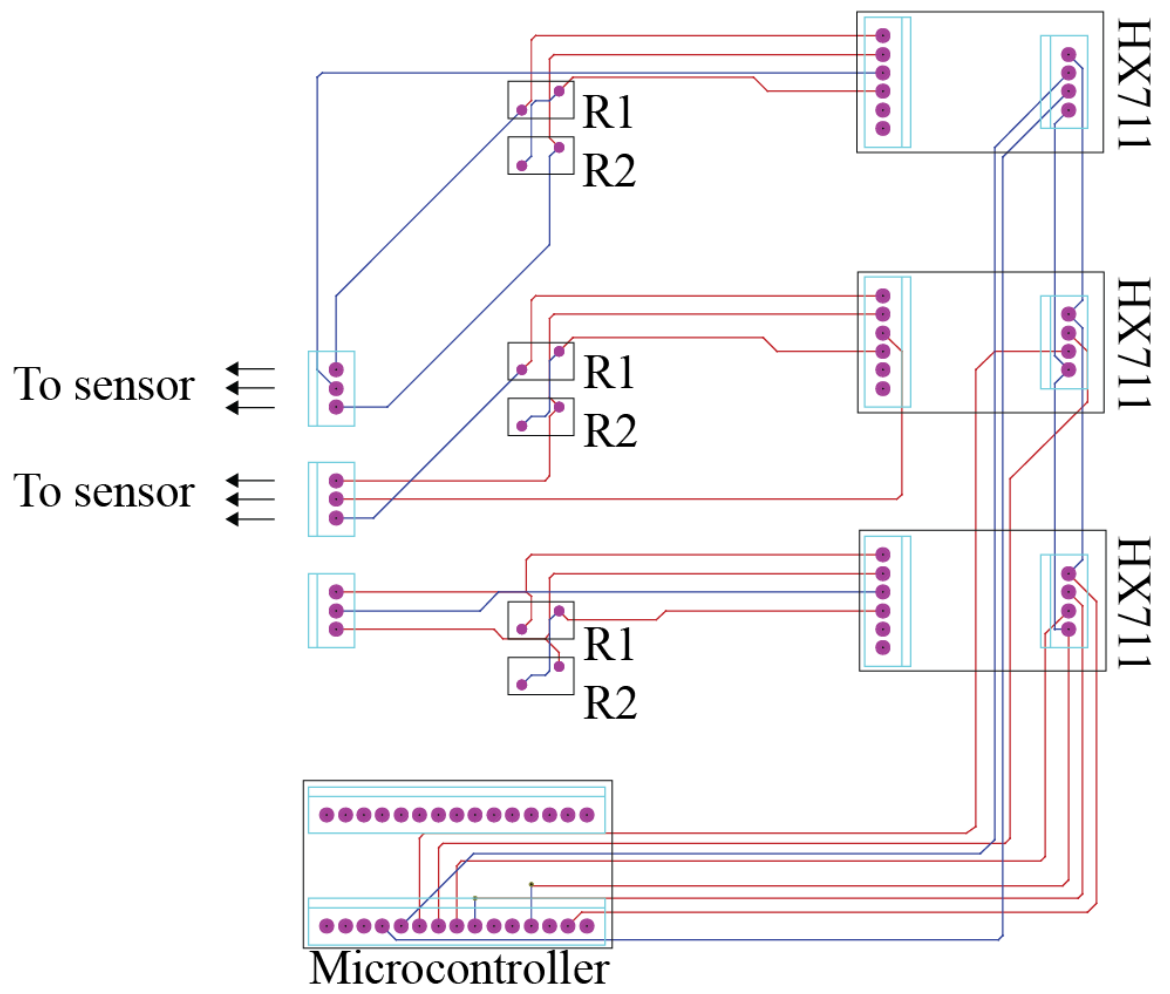
A.XVII.   Force sensor Matlab code

```matlab
function varargout = GUIA(varargin)
% GUIA MATLAB code for GUIA.fig
%      GUIA, by itself, creates a new GUIA or raises the existing
%      singleton*.
%
%      H = GUIA returns the handle to a new GUIA or the handle to
%      the existing singleton*.
%
%      GUIA('CALLBACK',hObject,eventData,handles,...) calls the local
%      function named CALLBACK in GUIA.M with the given input
arguments.
%
%      GUIA('Property','Value',...) creates a new GUIA or raises the
%      existing singleton*.  Starting from the left, property value
pairs are
%      applied to the GUI before GUIA_OpeningFcn gets called.  An
%      unrecognized property name or invalid value makes property
application
%      stop.  All inputs are passed to GUIA_OpeningFcn via varargin.
%
%      *See GUI Options on GUIDE's Tools menu.  Choose "GUI allows
only one
%      instance to run (singleton)".
%
% See also: GUIDE, GUIDATA, GUIHANDLES

% Edit the above text to modify the response to help GUIA

% Last Modified by GUIDE v2.5 12-May-2016 13:49:13

% Begin initialization code - DO NOT EDIT
gui_Singleton = 1;
gui_State = struct('gui_Name',       mfilename, ...
                   'gui_Singleton',  gui_Singleton, ...
                   'gui_OpeningFcn', @GUIA_OpeningFcn, ...
                   'gui_OutputFcn',  @GUIA_OutputFcn, ...
                   'gui_LayoutFcn',  [] , ...
                   'gui_Callback',   []);
if nargin && ischar(varargin{1})
    gui_State.gui_Callback = str2func(varargin{1});
end

if nargout
    [varargout{1:nargout}] = gui_mainfcn(gui_State, varargin{:});
else
    gui_mainfcn(gui_State, varargin{:});
end
% End initialization code - DO NOT EDIT


% --- Executes just before GUIA is made visible.
function GUIA_OpeningFcn(hObject, eventdata, handles, varargin)
% This function has no output args, see OutputFcn.
% hObject    handle to figure
% eventdata  reserved - to be defined in a future version of MATLAB
% handles    structure with handles and user data (see GUIDATA)
```

```matlab
% varargin   command line arguments to GUIA (see VARARGIN)

% Choose default command line output for GUIA
handles.output = hObject;

% Update handles structure
guidata(hObject, handles);

% UIWAIT makes GUIA wait for user response (see UIRESUME)
% uiwait(handles.figure1);


% --- Outputs from this function are returned to the command line.
function varargout = GUIA_OutputFcn(hObject, eventdata, handles)
% varargout  cell array for returning output args (see VARARGOUT);
% hObject    handle to figure
% eventdata  reserved - to be defined in a future version of MATLAB
% handles    structure with handles and user data (see GUIDATA)

% Get default command line output from handles structure
varargout{1} = handles.output;


% --- Executes on button press in Main.
function Main_Callback(hObject, eventdata, handles)
% hObject    handle to Main (see GCBO)
% eventdata  reserved - to be defined in a future version of MATLAB
% handles    structure with handles and user data (see GUIDATA)
global aa0 aa1 aa2 aa3 aa4 aa5
run('PLOTALLRAWDATA.m');
assignin('base','aa0',aa0);
assignin('base','aa1',aa1);
assignin('base','aa2',aa2);
assignin('base','aa3',aa3);
assignin('base','aa4',aa4);
assignin('base','aa5',aa5);


% --- Executes on button press in pushbutton2.
function pushbutton2_Callback(hObject, eventdata, handles)
% hObject    handle to pushbutton2 (see GCBO)
% eventdata  reserved - to be defined in a future version of MATLAB
% handles    structure with handles and user data (see GUIDATA)
run('CLOSEPORT.m');
pause(2);
run('GUIA.m');

%SAVE
% --- Executes on button press in pushbutton3.
function pushbutton3_Callback(hObject, eventdata, handles)
% hObject    handle to pushbutton3 (see GCBO)
% eventdata  reserved - to be defined in a future version of MATLAB
% handles    structure with handles and user data (see GUIDATA)
global   INZ OUTZ aa0 aa1 aa4 %%AVER

aa0=evalin('base','aa0');
aa1=evalin('base','aa1');
aa4=evalin('base','aa4');
aa0=aa0(:,2);
```

166

```matlab
aa1=aa1(:,2);
aa4=aa4(:,2);

INZ=[aa0 aa1];
OUTZ=aa4;
% AVER=(aa0+aa1)/2;
% INZ=evalin('base','[aa0,aa1]');
% assignin('base','INZ',INZ);
%
% % OUTZ=evalin('base','aa4');
% assignin('base','OUTZ',OUTZ);

% assignin('base','AVER',AVER);
assignin('base','INZ',INZ);
assignin('base','OUTZ',OUTZ);

% save('AVERIN.mat','AVER')
save('NEUIN.mat','INZ')
save('NEUOUT.mat','OUTZ')




% --- Executes on button press in pushbutton4.
function pushbutton4_Callback(hObject, eventdata, handles)
% hObject    handle to pushbutton4 (see GCBO)
% eventdata  reserved - to be defined in a future version of MATLAB
% handles    structure with handles and user data (see GUIDATA)
nftool

%plot after neural
% --- Executes on button press in pushbutton5.
function pushbutton5_Callback(hObject, eventdata, handles)
% hObject    handle to pushbutton5 (see GCBO)
% eventdata  reserved - to be defined in a future version of MATLAB
% handles    structure with handles and user data (see GUIDATA)
run('PLOTAFTERNEURALCALIBRATION.m');



% --- Executes on button press in pushbutton6.
function pushbutton6_Callback(hObject, eventdata, handles)
% hObject    handle to pushbutton6 (see GCBO)
% eventdata  reserved - to be defined in a future version of MATLAB
% handles    structure with handles and user data (see GUIDATA)



%CALIBRATE
% --- Executes on button press in pushbutton7.
function pushbutton7_Callback(hObject, eventdata, handles)
% hObject    handle to pushbutton7 (see GCBO)
% eventdata  reserved - to be defined in a future version of MATLAB
% handles    structure with handles and user data (see GUIDATA)
global  aa0 aa1 aa4 avergz plft

aa0=evalin('base','aa0');
aa1=evalin('base','aa1');
aa4=evalin('base','aa4');
aa0=aa0(:,2);
aa1=aa1(:,2);
aa4=aa4(:,1);
```

```matlab
avergz=(aa0+aa1)/2;

%polyfit
plft = polyfit(avergz,aa4,2);
assignin('base','plft',plft);
% save('POLYLINE.mat','plft')
POLYLINE = 'POLYLINE.xlsx';
xlswrite(POLYLINE,plft);

%plot after calibration
% --- Executes on button press in pushbutton8.
function pushbutton8_Callback(hObject, eventdata, handles)
% hObject    handle to pushbutton8 (see GCBO)
% eventdata  reserved - to be defined in a future version of MATLAB
% handles    structure with handles and user data (see GUIDATA)
run('PLOTAFTERpolyfitCALIBRATION.m');


-------------------------------
-------------------------------
-------------------------------
-------------------------------

clear all
close all
clc
global plft
plft = xlsread('POLYLINE.xlsx');
% plft=plftz;
ADCres=24; %bit
VIN=3.75; %volts

% arduin=serial('COM13','BaudRate',9600); % create serial
communication object on port COM18
arduin = Bluetooth('HC-05',1);
fopen(arduin); % initiate arduino communication

lenn2=1500;

aa0=zeros(lenn2,1);
aa1=zeros(lenn2,1);
aa2=zeros(lenn2,1);
aa3=zeros(lenn2,1);
aa4=zeros(lenn2,1);
aa5=zeros(lenn2,1);
aa6=zeros(lenn2,1);
aa7=zeros(lenn2,1);
aa8=zeros(lenn2,1);
%STRAIN GAUGE FILTER PARAMETERS
CH1filt=0;
CH2filt=0;
CH1filt0=0;
CH2filt0=0;

filtvalue1=0.5;
filtvalue2=0.5;

CH3filt=0;
CH4filt=0;
```

168

```matlab
ang1filt=0;
ang2filt=0;

CHa3filt=0;
CHa4filt=0;
filtvalue3=0.5;
filtvalue4=0.5;

mass=1000;    %gr
%cancel for initials
tic
while (toc<=5)

%view(-135,5);

% readz1=fscanf(arduin,'%f');
% readz2=fscanf(arduin,'%f');
if toc<2
    readz1=fscanf(arduin,'%f');
end
    readz3=fscanf(arduin,'%f');

%STRAIN
ang10=readz3(1);
ang20=readz3(2);
CH10=-readz3(3)/1;
CH20=-readz3(4)/1;
massz0=readz3(6);

CH1filt0=(1-filtvalue1)*CH1filt0+filtvalue1*CH10;
CH2filt0=(1-filtvalue1)*CH2filt0+filtvalue1*CH20;

%VOLTAGE STRAIN CONVERSION
%%%%%%%%%%%%%%%%%%
VoutCH1_unstrained=(VIN*CH1filt0)/2^ADCres;
VoutCH2_unstrained=(VIN*CH2filt0)/2^ADCres;

%%%%%%%%%%%%%%%%%%
toc

% CH1filt=(1-filtvalue1)*CH1filt+filtvalue1*CH1;
% CH2filt=(1-filtvalue1)*CH2filt+filtvalue1*CH2;
% ang1filt=(1-filtvalue2)*ang1filt+filtvalue2*ang1;
% ang2filt=(1-filtvalue2)*ang2filt+filtvalue2*ang2;

end

%
tic
while (toc<=400)

% readz1=fscanf(arduin,'%f');
% readz2=fscanf(arduin,'%f');
    readz3=fscanf(arduin,'%f');

%STRAIN
ang1=readz3(1);
ang2=readz3(2);
CH1=-readz3(3)/1;
```

```matlab
CH2=-readz3(4)/1;

contact=readz3(5);
massz=readz3(6);
% massz=massz-massz0;

CH1filt=(1-filtvalue1)*CH1filt+filtvalue1*CH1;
CH2filt=(1-filtvalue1)*CH2filt+filtvalue1*CH2;
% ang1filt=(1-filtvalue2)*ang1filt+filtvalue2*ang1;
% ang2filt=(1-filtvalue2)*ang2filt+filtvalue2*ang2;
%
% CH1filtZZZ=CH1filt-CH1filt0;
% CH2filtZZZ=CH2filt-CH2filt0;


%VOLTAGE STRAIN CONVERSION
%%%%%%%%%%%%%%%%%
VoutCH1_strained=(VIN*CH1filt)/2^ADCres;
VoutCH2_strained=(VIN*CH2filt)/2^ADCres;


Vr1=(VoutCH1_strained/VIN)-(VoutCH1_unstrained/VIN);
Vr2=(VoutCH2_strained/VIN)-(VoutCH2_unstrained/VIN);


% STRAIN1=(-4*Vr1)/(2.1*(1+2*Vr1));
% STRAIN2=(-4*Vr2)/(2.1*(1+2*Vr2));


STRAIN1=(-2*Vr1)/(2.1);
STRAIN2=(-2*Vr2)/(2.1);


STRAIN1=STRAIN1*10^6;
STRAIN2=STRAIN2*10^6;


%%%%%%%%%%%%%%%%%
ang1filt=ang1-ang10;
ang2filt=ang2-ang20;

%CALCULATING FORCE
Nforce=massz*cosd(ang1filt);
if contact<0.5
    Nforce=0;
end
%AVERAGING
aver=(STRAIN1+STRAIN2)/2;
%Coef of correction
% if CH2filtZZZ>CH1filtZZZ
%     aver=aver*0.65;
% end
polyout=polyval(plft,aver);

aa2 = [aa2(2:end) ; ang1filt];
aa3 = [aa3(2:end) ; ang2filt];
aa0 = [aa0(2:end) ; STRAIN1];
aa1 = [aa1(2:end) ; STRAIN2];
aa4 = [aa4(2:end) ; Nforce];
aa5 = [aa5(2:end) ; aver];
aa6 = [aa5(2:end) ; massz];
aa7 = [aa7(2:end) ; polyout];


figure(22)
```

```matlab
 plot(aa4,'linewidth',2,'color','black');
hold on
 plot(aa7,'linewidth',2,'color','r');

 ylim([-2 50]);
grid on
grid minor
title('Strains','FontSize',20);

text(50,10,'Normal Force','FontSize',14);
text(200,10,num2str(Nforce),'FontSize',14);
text(50,30,'Weight','FontSize',14);
text(200,30,num2str(massz),'FontSize',14);
title('Normal Force','FontSize',20);
 hold off

end
```